A Final Technical Report Submitted to the

U.S. Department of Energy
Nuclear Engineering Education Research (NEER) Program

By the

Office of Research and Graduate Programs
University of Florida
Gainesville, Florida 32611

For a project entitled

MicroCT-Based Skeletal Models for Use in Tomographic Voxel Phantoms for Radiological Protection

Grant DE-FG07-07ID14773

Wesley Bolch, PhD, PE, CHP, Principal Investigator
Department of Nuclear and Radiological Engineering
University of Florida

March 30, 2010

9. Health Physics:
MicroCT-Based Skeletal Models for Use in Tomographic Voxel Phantoms for Radiological Protection

Wesley E. Bolch, PhD, PE, CHP
Professor of Radiological and Biomedical Engineering
University of Florida, Principal Investigator

ABSTRACT

The University of Florida (UF) proposes to develop two high-resolution image-based skeletal dosimetry models for direct use by ICRP Committee 2's Task Group on Dose Calculation in their forthcoming Reference Voxel Male (RVM) and Reference Voxel Female (RVF) whole-body dosimetry phantoms. These two phantoms are CT-based, and thus do not have the image resolution to delineate and perform radiation transport modeling of the individual marrow cavities and bone trabeculae throughout their skeletal structures. Furthermore, new and innovative 3D microimaging techniques will now be required for the skeletal tissues following Committee 2's revision of the target tissues of relevance for radiogenic bone cancer induction. This target tissue had been defined in ICRP Publication 30 as a 10-μm cell layer on all bone surfaces of trabecular and cortical bone. The revised target tissue is now a 50-μm layer within the marrow cavities of trabecular bone only and is exclusive of the marrow adipocytes. Clearly, this new definition requires the use of 3D microimages of the trabecular architecture not available from past 2D optical studies of the adult skeleton. With our recent acquisition of two relatively young cadavers (males of age 18-years and 40-years), we will develop a series of reference skeletal models that can be directly applied to (1) the new ICRP reference voxel man and female phantoms developed for the ICRP, and (2) pediatric phantoms developed to target the ICRP reference children. Dosimetry data to be developed will include absorbed fractions for internal beta and alpha-particle sources, as well as photon and neutron fluence-to-dose response functions for direct use in external dosimetry studies of the ICRP reference workers and members of the general public.

A. Project Objectives

The International Commission on Radiological Protection (ICRP) is presently developing a revised set of radiological protection recommendations updating those given in ICRP Publication 60. Two very important decisions have been made regarding these revisions. First, ICRP Committee 2 was instructed to develop two tomographic voxel-based anatomic phantoms representing the ICRP 89 reference adult male and reference adult female. As these phantoms are based upon whole-body CT scans, limitations on image resolution preclude the ability to explicitly model the 3D micro-architecture of the bone trabeculae and marrow cavities within the skeletal regions of either phantom. Second, new information on the cells at risk for induction of radiogenic bone cancer have resulted in a revision of the 10-μm endosteal layer originally defined in the ICRP 30 bone model. The new target tissue is now defined as all non-adipose bone marrow located within 50-μm on the bone surfaces in trabecular bone (e.g., shallow active marrow). This new target tissue explicitly demands a 3D representation of not only the bone trabeculae by skeletal site, but also the active and inactive marrow tissues as a function of depth within the marrow cavities. The recent acquisition of two young cadavers at the University of Florida – an 18-year male and a 40-year male – provide us with a very unique and timely opportunity to significantly contribution to this ICRP effort. A 2-year comprehensive research project is thus proposed to DOE having the following three research objectives:

1. To construct a high-resolution skeletal dosimetry model for use with the ICRP Reference Voxel Male (RVM) and Reference Voxel Female (RVF) based upon CT and microCT images of skeletal specimens taken from the 18-year male. As the ICRP Publication 89 defines reference adults as between 20 and 50 years of age, this individual thus represents the lower end of the adult age range. Each bone and/or region of the skeleton will be modeled individually and will have two image-based descriptions. The first will be based on high-resolution ex-vivo CT scans with regions of cortical bone and interior spongiosa explicitly segmented. The second will be based on one or more ex-vivo microCT scans of cored spongiosa with bone trabeculae and marrow cavities explicitly defined in the voxelized image. The resulting model will be used to develop absorbed fraction data for internal electron and alpha-particle dosimetry of the skeletal tissues, as well as fluence-to-dose response functions needed for both photon and neutron dosimetry in the ICRP phantoms.

2. To construct a high-resolution skeletal dosimetry model for use with the ICRP reference voxel phantoms based upon ex-vivo CT and microCT scanning of skeletal specimens taken from the 40-year male cadaver. This individual thus represents the upper end of the ICRP adult age range. Along with Task 1, the ICRP will be able to report skeletal dosimetry values at each end of the adult age range, as well as average values for the median age of 35 years.

3. To construct high-resolution skeletal dosimetry models for use with UF and GSF series of pediatric phantoms for potential future use by the ICRP. In this task, we will rescale each of the ex-vivo CT skeletal images of the 18-year male cadaver of Task 1 to match the skeletal dimensions of the UF (9-mo M, 4-yr F, 8-yr F, 11-yr M, and 14-yr M) and GSF (2-mo F and 7-yr F) pediatric series. As existing chord-based models of electron transport in the skeleton do not account for energy loss to cortical bone, it is anticipated that Task 3 studies will significantly reduce conservative dose uncertainties in pediatric skeletal dosimetry as needed for dose reconstruction studies targeting members of the general public.

B. Graduate Students Supported

Masters Students

1. **Hasenauer, Deanna, MS** (Health Physics – May 2006)
   Thesis - *Image-based techniques for beta particle skeletal dosimetry*

2. **Kielar, Kayla, MS** (Health Physics – May 2006)
   Thesis - *A skeletal reference dosimetry model for the adult female*

3. **Hough, Matt, MS** (Health Physics – May 2007)
   Thesis - *A skeletal reference dosimetry model for the 40-year male*

PhD Students

4. **Kielar, Kayla PhD** (Health Physics – August 2009)
   Dissertation – Bone marrow dosimetry via microCT imaging and stem cell spatial mapping

5. **Pafundi, Deanna PhD** (Health Physics – August 2009)
   Dissertation – Image-based skeletal models for the ICRP reference pediatric age series

C. Meeting Presentations and Abstracts

1. KN Kielar*, WE Bolch, and AP Shah, "A skeletal reference dosimetry model for the adult female", *Transactions of the Computational Medical Physics Working Group – Workshop II – of the American Nuclear Society,* Gainesville, Florida, October 1-3, 2007.

2. D Hasenauer*, C Lee*, DL Lodwick*, CJ Watchman, and WE Bolch, "Development of hybrid computational newborn phantom for dosimetry calculation: the skeleton" *Transactions of the Computational Medical Physics Working Group – Workshop II – of the American Nuclear Society,* Gainesville, Florida, October 1-3, 2007.

3. KN Kielar*, AP Shah, and WE Bolch, "A skeletal dosimetry model for the adult female", 2007 Annual Meeting of the Society of Nuclear Medicine, Washington, DC, June 3-6, 2007 [Supplement to *J Nucl Med* **48** (6) 297P (2007)].

4. KN Kielar*, AP Shah, and WE Bolch, "A skeletal reference dosimetry model for the adult female", 2007 Annual Meeting of the Health Physics Society, Portland, Oregon, July 8-12, 2007 [Supplement to *Health Phys* **93** (1) S46 (2007)].

5. M Hough*, and WE Bolch, "A skeletal reference dosimetry model for the 40-year male", 2007 Annual Meeting of the Health Physics Society, Portland, Oregon, July 8-12, 2007 [Supplement to *Health Phys* **93** (1) S46 (2007)].

6. D Hasenauer*, C Lee*, D Lodwick*, C Watchman, and WE Bolch, "Development of hybrid computational newborn phantom for dosimetry calculations: The skeleton", 2007 Annual Meeting of the Health Physics Society, Portland, Oregon, July 8-12, 2007 [Supplement to *Health Phys* **93** (1) S47 (2007)].

7. C Lee*, D Lodwick*, J Hurtado*, D Pafundi*, and WE Bolch, "Development of a series of hybrid computational phantoms and their applications to assessment of photon and electron specific absorbed fractions", 2008 Annual Meeting of the European Association of Nuclear Medicine, Munich, Germany, October 11-15, 2008. [Supplement to *Eur J Nucl Med* **35** (2) S202, 2008].

8. D Pafundi*, C Lee*, DL Lodwick*, A Shahlaee, and WE Bolch, "Image-based pediatric skeletal dosimetry for the UF hybrid computational phantom series", 2008 Annual Meeting of the European Association of Nuclear Medicine, Munich, Germany, October 11-15, 2008 [Supplement to *Eur J Nucl Med* **35** (2) S135, 2008].

9. D Hasenauer*, C Lee*, D Lodwick*, A Shahlaee, and WE Bolch, "Image-based pediatric skeletal dosimetry for the UF hybrid computational phantom series", 2008 Annual Meeting of the Society of Nuclear Medicine, New Orleans, LA, June 14-18, 2008. [Supplement to *J Nucl Med* **49** (5) 281P (2008)].

10. L Sinclair, D Pafundi, and W Bolch, "A skeletal model for marrow dosimetry in the ICRP reference adult female", 2009 Annual Meeting of the American Association of Physicists in Medicine, Anaheim, CA, July 26-30, 2009. [Supplement to *Medical Physics* **36** (6) 2450 (2009)].

11. A Bahadori, K Eckerman, D Jokisch, and W Bolch, "Skeletal neutron dose response functions development for use in proton therapy," 2009 Annual Meeting of the American Association of Physicists in Medicine, Anaheim, CA, July 26-30, 2009. [Supplement to *Medical Physics* **36** (6) 2668 (2009)].

12. D Pafundi*, C Lee, C Watchman, V. Bourke, J. Aris, and WE Bolch, "Image-based skeletal dosimetry models for the ICRP reference pediatric series", Third International Symposium on Radionuclide Therapy and Radiopharmaceutical Dosimetry (ISRTRD), Toronto, Canada, June 13-17, 2009 [Supplement to *J Nucl Med* **50** (2) 70P (2009)].

D. Journal Articles Published

1. CJ Watchman, D Hasenauer*, **WE Bolch**, "Derivation of site-specific skeletal masses within the current ICRP age series" *Phys Med Biol* **52** (11) 3133-3150 (2007).

2. **WE Bolch**, AP Shah, CJ Watchman, DW Jokisch, PW Patton, DA Rajon, M Zankl, N Petoussi-Henss, and KF Eckerman, "Skeletal absorbed fractions for electrons in the adult male – considerations of a revised 50-μm definition of the bone endosteum" *Radiat Prot Dosim* (Adv Access June 7, 2007) **127** (1-4) 169-173 (2008). **[Invited Paper]**

3. **CJ Watchman** and WE Bolch, "Absorbed fractions for alpha particles in tissues of cortical bone" *Phys Med Biol* **54** 6009-6027 (2009).

E. Journal Articles In Preparation for Submission

1. ***A microCT-based skeletal dosimetry model for the reference adult male: Internal electron sources***
   Matt Hough, Didier Rajon, Perry Johnson, and Choonsik Lee
   Physics in Medicine and Biology (in preparation)

2. ***Skeletal dose response functions: A comprehensive method for evaluating absorbed dose to active marrow and bone endosteum from external and internal photon sources***
   Perry Johnson, Amir Bahadori, Keith Eckerman, Choonsik Lee, and Wesley Bolch
   Physics in Medicine and Biology (in preparation)

3. ***A microCT-based skeletal dosimetry model for the reference adult female: Internal electron sources***
   Lindsay Sinclair and Wesley Bolch
   Physics in Medicine and Biology (in preparation)

4. ***A microCT-based skeletal dosimetry model for the reference 15-year adolescent: Internal electron sources***
   Deanna Pafundi and Wesley Bolch
   Physics in Medicine and Biology (in preparation)

Appendix A

A Skeletal Reference Dosimetry Model for the 40-Year Male

A Skeletal Reference Dosimetry Model for the 40-Year Male: Skeletal Masses

Matthew C Hough[1] and Wesley Bolch[1]

[1] Department of Nuclear and Radiological Engineering

University of Florida, Gainesville, FL 32611

ABSTRACT

Accurate estimates of absorbed dose to skeletal tissues (hematopoietic stem cells in active bone marrow and osteoprogenitor cells in shallow marrow) are essential in risk assessment in both occupational and medical dosimetry. Currently, the majority of skeletal reference models (SRMs) used in dosimetry utilizes chord-length data from a single 44-year male that was obtained in the late 1960s and early 1970s at the University of Leeds. Seeing a need for skeletal data for patients/workers at various ages, the University of Florida Bone Imaging and Dosimetry (UF BID) project set out to create scalable SRMs of male and female subjects representative of pediatric, adolescent, young adult, and geriatric ages that can be applied to patient/worker specific cases. Recently, the UF BID project has developed image-based SRMs of a 66-year male and a 64-year female, as representative of cancer patients undergoing radionuclide therapy. For this study, a 40-year male SRM is under development as representative of a typical radiation worker or cancer patient. A 40 year-old male cadaver was selected with a body-mass index of 28.6 kg m^{-2} and a cause of death precluding skeletal deterioration. *In-vivo* Computed Tomography (CT) images were acquired prior to removal of 38 bone sites, including 14 sites from the axial skeleton and 24 sites from the appendicular skeleton (proximal and distal sites of

the arm and leg bones). Next, high-resolution *ex-vivo* CT images of all skeletal sites were acquired from which volumes of both cortical bone and trabecular spongiosa were determined via image segmentation. Finally, samples of trabecular spongiosa from all bone sites were imaged at 30 μm resolution utilizing microCT to determine the micro-structure and marrow volume fraction of the trabecular spongiosa. From knowledge of macrostructural information (*ex-vivo* CT contoured spongiosa volumes) and microstructural information (*ex-vivo* microCT marrow and bone volume fraction, cellularity, etc.) a skeletal mass database was created for the 40 year-old male. These reference masses are reported and compared to both the UF 66 year-old male and ICRP 70/89 Reference Man.

INTRODUCTION

The skeleton is of critical interest in internal radiation dosimetry for both radiation protection and radionuclide therapy. Accurate absorbed dose estimates to the hematopoietic tissues in the active (red) bone marrow and osteogenic tissues in the shallow active bone marrow are of primary importance in order to better predict the short-term deterministic (myelotoxicity) and long-term stochastic (leukemia and/or osteosarcomas induction) effects of radiation exposure. Unlike many other organs of interest in internal dosimetry, however, the skeleton is composed of many bones with highly heterogeneous tissues: cortical and trabecular bone and hematopoietically active and inactive bone marrow. Explicit knowledge of each bone site's shape and volume of: (1) trabecular spongiosa (combination of trabecular bone and active and inactive marrow) and the exterior cortex of cortical bone (the hard compact bone that forms the dense but smooth external layer), or macrostructure, (2) trabecular bone (the spongy or cancellous bone that forms the honeycomb structure within the dense shell) distribution, or microstructure, (3) bone volume fraction and marrow volume fraction, (4) and marrow cellularity (the fraction of marrow present that is hematopoietically active) is paramount to accurately create Skeletal Reference Models (SRMs) used to calculate absorbed dose to both red bone marrow and osteogenic shallow marrow.

Currently, the majority of SRMs used in dosimetry utilizes chord-length data from a single 44-year male that was obtained in the late 1960s and early 1970s at the University of Leeds. This data forms an essential component of the International Commission on Radiological Protection's (ICRP) SRM published in ICRP Publications 30, 70, and 89. Unfortunately, this study only set out to describe the trabecular microstructure of seven bone sites and did not incorporate each bone sites' macrostructure. Ideally this model should have taken into account

both the microscopic structure of the bone trabeculae and marrow cavities, as well as the macroscopic structure of the bone site itself. Indeed, for alpha emitters and low-energy beta emitters, only the microscopic characterization is needed to model each bone site and accurately predict its absorbed dose, as these particles typically expend their full emission energy within the trabecular spongiosa. However, for intermediate- to higher-energy beta emitters, energy loss to the exterior cortical bone or even particle escape from the bone site can be expected, especially at those skeletal sites with high spongiosa surface-to-volume ratios (flat bones such as the cranium and ribs). In the later cases, the SRMs based on the University of Leeds' data will overestimate skeletal absorbed dose, which could possibly lead to overly conservative treatment planning for radionuclide therapy patients.

Previous work by Shah *et al.* at the University of Florida (UF) created the Paired-Image Radiation Transport (PIRT) model, a means to account for both the macro- and microstructure of each individual bone site. PIRT allows particles to be tracked simultaneously through two segmented digital images: (1) an *ex-vivo* Computed Tomography (CT) scan of each individual bone site's macrostructure, and (2) a high-resolution microCT scan of each individual bone site's microstructure. This form of radiation transport allows for both energy losses to the exterior cortical bone as well as particle escape from the bone site, which leads to a much more accurate absorbed dose calculation for higher-energy beta emitters. Furthermore, the technique increases the prospects for expanded availability of SRMs for both genders and of individuals of varying stature and skeletal size.

In addition, while the University of Leeds' data has formed the backbone of all skeletal dosimetry for the past three decades, recent studies have shown that predictions of myelotoxicity must be based on patient/worker-specific skeletal absorbed doses. This is due to highly variable

skeletal macro- and microstructures as well as marrow cellularities. An important example of this skeletal variability is osteoporosis in females over the age of 50. Osteoporosis, which is the most common bone disease in the United States, is a disorder which causes the rate of bone resorption to become much greater than that of bone formation. This leads to a much thinner trabecular structure, which greatly affects the microstructure and dosimetry of certain skeletal sites. Yet another variable is the shape and size of bone sites with age. Obviously, the skeletal structure of a teenage male is much different than that of a middle-aged male. Hence, trying to accurately predict myelotoxicity in a 65 year-old female Non-Hodgkin's Lymphoma patient or a 15 year-old male leukemia patient utilizing the University of Leeds' 44 year-old male skeletal data would be extremely difficult. For this reason, it is evident that the creation of SRMs that are able to be matched to patient-specific cases is essential. In fact, as radionuclide therapies such as radioimmunotherapy become more prevalent in everyday clinical practice, the need for patient-specific dosimetry intensifies.

Seeing a need for skeletal data for patients/workers at various ages, the University of Florida Bone Imaging and Dosimetry (UF BID) project set out to create scalable SRMs of male and female subjects representative of pediatric, adolescent, middle, and geriatric ages that can be applied to patient/worker-specific cases. Recently, the UF BID project has developed image-based SRMs of a 66 year-old male and a 64 year-old female, as representative of cancer patients undergoing radionuclide therapy. Studies at UF have also established a methodology by which these voxel based SRMs can be converted to deformable polygon-mesh models via Non-Uniform Rational B-Spline (NURBS) technology in order to account for varying macrostructures. Also, linear regression models have been created to predict skeletal total spongiosa volumes from a

few simple radiographic measurements. These advances will allow the age and gender dependent SRMs developed at UF to be scaled to patient/worker-specific cases.

In the current study, a 40-year male SRM is under development as representative of a typical radiation worker or cancer patient. Creation of an SRM is a two step process, in that radionuclide S-values require knowledge of both the absorbed fraction (AFs), the fractional energy deposited within a target region from a source region, as well as the mass of the target region. In this phase of the study, the later will be determined for the entire skeletal system and compared to the masses of the 66 year-old male SRM developed at UF and ICRP Reference Man.

MATERIALS AND METHODS

Cadaver Selection

A male candidate subject for this study was obtained through the State of Florida Anatomical Board located on the University of Florida (UF) campus. Cadaver selection criteria included (1) an age between 30 – 50 years (representative of typical radiation worker or radionuclide therapy patient), (2) a body mass index close to between 18.5 – 25 kg m^{-2} (CDC recommended healthy range), and (3) a cause of death that would preclude significant skeletal deterioration. The subject identified was a 44 year-old male approximately 82 kg in total mass and 170 cm in total height at the time of death (BMI of 28.5 kg m^{-2}). The subject died suddenly of complications associated with cardiopulmonary arrest due to myocardial infarction.

In-Vivo Computed Tomography Scanning

Prior to bone harvesting, the male cadaver was subjected to whole-body imaging via multi-slice helical CT at a pitch necessary to reconstruct contiguous 1-mm axial slices. The images were

acquired on a Siemens Sensation 16 unit within the Department of Radiology at UF Shands Hospital. Image reconstruction was performed with a bone filter at a maximum in-plane pixel resolution of 977 μm x 977 μm. The CT image sets were then transferred to workstations within the Advanced Laboratory for Radiation Dosimetry Studies (ALRADS) in the UF Department of Nuclear & Radiological Engineering for image processing and data storage. The *in-vivo* CT scans provided image data for (1) selecting the anatomical region from which the bone site would be harvested, and (2) constructing 3D anatomic models of skeletal sites where bone harvesting (and thus *ex-vivo* CT scanning) might be incomplete (e.g., facial bones of the skull and shafts of all long bones).

Bone Harvesting and *Ex-Vivo* Computed Tomography Scanning

Following detailed review of the whole-body in-vivo CT images, bone harvesting was conducted. Thirty-eight major skeletal sites were taken from the male cadaver: clavicles (2), cranium cap (2), distal and proximal femur (4), distal and proximal fibula (3 – the left distal fibula could not be excised due to the presence of a surgical pin), distal and proximal humerus (4), mandible (1), distal and proximal radius (4), lower rib (2), middle rib (2), upper rib (2), scapula (2), pelvis (1 – including osae coxae and sacrum), spinal column (1 – including lumbar, thoracic, and cervical vertebrae), sternum (1), distal and proximal tibia (3 – the left distal tibia could not be excised due to the presence of a surgical pin), and the distal and proximal ulna (4). Once each skeletal site was excised, it was cleaned of excess tissue, bagged, labeled, and stored frozen until *ex-vivo* CT imaging could be scheduled.

Ex-vivo CT imaging was again conducted with a Siemens Sensation 16 unit within the Department of Radiology at UF Shands Hospital utilizing the highest resolution permitted based on each samples' required field of view (1.0 mm slice thickness with an in-plane resolution of

0.57 mm x 0.57 mm for the pelvis, 0.11 mm x 0.11 mm for the clavicles). The *ex-vivo* CT scans provided image data for (1) identifying the location and extent of trabecular spongiosa to be sectioned for microCT imaging; (2) quantifying both trabecular spongiosa and cortical bone volumes within the bone site; and (3) constructing 3D anatomic models of the bone site for subsequent paired-image radiation transport simulations ((2) and (3) were accomplished via detailed image segmentation).

Micro- Computed Tomography Scanning

After review of each bone site's *ex-vivo* CT scan, samples, or cores, of marrow intact spongiosa were strategically excised for imaging via microCT. Samples were taken to ensure that the largest volume of trabecular spongiosa possible would be imaged. Sample sizes were, however, limited to a maximum of 35 mm cubes due to restrictions of the microCT bore. Nonetheless, each sample was then shipped to Scanco Medical AG, in Bassersdorf, Switzerland for imaging with the μCT80 scanner at 30 micron resolution. It should be noted that in some cases, multiple samples were taken from each bone site (*e.g.* the cranium was split into the frontal, parietal, and occipital). Also, in an effort to include more samples from the long bones, only samples from the cadaver's right side were sent off for imaging.

Post-acquisition Image Processing

Image Segmentation of Spongiosa and Cortical Bone Regions from Ex-Vivo CT Scans

To create SRM tomographic anatomic models for use in internal dosimetry, boundaries must be delineated between each tissue region for which an independent dose assessment is to be made. For this reason, it is necessary to separate the cortical region of each bone site from the trabecular spongiosa region. Unfortunately, limitations of CT image acquisition results in an overlap of grayscale values for tissues of interest, which does not allow for simple automated

methods of this boundary definition. For this reason, an in-house program called CT_Contours was adopted for use in segmenting the spongiosa and cortical bone within each *ex-vivo* or *in-vivo* CT image set. This program allows for a labeled contour file output in a variety of formats including binary files for EGSnrc and ASCII text for MCNP. In this program, the CT image data set is displayed in a two-dimensional array and the user can create colored overlays, or contours, to delineate the cortical from the spongiosa regions. An example of this program's user interface can be seen in Fig. 1.

Image Segmentation of Trabecular Spongiosa Regions from MicroCT Scans

In order to determine marrow volume fraction (MVF), trabecular shallow marrow volume fraction (SMVF), and trabecular bone volume fraction (BVF), multiple steps were applied to the microCT data sets. These steps included (1) extraction of a region of interest (ROI) to remove any intrusive cortical bone from the image; (2) applying a median filter to improve the signal-to-noise ratio (SNR); (3) determining a threshold to best classify the voxels as either bone or marrow; and (4) segmentation of the ROI into a binary image based on the threshold gray-level value. The thresholding technique used visual inspection of the image gradient magnitude in order to retrieve sample volume fractions at 30-μm voxel resolution. An example of the user interface used to determine all microstructure data can be seen in Fig. 2.

Comparison of Relative Spongiosa Volumes and Mass Calculations

Relative Spongiosa Volumes

In an effort to quantify how well the 40 year-old male subject matched to average population parameters, relative spongiosa volumes, or the fraction of each bone site's spongiosa volume to the total spongiosa volume, were compared to those of the 66 year-old male SRM. Comparisons were also made to those of 19 other males, which were segmented in a previous study at UF.

Mass Calculations

Mass estimates require both macrostructural volumetric information (obtained from the contours of segmented *ex-vivo* or *in-vivo* CT images), microstructural volume information (obtained from the filtered and segmented microCT spongiosa images), and the volume percentage of hematopoietically active versus inactive bone marrow for each skeletal site (marrow cellularity). It is important to note that marrow cellularity can vary from 0% (no active bone marrow) to 100% (no adipose tissue). For this reason, reference individuals could have a multitude of total active marrow masses, where the potential masses depend upon the marrow cellularity chosen. In an effort to create a SRM that is representative of average parameters, the reported masses utilize average age dependent cellularities provided by ICRP Publication 70 for a 40 year-old male, values of which can be seen in Table 1. Also, ICRU 46 tissue elemental compositions and densities, which can be seen in Table 2, were used for the appropriate skeletal regions.

Trabecular and Cortical Bone Masses in all Skeletal Sites

The mass of the Trabecular Bone Volume (TBV) was calculated as:

$$(m_{TBV})_j = (SV)_j (BVF)_j (\rho_{TBV}) \qquad (3\text{-}1)$$

where SV_j is the spongiosa volume for skeletal site j, BVFj is the Trabecular Bone Volume fractions at skeletal site j, and ρ_{TBV} is the mass densities of the trabeculae bone (1.92 g cm^{-3}).

The mass of the Cortical Bone Volume was calculated as:

$$(m_{CBV})_j = (CBV)_j (\rho_{CBV}) \qquad (3\text{-}2)$$

where CBV_j is the cortical bone volume of skeletal site j, and ρ_{CBV} is the density of cortical bone (1.92 g cm^{-3}).

Marrow Masses in the Cortical Medullary Regions

In the six skeletal long bones' (distal femur, distal fibula, distal humerus, distal radius, distal tibia, and distal ulna) cortical medullary regions, which lack active marrow (except in the upper half of the femur and humerus where CF is 0.25) and trabecular structure (*i.e.* MVF = 1.0), the inactive marrow masses were calculated using the following approach.

Unfortunately, the volume of the Cortical Medullary Inactive Shallow Marrow (CIM_{50}) is not easily attained from the segmented *in-vivo* images. For this reason, an approximation was made in which the cortical medullary region, or shafts, of the long bones were modeled as concentric cylinders. From these approximations, effective radii, which can be seen in Table 3, allowed the volume and mass of CIM_{50} to be calculated as:

$$(V_{CIM_{50}})_j = 1 - \frac{R_{eff.} - 0.005cm}{R_{eff.}} \tag{3-3}$$

$$(m_{CIM_{50}})_j = (V_{CIM_{50}})_j (1 - CF)_j (\rho_{CIM_{50}}) \tag{3-4}$$

where V_{CIM50j} is the volume of Cortical Medullary Inactive Shallow Marrow of skeletal site j, CF_j is the cellularity factor for skeletal site j, and ρ_{CIM50} is the mass density of inactive marrow (0.98 g cm^{-3}).

Marrow Masses in Skeletal Sites Containing Active and Inactive Marrow

For the thirteen skeletal sites that contain a relatively large portion of active marrow (clavicles, cranium and facial bones, proximal femur, proximal humerus, mandible, ribs, scapula, osae coxae, sacrum, lumbar vertebrae, thoracic vertebrae, cervical vertebrae, sternum), as well as the eight skeletal sites that contain minimal, if any, active marrow (distal femur, distal fibula, distal humerus, distal radius, distal tibia, distal ulna, hands, and feet),marrow masses were calculated using the following approach.

The mass of Trabecular Active Marrow (TAM) at skeletal site *j* was calculated as:

$$(m_{TAM})_j = (SV)_j (MVF)_j (CF)_j (\rho_{TAM}), \quad (3\text{-}5)$$

where SV_j is the spongiosa volume for skeletal site j, MVF_j is the marrow volume fraction for skeletal site j, CF_j is the cellularity factor for skeletal site j, and ρ_{TAM} is the mass density of active marrow (1.03 g cm^{-3}).

The mass of the Trabecular Inactive Marrow (TIM) was calculated as:

$$(m_{TIM})_j = (SV)_j (MVF)_j (1-CF)_j (\rho_{TIM}) \quad (3\text{-}6)$$

where SV_j is the spongiosa volume of skeletal site j, MVF_j is the marrow volume fraction of skeletal site j, CF_j is the cellularity factor for skeletal site j, and ρ_{TIM} is the mass density of inactive marrow (0.98 g cm^{-3}).

The mass of the Trabecular Marrow (TM), which includes both active and inactive marrow, was calculated as:

$$(m_{TM})_j = (m_{TAM})_j + (m_{TIM})_j \quad (3\text{-}7)$$

The mass of the Trabecular Shallow Active Marrow (TAM_{50}), the 50 micron thick layer which contains the osteogenic tissues, was calculated as:

$$(m_{TAM_{50}})_j = (SV)_j (SMVF)_j (CF)_j (\rho_{TAM}) \quad (3\text{-}8)$$

where SV_j is the spongiosa volume for skeletal site j, $SMVF_j$ is the shallow marrow volume fraction for skeletal site j, CF_j is the cellularity factor for skeletal site j, and ρ_{TAM} is the mass density of active marrow (1.03 g cm^{-3}).

The mass of the Trabecular Shallow Inactive Marrow (TAM_{50}), was calculated as:

$$(m_{TIM_{50}})_j = (SV)_j (SMVF)_j (1-CF)_j (\rho_{TIM}) \quad (3\text{-}9)$$

where SV_j is the spongiosa volume for skeletal site j, $SMVF_j$ is the shallow marrow volume fraction for skeletal site j, CF_j is the cellularity factor for skeletal site j, and ρ_{TIM} is the mass density of inactive marrow (0.98 g cm^{-3}).

The mass of the Trabecular Shallow Marrow (TM_{50}), which includes both active and inactive marrow, was calculated as:

$$(m_{TM_{50}})_j = (m_{TAM_{50}})_j + (m_{TIM_{50}})_j \quad (3\text{-}10)$$

RESULTS AND DISCUSSION

Relative Spongiosa Volumes

The spongiosa volumes for all skeletal sites of the 40 year-old male can be seen in Table 4. A comparison of the 13 active marrow skeletal sites' spongiosa volumes and relative spongiosa volumes as well as percent difference between the 40 year-old male and 66 year-old male's relative spongiosa volumes can be seen in Table 5. It is interesting to note the relatively large difference between the total skeletal spongiosa volumes of the 40 year-old male and the 66 year-old male; 1803.5 cm^3 and 2413 cm^3, respectively. This large difference, however, is not unexpected due to natural skeletal variations. Also of interest, is that the top three relative spongiosa volumes come from the same sites for both subjects: the osae coxae, proximal femurs, and the thoracic vertebrae. However, after this point some very large discrepancies begin to appear. For example, the percent differences between relative spongiosa volumes range from -51.19% in the cranium (the relative spongiosa volume of the cranium is much higher in the 44 year-old male than the 66 year-old) to 44.32% in the proximal femurs (even though they are the second largest relative contributor to total spongiosa volume, the 66 year-old male has a much

higher relative spongiosa volume than the 44 year-old). These differences show the great variability in skeletal structure and spongiosa volumes that can occur between two individuals.

A comparison of the 13 active marrow skeletal sites' spongiosa volumes and relative spongiosa volumes as well as percent difference between the 40 year-old male and 19 other males' relative spongiosa volumes can be seen in Table 6. Again, large discrepancies can be seen between the relative spongiosa volumes of the 40 year-old male and nineteen other males. For example, percent differences range from -27.0% in the ribs to -40.0% in the mandible. These differences, however, are not to say that the 44 year-old male subject is not a good candidate for a SRM, but rather to highlight the significant errors that can be encountered when trying to utilize a single SRM's skeletal spongiosa volumes (and in turn skeletal masses) to accurately predict skeletal absorbed doses to other non-population average individuals.

In fact, these differences underscore the importance of the studies being performed by the UF BID project to develop scalable SRMs for use in patient/worker-specific cases. One such study, performed by Brindle *et al.,* realized that marrow masses can easily be scaled from an SRM to patient/worker-specific cases by simply multiplying by the ratio of the patient/worker-specific total spongiosa volume to that of the SRMs total spongiosa volume. However, attaining such information on a patient/worker-specific case via manual image segmentation is quite labor intensive. Realizing this, Brindle *et al.* created a database of 20 cadaver (10 male and 10 female) total and relative spongiosa volumes as well as radiographic measurements of such parameters as osae coxae height and width. From this data, linear regression models were created to predict a patient/worker-specific total spongiosa volume from a few simple radiographic measurements. This total spongiosa volume can then be applied to more accurately predict patient/worker-specific active marrow masses and hence skeletal absorbed doses. Pichardo *et al.*, recently

extended this study to a data set of 40 cadavers (20 male and 20 female) and added a gender based component to the regression model to help improve the model's predictive accuracy.

Marrow Volume Fractions

The Marrow and Bone Volume Fractions (MVF and BVF, respectively) for all of the skeletal sites of which microstructural data was collected can be seen in Table 4. It should be noted, that as MVF and BVF are fractions of total spongiosa volumes, they must sum to 1. For this reason, only the MVF were used for comparison purposes between the 40 year-old male and the 66 year-old male.

A comparison of the 40 year-old male and the 66 year-old male's MVFs can be found in Table 7. There seems to be fairly good agreement between the MVFs as 17 of the 22 skeletal sites display relative percent differences of less than 10%. The one extreme difference is for the occipital bone with a relative difference of 512%. This is probably due to were the sample was taken for microstructural imaging. The comparisons are only made between the right side of the 40 year-old male and the 66 year-old male. If an average is taken for the left and right sides of the 66 year-old male the differences shown in Table 7 are drastically reduced. For example, the clavicles yield around a 9.1% relative difference when comparing only the right side. However, if you compare an average, which can be seen in Table 8, of the right and left scapulae's MVF for the 66 year-old male and compare that to the 40 year-old male right scapula MVF, this relative difference is reduced to 0.2%. This may seem insignificant for comparison purposes, as the comparison of the right sides seems more pertinent. However, when calculating the overall marrow volumes and masses comparing the right side of the 44 year-old male to the average of the 66 year-old male holds more weight. That is to say that in the case of the 66 year-old male,

knowledge of the right and left side MVFs was used in conjunction with knowledge of the right and left side spongiosa volumes to explicitly calculate left and right side marrow volumes and masses. In the case of the 40 year-old male, only the right side MVF information is used along with the right and left side spongiosa volumes to calculate marrow volumes and masses. However, using the right side value only in the case of the 40 year-old male can be considered equivalent to using the average MVF for the 66 year-old male when it comes to calculating overall marrow volumes and masses. Hence, the fact that the average of the left and right side MVFs in the 66 year-old male are relatively close to those of the 40 year-old male demonstrates that explicit knowledge of both the left and right side MVFs for the 40 year-old male may not be necessary for accurate assessment of marrow volumes and masses.

Also, this lack of relatively large differences between the 40 year-old male and 66 year-old male, both of whom were considered to have normal skeletal structures (*e.g.* not osteoporetic), is of great importance. Studies by Hasenauer and Shah at UF have shown that microstructural differences do not demonstrate large differences in absorbed fraction calculations. In fact, differences in macrostructure seem to dominate absorbed fraction values at intermediate- to high-energy beta emitters. Therefore, explicit knowledge of each patient/worker's microstructure, which is practically impossible to attain, may not be necessary to accurately predict skeletal doses. These facts demonstrate, at least, that other factors such as spongiosa volumes and cellularity may have a much more direct impact on not only mass estimates but also absorbed fraction estimates. This is not to say, however, that patients/workers who demonstrate abnormal trabecular microstructure should be treated using the same microstructural data as a normal patient. Indeed, reference microstructural data for these

patients/workers should be collected and assessed in order to more accurately estimate skeletal absorbed doses for their specific cases.

Mass Calculations

Trabecular and Cortical Bone Masses in all Skeletal Sites

Masses for trabecular and cortical bone in all skeletal sites can be seen in Table 9. Also, total mineral bone masses, the sum of trabecular and cortical bone, are given. The top three largest trabecular bone mass contributors in descending order are the craniofacial bones (199.6 g), the osae coxae (73.5 g), and the distal femora (68.3 g). The top three largest cortical bone mass contributors in descending order are the craniofacial bones (741.5 g), the ribs (427.6 g), and the osae coxae (269.9 g). Overall, the top three largest mineral bone mass contributors in descending order are the craniofacial bones (941.1 g), the ribs (462.1 g), and the osae coxae (343.4 g). It is interesting to note, that while the ribs do not contribute that much trabecular bone mass, 34.5 g, their high cortical bone mass, 427.6 g, allows them to be one of the top three total mineral bone mass contributors. The ribs, in particular, along with the craniofacial bones represent skeletal sites that have high surface-to-volume ratios. For this reason, these sites' absorbed fractions for intermediate to high beta energies are affected by macrostructural effects.

Comparisons of the trabecular, cortical, and total mineral bone masses between the 40 year-old male and ICRP Reference Man can be found at the bottom of the Table 9. It is evident that the 40 year-old male has much less trabecular, cortical, and total mineral bone mass than ICRP Reference Man with relative ratios of 0.76, 0.82, and 0.81, respectively. This again, however, is not unexpected as skeletal structures and masses can be highly variable. The one important aspect that ensures the 40 year-old male's viability as a SRM is the relative fractions of trabecular and cortical bone mass. ICRP Reference Man displays a fractional 80% cortical

bone mass and 20% trabecular bone mass, while the 40 year-old male displays a fractional 81% cortical bone mass and 19% trabecular bone mass. Even though the 40 year-old male's total mineral bone mass is 81% that of ICRP Reference Man, the overall important factor is that he displays appropriate relative trabecular and cortical bone masses.

Active and Inactive Shallow Marrow Masses in all Skeletal Sites

Masses for active and inactive shallow marrow in all skeletal sites can be seen in Table 10. Also, the total shallow marrow mass, the sum of active and inactive shallow marrow, is given along with the relative percents of active and inactive shallow marrow. The top three largest inactive shallow marrow mass contributors in descending order are the distal femora (33.0 g), the feet (32.5 g), and the craniofacial bones (19.7 g). The top three largest active shallow marrow mass contributors in descending order are the osae coxae (16.0 g), the craniofacial bones (12.7 g), and the thoracic vertebrae (10.8 g). Overall, the top three largest shallow marrow mass contributors in descending order are the distal femora (33.0 g), the craniofacial bones (32.4 g), and the osae coxae (32.4 g).

Direct comparisons of skeletal site specific and total active and inactive shallow marrow between the 40 year-old male and ICRP Reference Man are not possible due to the lack of Reference Man data. Nonetheless, comparisons of the relative active and inactive shallow marrow masses of the 40 year-old male and the relative active and inactive marrow masses of Reference Man are possible. The 40 year-old male again shows good agreement with Reference Man on a relative scale with 69% inactive shallow marrow and 31% active shallow marrow compared to Reference Man's values of 68% inactive marrow and 32% active marrow.

Active and Inactive Marrow Masses in all Skeletal Sites

Masses for active and inactive marrow in all skeletal sites can be seen in Table 11. Also, the total marrow mass, the sum of active and inactive marrow, and relative percents of active and inactive marrow are shown. The top three largest inactive marrow mass contributors in descending order are the distal femora (241.0 g), the feet (237.7 g), and the osae coxae (176.6 g). The top three largest active marrow mass contributors in descending order are the osae coxae (163.1 g), the thoracic vertebrae (132.7 g), and the lumbar vertebrae (112.0 g). Overall, the top three largest marrow mass contributors in descending order are the osae coxae (339.7 g), the distal femora (241.0 g), and the feet (237.7 g).

Comparisons of total and relative active and inactive marrow masses for the 40 year-old male and ICRP Reference Man can be found at the bottom of Table 11. Again, it is evident that the 40 year-old male has much less inactive, active, and total bone marrow mass than ICRP Reference Man with relative ratios of 0.76, 0.70, and 0.74, respectively. This again, however, is due to normal variability in skeletal structure and size. It is important to realize that the aspect that ensures the 40 year-old male's viability as a SRM is the relative fractions of inactive and active marrow mass. ICRP Reference Man displays a fractional 68% inactive marrow mass and 32% active marrow mass, while the 40 year-old male displays a fractional 70% inactive marrow mass and 30% active marrow mass. Even though the 40 year-old male's total marrow mass is 74% that of ICRP Reference Man, the overall important factor is that he displays appropriate relative inactive and active marrow masses. These masses can easily be adjusted by the methods described by Brindle *et al.* and Pichardo *et al.* to match patient/worker specific cases.

CONCLUSION

A complete skeletal mass database is presented for a 40 year-old male for use in internal radiation dosimetry for both radiation protection and radionuclide therapy. The masses reported are representative of those at ICRP 70/89's reference cellularity for a 40 year-old male for comparison purposes. However, the database presented includes all of the necessary data to recalculate patient/worker specific skeletal masses via scaling of spongiosa volumes and/or modification of skeletal site cellularities.

Overall, the 40 year-old male SRM masses presented were approximately 20-30% lower than that of ICRP Reference Man. This, however, does not represent any problems with the viability of the SRM to clinical use, as these differences are not unexpected. The subject chosen simply did not have as massive a skeletal system as Reference Man. Again, simple scaling to patient/worker cases can overcome this factor.

FUTURE WORKS

The *ex-vivo* CT, macrostructure, and microCT, microstructure, images will be combined utilizing PIRT as described by Shah *et al* to calculate Specific Absorbed Fractions (SAFs) for each skeletal site as well as skeletal averaged SAFs at cellularities ranging from 0-100%. These skeletal absorbed dose estimates will complete the detailed skeletal reference model for the UF 40 year-old male.

REFERENCES

Aubin JE, Liu F, Malaval L, Gupta AK 1995 Osteoblast and chondroblast differentiation. Bone **17**(2) 77S-83S

Beddoe AH. The microstructure of mammalian bone in relation to the dosimetry of bone-seeking radionuclides [Thesis]. Leeds, UK: University of Leeds. 165 p; 1976.

Beddoe AH, Darley PJ, and Spiers FW 1976 Measurements of trabecular bone structure in man. Phys. Med. Biol. **21**(4) 589-607

Bianco P, Riminucci M, Gronthos S, Robey PG 2001 Bone marrow stromal stem cells: nature, biology, and potential applications. Stem Cells **19** 180-192

Bouchet LG, Bolch WE, Howell RW, and Rao DV 2000 S values for radionuclides localized within the skeleton. *J. Nucl. Med.* **41**(1) 189-212

Bovée JVMG, Cleton-Jansen AM, Taminiau AHM, Hogendoorn PCW 2005 Emerging pathways in the development of chondrosarcoma of bone and implications for targeted treatment. Lancet Oncology **6** 599-607

Cristy M 1981 Active bone marrow distribution as a function of age in humans. Phys. Med. Biol. **26** 389-400

Cristy M, and Eckerman KF 1987 Specific absorbed fractions of energy at various ages from internal photon sources. Oak Ridge, TN: Oak Ridge National Laboratory. ORNL/TM-8381/Volumes I-VII.

Dominici M, Hofmann TJ, Horwitz EM 2001 Bone marrow mesenchymal cells: biological properties and clinical applications. J Biol Regul Homeost Agents **15** 28-37

Eckerman KF Aspects of the dosimetry of radionuclides within the skeleton with particular emphasis on the active marrow. In: Proceedings of the Fourth International Radiopharmaceutical Dosimetry Symposium. Schlafke-Stelson AT, Watson EE, editors; 1985; Oak Ridge, Tennessee. Oak Ridge Associated Universities; 1985: p 514-534.

Eckerman KF, and Stabin MG 2000 Electron absorbed fractions and dose conversion factors for marrow and bone by skeletal regions. Health Phys. **78**(2) 199-214

Fitzwater JE, Cabaud HE, Farr GH 1976 Irradiation-induced chondrosarcoma. A case report. J Bone & Joint Surgery **58** 1037-1039

Gossner W, Masse R, and Stather JW 2000 Cells at risk for dosimetric modeling relevant to bone tumour induction. *Radiat Prot Dosimetry* **92**(1-3) 209-213

Gossner W 2003 Target cells in internal dosimetry. *Radiat Prot Dosimetry* **105**(1-4) 39-42

ICRP 1979 Limits for intakes of radionuclides by workers. Oxford, UK: International Commission on Radiological Protection. ICRP Publication 30 (Part 1).

ICRP 1995 Basic anatomical and physiological data for use in radiological protection: the skeleton. Oxford, UK: International Commission on Radiological Protection. ICRP Publication 70.

Jokisch DW, Bouchet LG, Patton PW, Rajon DA, and Bolch WE 2001 Beta-particle dosimetry of the trabecular skeleton using Monte Carlo transport within 3D digital images. Med Phys **28**(7) 1505-1518

Lee C, Lee C, Park SH, and Lee JK 2006b Development of the two Korean adult tomographic computational phantoms for organ dosimetry. Med Phys **33**(2) 380-90

Lee C, Lee C, Shah AP, and Bolch WE in press An assessment of bone marrow and bone endosteum dosimetry methods for photon sources. Phys Med Biol

Mechanik N 1926 Studies of the weight of bone marrow in man. Zeitschrift fur die Gest. *Anatomy* **79** 58-99

Nagaoka T, Watanabe S, Sakurai K, Kunieda E, Taki M, and Yamanaka Y 2004 Development of realistic high-resolution whole-body voxel models of Japanese adult males and females of average height and weight, and application of models to radio-frequency electromagnetic-field dosimetry. *Phys Med Biol* **49**(1) 1-15

Parker RG, Berry HC 1976 Late effects of therapeutic irradiation on the skeleton and bone marrow. Cancer **37** 1162-1171

Patton PW, Rajon DA, Shah AP, Jokisch DW, Inglis B, and Bolch WE 2002b Site-specific variability in trabecular bone dosimetry: considerations of energy loss to cortical bone. Med Phys **29**(1) 6-14

Patton PW, Jokisch DW, Rajon DA, Shah AP, Myers SL, and Bolch WE 2002a Skeletal dosimetry via NMR microscopy: investigations of sample reproducibility and signal source. Health Phys **82**(3) 316-326

Peimer CA, Yuan HA, Sagerman RH 1976 Postirradiation chondrosarcoma. A care report. J Bone & Joint Surgery **58** 1033-1036

Petoussi-Henss N, Zankl M, Fill U and Regulla D 2002 The GSF family of voxel phantoms *Phys. Med. Biol.* **47** 89-106

Piegl L 1991 On NURBS: A survey. IEEE Computer Graphics and Applications **11** 55-71

Rajon D, Pichardo J, Brindle J, Kielar K, Jokisch D, Patton P, and Bolch W 2006 Image segmentation of trabecular spongiosa by visual inspection of the gradient magnitude. Phys Med Biol **51**(16) 4447-67

Roschger P, Grabner BM, Rinnerthaler S, Tesch W, Kneissel M, Berzlanovich A, Klaushofer K, Fratzl P 2001 Structural development of the mineralized tissue in the human L4 vertebral body. J Structural Biology **136** 126-136

Shagina NB, Degteva MO, Tolstykh EI, Anspaugh LR, and Napier BA 2005 Dosimetric Models for Strontium in the Human Bone: A Review of Available Data and Recommendations on Needed Research. *Further Studies on Uncertainty and Validation of Doses in the Techa River Dosimetry System*.: US-Russian Coordinating Committee on Radiation Effects Research - Project 1.1.

Shah AP, Jokisch D, Watchman C, Rajon D, Patton P, and Bolch W 2005a Chord-based versus voxel-based methods of electron transport in the skeletal tissues. Med Phys **32**(10) 3151-3159

Shah AP, Rajon D, Jokisch D, Patton P, and Bolch W 2005b A comparison of skeletal chord-length distributions in the adult male. Health Phys **89**(3) 199-215

Shah AP, Rajon D, Patton P, Jokisch D, and Bolch W 2005c Accounting for beta-particle energy loss to cortical bone via Paired-Image Radiation Transport (*PIRT*). Med Phys **32**(5) 1354-1366

Shah AP, Patton PW, Rajon DA, and Bolch WE 2003 Adipocyte spatial distributions in bone marrow: Implications for skeletal dosimetry models. J Nucl Med **44**(5) 774-783

Snyder WS, Ford MR, Warner GG, and Watson SB 1975 "S," absorbed dose per unit cumulated activity for selected radionuclides and organs. New York, NY: Society of Nuclear Medicine. MIRD Pamphlet No. 11.

Stabin MG, and Siegel JA 2003 Physical models and dose factors for use in internal dose assessment. Health Phys **85**(3) 294-310

Tanaka C, and Kawamura H 1996 Anatomical and physiological characteristics for Asian reference man. National Institute of Radiological Sciences. NIRS-M-115.

Watchman CJ, Hasenauer D, Bolch WE 2007 in press Derivation of Site-Specific Skeletal Masses within the Current ICRP Age Series. *Phys. Med. Biol.*

Whitwell JR. Theoretical investigations of energy loss by ionizing particles in bone [Thesis]. Leeds, UK: University of Leeds. 268 p; 1973.

Whitwell JR, and Spiers FW 1976 Calculated beta-ray dose factors for trabecular bone. Phys. Med. Biol. **21**(1) 16-38

Zankl M, and Wittmann A 2001 The adult male voxel model "Golem" segmented from whole-body CT patient data. *Radiation and Environmental Biophysics* **40**(2) 153-162

Zubal IG, Harrell CR, Smith EO, Rattner Z, Gindi G, and Hoffer PB 1994 Computerized three-dimensional segmented human anatomy. *Med Phys* **21**(2) 299-302

Table 1. ICRP 70 marrow cellularities for a 40 year-old male. Marrow cellularity is the fraction of active bone marrow within the total marrow volume.

Skeletal Sites	Cellularity *(% of MV)*
Craniofacial Bones	38%
Mandible	38%
Scapulae	38%
Clavicles	33%
Sternum	70%
Ribs	70%
Cervical Vertebra	70%
Thoracic Vertebra	70%
Lumbar Vertebra	70%
Sacrum	70%
Os Coxae	48%
Humeri, proximal	25%
Femora, proximal	25%
Humeri, shaft (upper 1/2)	25%
Humeri, shaft (lower 1/2)	0%
Humeri, distal	0%
Ulnae, proximal	0%
Ulnae, shaft	0%
Ulnae, distal	0%
Radii, proximal	0%
Radii, shaft	0%
Radii, distal	0%
Hands	0%
Femora, shaft (upper 1/2)	25%
Femora, shaft (lower 1/2)	0%
Femora, distal	0%
Tibiae, proximal	0%
Tibiae, shaft	0%
Tibiae, distal	0%
Fibulae, proximal	0%
Fibulae, shaft	0%
Fibulae, distal	0%
Feet	0%

Table 2. ICRU 46 skeletal tissue elemental compositions and mass densities used to calculate marrow and bone masses as well as for transport in PIRT.

Tissue	H	C	N	O	Trace	Mass Density ($g\ cm^{-3}$)
Red Bone Marrow (RBM)	10.5	41.4	3.4	43.9	0.1 P, 0.2 S, 0.2 Cl, 0.2 K, 0.1 Fe	1.03
Yellow Bone Marrow (YBM)	11.5	64.4	0.7	23.1	0.1 Na, 0.1 S, 0.1 Cl	0.98
Trabecular Shallow Active Marrow (TIM_{50})	10.5	25.6	2.7	60.2	0.1 Na, 0.2 P, 0.3 S, 0.2 Cl, 0.2 K	1.03
Trabecular Bone Volume (TBV)	3.4	15.5	4.2	43.5	0.1 Na, 0.2 Mg, 10.3 P, 0.3 S, 22.5 Ca	1.92
Cortical Bone Volume (CBV)	3.4	15.5	4.2	43.5	0.1 Na, 0.2 Mg, 10.3 P, 0.3 S, 22.5 Ca	1.92
Surrounding tissues	10.5	25.6	2.7	60.2	0.1 Na, 0.2 P, 0.3 S, 0.2 Cl, 0.2 K	1.03

Table 3. Values of the shaft marrow volume, cortical bone volume, and shaft length were obtained from segmentation and measurement of the *in-vivo* images of the long bones. The effective radii were calculated using the principle of concentric cylinders. These radii were then used to calculate the shallow marrow volume and shallow marrow masses for the cortical medullary regions of the long bones.

	Shaft Marrow Volume (cm^3)	Cortical Bone Volume (cm^3)	Shaft Length (cm)	Effective Radius (cm)			
				Shallow Marrow	Spongiosa	Cortical Shell	Total
Humerus	22.1	38.7	22.3	0.556	0.561	0.370	0.931
Radius	5.2	10.5	19.6	0.287	0.292	0.214	0.506
Ulna	3.2	13.9	23.7	0.204	0.209	0.271	0.480
Femur	43.7	35.1	20.8	0.812	0.817	0.280	1.097
Tibia	68.2	63.0	25.4	0.919	0.924	0.358	1.282
Fibula	7.9	17.8	26.7	0.302	0.307	0.247	0.554

Table 4. Spongiosa volumes, Marrow Volume Fractions, and Bone Volume Fractions for all skeletal sites of the 40 year-old male.

Skeletal Sites	Spongiosa Volume (cm^3)		Trabecular Spongiosa Regions: Bone Volume Fraction (BVF)	Trabecular Spongiosa Regions: Marrow Volume Fraction (MVF)
Craniofacial Bones[d]		**185.48**		
Frontal	40.34		0.445	0.555
Occipital	54.94		0.912	0.088
Right Parietal / Temporal	41.09		0.394	0.606
Left Parietal / Temporal	41.09		-	-
Sphenoid, Ethmoid, Facial[e]	8.01		-	-
Mandible		**26.30**	0.089	0.911
Scapulae		**108.22**		
Right	55.69		0.153	0.847
Left	52.53		-	0.847
Clavicles		**34.01**		
Right	17.00		0.116	0.884
Left	17.01		-	-
Sternum		**34.86**	0.082	0.918
Ribs[d]		**148.60**		
Ribs 1-4 (Right)	22.25		0.103	0.897
Ribs 5-8 (Right)	35.40		0.142	0.858
Ribs 9-12 (Right)	16.65		0.101	0.899
Ribs 1-4 (Left)	22.25		-	-
Ribs 5-8 (Left)	35.40		-	-
Ribs 9-12 (Left)	16.65		-	-
Cervical Vertebra		**45.97**		
C1 - C3	20.51		0.159	0.841
C4 - C7	25.46		0.194	0.806
Thoracic Vertebra		**203.15**		
T1 - T4	49.93		0.132	0.868
T5 - T8	63.64		0.042	0.959
T9 - T12	89.58		0.111	0.889
Lumbar Vertebra		**173.33**		
L1 - L3	98.87		0.114	0.887
L4- L5	74.46		0.091	0.909
Sacrum		**132.19**	0.118	0.882
Os Coxae		**384.93**		
Ilium	-		0.100	0.901
Ischium	-		-	-
Pubis	-		-	-
Humeri, proximal		**109.03**	-	
Right	52.93		0.096	0.904
Left	56.10		-	-
Femora, proximal		**223.07**	-	
Right Head	48.36		0.229	0.771
Right Neck	67.82		0.103	0.897
Left Head	50.98		-	-
Left Neck	55.92		-	-
Totals:		*1809.14*		

	Spongiosa Volume (cm^3)	Bone Volume Fraction (BVF)	Marrow Volume Fraction (MVF)
Humeri, shaft	**44.12**	-	-
Humeri, distal	**46.24**	0.151	0.849
Ulnae, proximal	**29.94**	0.161	0.839
Ulnae, shaft	**10.46**	-	-
Ulnae, distal	**4.15**	0.139	0.861
Radii, proximal	**12.53**	0.089	0.911
Radii, shaft	**6.48**	-	-
Radii, distal	**17.22**	0.116	0.884
Hands	**44.29**	-	-
Femora, shaft	**87.31**	-	-
Femora, distal	**287.98**	0.146	0.854
Tibiae, proximal	**213.66**	0.115	0.885
Tibiae, shaft	**136.42**	-	-
Tibiae, distal	**87.04**	0.125	0.875
Fibulae, proximal	**16.06**	0.078	0.922
Fibulae, shaft	**15.82**	-	-
Fibulae, distal	**13.94**	0.147	0.853
Feet	**284.04**	-	-
Totals:	*1357.68*		
Total for UF Model:	*3166.82*		

Table 5. Relative spongiosa volumes for all 13 active marrow containing skeletal sites for the 40 year-old male and 66 year-old male and comparison.

Skeletal Sites	Relatvie Spongiosa Volumes		Ratio	
	40 Year-old Male	66 Year-old Male	(40 YOM / 66 YOM)	% Difference
Pelvis				
- Os Coxae	21.34%	23.14%	0.922	8.41%
- Sacrum	7.33%	6.61%	1.109	-9.83%
Vertebrae				
- Cervical	2.55%	2.37%	1.074	-6.86%
- Thoracic	11.26%	12.10%	0.931	7.45%
- Lumbar	9.61%	9.83%	0.977	2.31%
Skull				
- Cranium	9.97%	4.87%	2.049	-51.19%
- Mandible	1.46%	0.74%	1.966	-49.14%
Ribs	8.24%	8.06%	1.023	-2.23%
Clavicles	1.89%	1.07%	1.757	-43.09%
Scapulae	6.00%	4.78%	1.256	-20.38%
Sternum	1.93%	1.40%	1.376	-27.32%
Femora, proximal	12.37%	17.85%	0.693	44.32%
Humeri, proximal	6.05%	7.17%	0.843	18.65%

Table 6. Relative spongiosa volume for all 13 active marrow containing skeletal sites for the 40 year-old male and nineteen other males from studies by Brindle *et al.* and Pichardo *et al.* and comparison.

Skeletal Sites	Relatvie Spongiosa Volumes		Ratio	
	40 Year-old Male	Nineteen Other Males	(40 YOM / 19 OM)	% Difference
Pelvis				
- Os Coxae	21.34%	22.9%	0.932	7.3%
- Sacrum	7.33%	6.8%	1.071	-6.6%
Vertebrae				
- Cervical	2.55%	2.5%	1.018	-1.8%
- Thoracic	11.26%	12.0%	0.937	6.8%
- Lumbar	9.61%	10.1%	0.950	5.3%
Skull				
- Cranium	9.97%	7.0%	1.432	-30.2%
- Mandible	1.46%	0.9%	1.667	-40.0%
Ribs	8.24%	10.5%	0.787	27.0%
Clavicles	1.89%	1.6%	1.165	-14.2%
Scapulae	6.00%	4.6%	1.305	-23.4%
Sternum	1.93%	2.2%	0.875	14.3%
Femora, proximal	12.37%	13.0%	0.952	5.0%
Humeri, proximal	6.05%	5.9%	1.027	-2.6%

Table 7. Marrow Volume Fractions sampled from all13 active marrow containing skeletal sites for the 40 year-old male and 66 year-old male and comparison of the right side Marrow Volume Fractions.

Skeletal Sites	*Trabecular Spongiosa Regions Marrow Volume Fraction (MVF)* 44 Year-Old Male	64 Year-Old Male	Ratio (44 YOM / 66 YOM)	Relative % Difference
Cranium				
Frontal	0.555	0.596	0.931	7.4%
Occipital	0.0884	0.541	0.163	512.0%
Right Parietal	0.6062	0.643	0.943	6.1%
Left Parietal	-	0.656	-	-
Mandible	0.9114	0.835	1.091	-8.4%
Scapulae				
Right	0.8471	0.819	1.034	-3.3%
Left	-	0.877	_	-
Clavicles				
Right	0.8844	0.804	1.100	-9.1%
Left	-	0.962	_	-
Sternum	0.9181	0.909	1.010	-1.0%
Ribs				
Upper Right	0.8974	0.863	1.040	-3.8%
Middle Right	0.858	0.941	0.912	9.7%
Lower Right	0.8989	0.914	0.983	1.7%
Upper Left	-	0.929	-	-
Middle Left	-	0.929	-	-
Lower Left	-	0.942	-	-
Cervical Vertebra				
C3	0.8411	0.894	0.941	6.3%
C6	0.8059	0.859	0.938	6.6%
Thoracic Vertebra				
T3	0.868	0.9	0.964	3.7%
T6	0.9585	0.924	1.037	-3.6%
T11	0.8892	0.762	1.167	-14.3%
Lumbar Vertebra				
L2	0.8865	0.92	0.964	3.8%
L4	0.9092	0.771	1.179	-15.2%
Sacrum	0.8822	0.876	1.007	-0.7%
Os Coxae				
Ilium	0.9005	0.887	1.015	-1.5%
Ischium	-	0.923	-	-
Pubis	-	0.884	-	-
Humeri, proximal				
Right	0.904	0.837	1.080	-7.4%
Left	-	0.779	-	-
Femora, proximal				
Right Head	0.7709	0.647	1.191	-16.1%
Right Neck	0.8966	0.896	1.001	-0.1%
Left Head	-	0.707	-	-
Left Neck	-	0.884	-	-

Table 8. Marrow Volume Fractions sampled from all13 active marrow containing skeletal sites for the 40 year-old male and 66 year-old male and comparison of the average Marrow Volume Fractions.

Skeletal Sites	*Trabecular Spongiosa Regions Average Marrow Volume Fraction (MVF)* 44 Year-Old Male	64 Year-Old Male	Ratio (44 YOM / 66 YOM)	Relative % Difference
Cranium				
Frontal	0.555	0.596	0.931	7.4%
Occipital	0.0884	0.541	0.163	512.0%
Parietal	0.6062	0.6495	0.933	7.1%
Mandible	0.9114	0.835	1.091	-8.4%
Scapulae	0.8471	0.848	0.999	0.1%
Clavicles	0.8844	0.883	1.002	-0.2%
Sternum	0.9181	0.909	1.010	-1.0%
Ribs				
Upper	0.8974	0.896	1.002	-0.2%
Middle	0.858	0.935	0.918	9.0%
Lower	0.8989	0.928	0.969	3.2%
Cervical Vertebra				
C3	0.8411	0.894	0.941	6.3%
C6	0.8059	0.859	0.938	6.6%
Thoracic Vertebra				
T3	0.868	0.9	0.964	3.7%
T6	0.9585	0.924	1.037	-3.6%
T11	0.8892	0.762	1.167	-14.3%
Lumbar Vertebra				
L2	0.8865	0.92	0.964	3.8%
L4	0.9092	0.771	1.179	-15.2%
Sacrum	0.8822	0.876	1.007	-0.7%
Os Coxae	0.9005	0.898	1.003	-0.3%
Humeri, proximal	0.904	0.808	1.119	-10.6%
Femora, proximal				
Head	0.7709	0.677	1.139	-12.2%
Neck	0.8966	0.89	1.007	-0.7%

Table 9. Trabecular, cortical, and total mineral bone masses for all skeletal sites of the 40 year-old male and comparison with ICRP Reference Man.

Skeletal Sites	Trabecular Bone *Mass (g)*	Cortical Bone Mass (g)	Total Bone *Mass (g)*
Craniofacial Bones [d]	199.6	741.5	941.1
Mandible	4.5	54.1	58.5
Scapulae	31.8	121.8	153.6
Clavicles	7.5	45.3	52.8
Sternum	5.5	32.2	37.7
Ribs	34.5	427.6	462.1
Cervical Vertebra	15.7	78.5	94.3
Thoracic Vertebra	36.8	175.0	211.8
Lumbar Vertebra	34.5	122.9	157.4
Sacrum	29.9	98.8	128.7
Os Coxae	73.5	269.9	343.4
Humeri, proximal	20.1	38.8	58.9
Femora, proximal	68.3	75.5	143.8
Totals:	*562.3*	*2282.0*	*2844.2*
	Trabecular Bone *Mass* (g)	**Cortical Bone** *Mass* (g)	**Total Bone** *Mass* (g)
Humeri, shaft	-	148.7	148.7
Humeri, distal	13.4	43.2	56.7
Ulnae, proximal	9.3	28.8	38.0
Ulnae, shaft	-	53.2	53.2
Ulnae, distal	1.1	3.1	4.2
Radii, proximal	2.1	10.8	13.0
Radii, shaft	-	40.2	40.2
Radii, distal	3.8	14.6	18.4
Hands	12.9	131.7	144.6
Femora, shaft	-	134.9	134.9
Femora, distal	80.8	71.7	152.5
Tibiae, proximal	47.3	48.5	95.9
Tibiae, shaft	-	241.9	241.9
Tibiae, distal	20.9	30.2	51.1
Fibulae, proximal	2.4	8.7	11.1
Fibulae, shaft	-	68.4	68.4
Fibulae, distal	3.9	10.6	14.5
Feet	79.7	248.0	327.7
Totals:	*277.8*	*1337.3*	*1615.0*
Totals for UF Model:	**840**	**3619**	**4459**
% mineral bone	19%	81%	-
ICRP 89 Ref Male:	**1100**	**4400**	**5500**
% mineral bone	20%	80%	-
Ratio (UF / ICRP):	**0.76**	**0.82**	**0.81**

Table 10. Inactive, active, and total shallow marrow masses for all skeletal sites of the 40 year-old male.

Skeletal Sites	Shallow Inactive Marrow *Mass (g)*	Shallow Active Marrow *Mass (g)*	Shallow Total Marrow *Mass (g)*
Craniofacial Bones	19.7	12.7	32.4
Mandible	1.0	0.6	1.6
Scapulae	5.5	3.5	9.0
Clavicles	1.6	0.8	2.4
Sternum	0.8	1.9	2.6
Ribs	4.0	9.9	13.9
Cervical Vertebra	1.8	4.4	6.2
Thoracic Vertebra	4.4	10.8	15.2
Lumbar Vertebra	4.0	9.8	13.8
Sacrum	3.2	7.8	11.0
Os Coxae	16.5	16.0	32.4
Humeri, proximal	4.7	1.6	6.3
Femora, proximal	17.0	5.9	22.9
Totals:	*84.1*	*85.8*	*169.9*

	Shallow Inactive Marrow *Mass (g)*	Shallow Active Marrow *Mass (g)*	Shallow Total Marrow *Mass (g)*
Humeri, distal	4.3	0.0	4.3
Ulnae, proximal	2.6	0.0	2.6
Ulnae, distal	0.5	0.0	0.5
Radii, proximal	0.6	0.0	0.6
Radii, distal	1.6	0.0	1.6
Hands	4.1	0.0	4.1
Femora, distal	33.0	0.0	33.0
Tibiae, proximal	15.9	0.0	15.9
Tibiae, distal	5.8	0.0	5.8
Fibulae, proximal	0.9	0.0	0.9
Fibulae, distal	1.5	0.0	1.5
Feet	32.5	0.0	32.5
Totals:	*103.3*	*0.0*	*103.3*
Humeri, shaft (upper 1/2)	0.3	0.1	0.3
Humeri, shaft (lower 1/2)	0.4	0.0	0.4
Ulnae, shaft	0.3	0.0	0.3
Radii, shaft	0.3	0.0	0.3
Femora, shaft (upper 1/2)	0.4	0.1	0.4
Femora, shaft (lower 1/2)	0.5	0.0	0.5
Tibiae, shaft	1.4	0.0	1.4
Fibulae, shaft	0.5	0.0	0.5
Totals:	*4.2*	*0.2*	*4.2*
Totals for UF Model:	**191.5**	**86.0**	**277.4**
% total shallow marrow:	69%	*31%*	

Table 11. Inactive, active, and total marrow masses for all skeletal sites of the 40 year-old male and comparison with ICRP Reference Man.

Skeletal Sites	Inactive Marrow *Mass (g)*	Active Marrow *Mass (g)*	Total Marrow *Mass (g)*
Craniofacial Bones	49.5	31.9	81.4
Mandible	14.6	9.4	23.9
Scapulae	55.7	35.9	91.6
Clavicles	19.7	10.2	30.0
Sternum	9.4	23.1	32.5
Ribs	38.4	94.2	132.6
Cervical Vertebra	11.1	27.2	38.3
Thoracic Vertebra	54.1	132.7	186.8
Lumbar Vertebra	45.7	112.0	157.7
Sacrum	34.3	84.1	118.4
Os Coxae	176.6	163.1	339.7
Humeri, proximal	72.4	25.4	97.8
Femora, proximal	137.8	48.3	186.1
Totals:	*719.4*	*797.3*	*1516.8*
	Inactive Marrow *Mass (g)*	**Active Marrow** *Mass (g)*	**Total Marrow** *Mass (g)*
Humeri, shaft (upper 1/2)	16.2	5.7	21.9
Humeri, shaft (lower 1/2)	21.6	0.0	21.6
Humeri, distal	38.0	0.0	38.0
Ulnae, proximal	24.6	0.0	24.6
Ulnae, shaft	10.3	0.0	10.3
Ulnae, distal	3.5	0.0	3.5
Radii, proximal	11.2	0.0	11.2
Radii, shaft	6.3	0.0	6.3
Radii, distal	14.9	0.0	14.9
Hands	36.8	0.0	36.8
Femora, shaft (upper 1/2)	32.1	11.2	43.3
Femora, shaft (lower 1/2)	42.8	0.0	42.8
Femora, distal	241.0	0.0	241.0
Tibiae, proximal	185.2	0.0	185.2
Tibiae, shaft	133.7	0.0	133.7
Tibiae, distal	74.6	0.0	74.6
Fibulae, proximal	14.5	0.0	14.5
Fibulae, shaft	15.5	0.0	15.5
Fibulae, distal	11.7	0.0	11.7
Feet	237.7	0.0	237.7
Totals:	*1172.2*	*16.9*	*1189.1*
Totals for UF Model:	**1891.62**	**814.26**	**2705.9**
% total marrow	0.70	0.30	-
ICRP 89 Ref Male:	**2480.00**	**1170.00**	**3650.0**
% total marrow	0.68	0.32	-
Ratio (UF / ICRP):	**0.76**	**0.70**	**0.74**

Fig. 1. CT Contours graphic user interface. An *ex-vivo* CT image is overlaid with tag values to distinguish soft tissue, cortical bone, and spongiosa volumes.

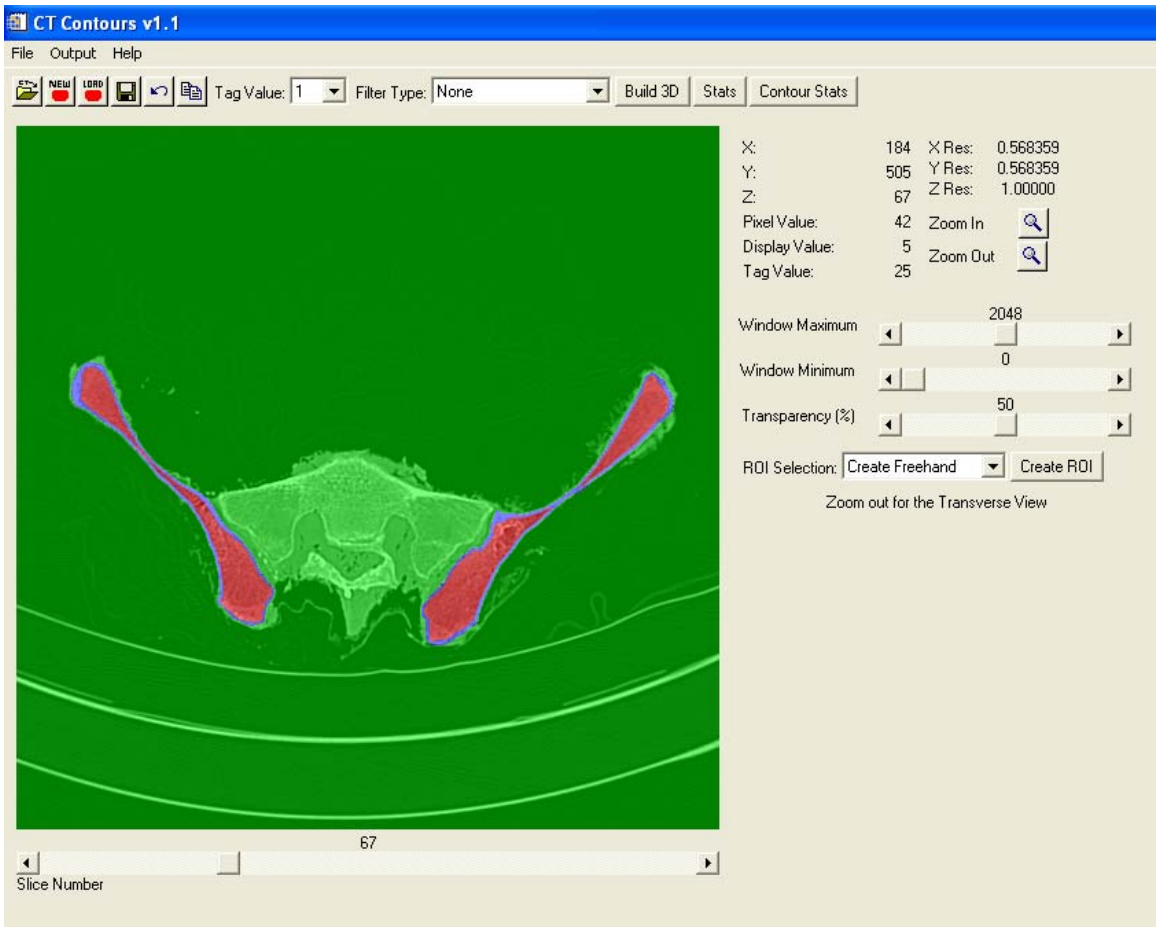

Fig. 2. BID graphic user interface. This program is used extract a region of interest from the trabecular spongiosa microCT image as well as to determine the appropriate threshold value and segment the image to contain only marrow (black) and trabecular bone (green).

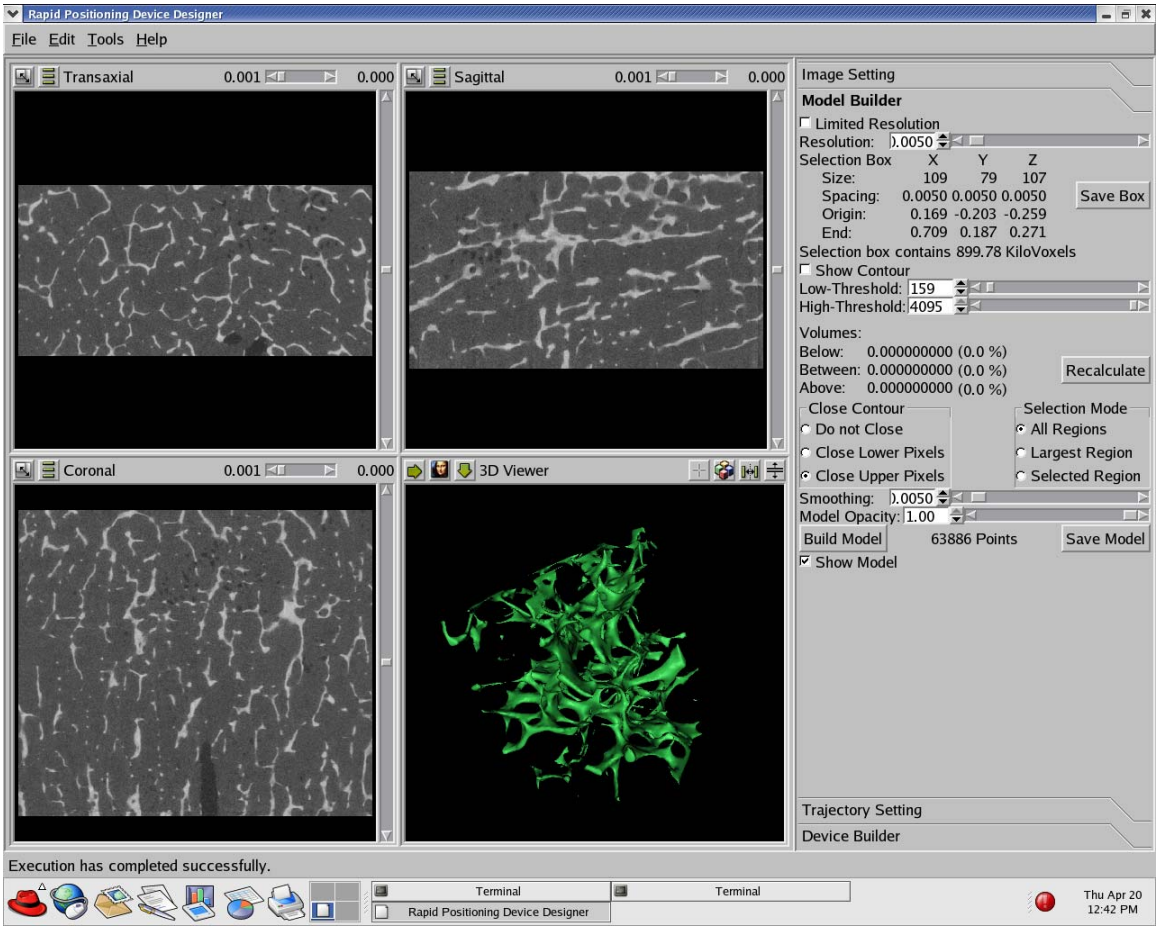

Appendix B

A Skeletal Reference Dosimetry Model for the 15-Year Adolescent

CHAPTER 4
AN IMAGE-BASED SKELETAL TISSUE AND DOSIMETRY MODEL FOR THE ICRP REFERENCE 15-YEAR MALE AND FEMALE

Introduction

The goals of this chapter were to (1) develop and apply a methodology for the sub-segmentation of the skeleton into all skeletal tissues by bone site within the hybrid computational 15 year-old male and female phantoms analogous to Chapter 2, and (2) implement the dosimetry methods utilized in Chapter 3 for dose assessment to active marrow and endosteal tissues for the 15 year-old female phantom of Lee *et al.* (2008). Detailed methods on the development of the homogeneous 15-year male and female hybrid phantoms are discussed in Lee *et al.* (2008). The methodology presented here targets total skeletal tissue masses for the reference 15 year-old male and female as defined in ICRP Publication 89 (ICRP 2002). However, the study further distributes those masses in a bone-specific manner based upon ICRP reference data, ex-vivo CT data from an 18 year-old male cadaver, microCT-based images of the 18 year-old male spongiosa from cadaver specimen collection, and the individual bone volumes defined within the UF hybrid 15-year male and female phantoms (Lee *et al.* 2008). The tissue masses presented here are thus offered as a revision to those given previously by Cristy (1981) for the 15-year active marrow distribution, and by Watchman *et al.* (2007) for all skeletal tissues. Electron dosimetry results are based on a large sample selection of 3D image data from an 18 year-old cadaver instead of limited 2D chord-distributions from 1.7-year and 9-year children. A glossary of acronyms for both tissue regions of the skeleton and model parameters used in this study is included at the beginning of this dissertation.

Materials and Methods

Cadaver Selection and Sample Acquisition

The 66-year adult cadaver in Shah *et al.* (2005) was selected based on criteria including BMI 18.5 – 25 kg m^{-2}(CDC recommended healthy range), and cause of death that would preclude any significant skeletal deterioration. However, obtaining samples from children and young adults is rare due to limited availability and the sensitive nature in getting permission to acquire bone samples. After receiving IRB approval, the Florida State Anatomical Board and the University of Florida Shands Hospital was able to provide us with an 18 year-old male cadaver to be used as a surrogate for the 15 year-old male and female skeletal modeling in this study. Unlike the selection criteria for the adult, limited cadaver availability for this age group restricts the criteria. It was estimated that this cadaver was 180 lbs. (81.6 kg) in weight and 72 inches (1.83 m) in height, which is approximately a BMI of 24.4 kg m^{-2}. It should be noted that the cause of death was due to complications from graft versys host disease (GVHD). It should also be noted that this individual was given total body irradiation (TBI) during the treatment of his leukemia, external beam treatment to the sternum, and a bone marrow transplant. The literature suggests that suppression of bone growth in children, along with bone marrow suppression could occur with TBI (Parker and Berry 1976). However, the skeleton is considered to be mature by 18 years of age. Therefore, it is assumed that significant changes in the trabecular microarchitecture from TBI are negligible for the dosimetry assessment. Bone marrow changes are taken into account during transport.

In-vivo cadaver imaging, cadaver harvest, and ex-vivo bone sample imaging

The cadaver was scanned, in-vivo, with the Siemens Sensation 16 unit in the Department of Radiology at UF Shands Hospital prior to the bone harvest. The cadaver was scanned at 1 mm slice thickness and reconstructed using both a bone filter and soft tissue filter. The in-plane

resolution was selected as to maximize the resolution by minimizing the field-of-view (FOV) around the cadaver. 120 kVp and 200-250 mA were chosen as the scanning protocols in order to maximize tissue contrast. The head and extremities were scanned separately for highest contrast and spatial resolution.

The bone tissue specimen collection from the 18 year-old male cadaver was performed on December 9, 2005. Representative samples from the entire skeleton were acquired during the bone harvest to further develop information on the relative cortical and spongiosa percentages, as well as 3D microstructure information of 18-year trabecular spongiosa for future transport. The following bone sites were acquired from the 18 year-old male: cranium, mandible, whole spine, sacrum, os coxae, mandible, right scapula, right clavicle, os coxae, sacrum, sternum, rib samples from the 1^{st}, 6^{th} and 12^{th} right ribs, right proximal humerus, right proximal radius, right proximal ulna, right distal humerus, right distal radius, right distal ulna, right proximal femur, right proximal tibia, right proximal fibula, right distal femur, right distal tibia, and right distal fibula. These bone samples were then scanned, ex-vivo (outside the cadaver), in the same manner as the in-vivo imaging. Again, maximizing the in-plane resolution with the smallest scanning FOV, 1 mm slice thickness axial resolution, and both bone and soft tissue filter reconstruction, in order to obtain the best contrast resolution and spatial resolution necessary for accurate cortical bone and spongiosa segmentation.

Spongiosa image analysis using microCT

As done in Chapters 2 and 3 for the newborn, bone specimens from the 18 year-old were subjected to microCT imaging (Scanco Medical AG, Brüttisellen, Switzerland) at 30 μm isotropic resolution. Prior to sample shipment, each bone was cut using a bone saw, and cored with a drill press in order to (1) maintain the microCT size restrictions of the bore (4 cm height

and 3.8 cm in-plane) and (2) obtain a large, representative sample of spongiosa. The resulting images were converted to binary format using techniques previously given in Rajon *et al.* (2006). Cored cranial samples from the parietal bone, occipital bone and frontal bone, cored vertebral samples from C_3, C_6, T_1, T_3, T_6, T_9, T_{12} and L_1-L_5, manubrium cut from the sternum, cored samples from the proximal humerus and femur, cut samples from the distal femur and humerus, cut samples from both the proximal and distal fibula, ulna, radius and tibia, cored sample from the subscapular fossa region of the right scapula, cut sample of the sternal end to shaft region of the right clavicle, cored sample from the mandible body, cut sample of the shaft region in right rib-1, rib-6 and rib-12, cored sample of the right ilium from the os coxae, and cored sample from the medial sacral region were imaged.

Segmentation of Skeletal Tissues from the 18-Year Male Cadaver CT and microCT Data

As previously mentioned, the 15-year male and female skeleton developed in Lee *et al.* (2008) contain only homogeneous bone (no delineation between cortical bone and spongiosa). Similar to Chapter 2 for the newborn, skeletal tissue volume fractions are needed to partition the 15-year male and female homogeneous skeletons into detailed skeletal models. The *CBVF* and *SVF* were determined from manual image segmentation in *3D-DOCTOR*^{TM} (Able Software Corp., Lexington, MA) of the 18-year male ex-vivo scans. The *MVF* and *TBVF*, with both in reference to the total volume of spongiosa (homogeneous bone exclusive of its cortical bone cortex), were determined based on image segmentation described in Chapter 2. The *SMVF* – was derived though an image analysis software using *EGSnrc*, which is described in detail in Chapter 2. As previously discussed, the *SMVF* defines the fraction of spongiosa occupied by marrow space within 50-μm of the bone trabeculae surfaces. This latter parameter is used to define the surrogate tissue region for the osteoprogenitor cells.

Skeletal Tissue Derivations for the UF 15-Year Male and Female Hybrid Phantoms

Calculations of reference 15-year male and female site-specific skeletal tissue masses, elemental compositions, and mass densities were performed using data from three sources. The first were reference data given in ICRP Publications 70 (ICRP 1995) and 89 (ICRP 2002), ICRU Publication 44 (ICRU 1989), and ICRU Publication 46 (ICRU 1992). The second were CT and microCT images from skeletal specimens acquired from the 18-year male cadaver. The third were homogeneous skeleton volumes defined within the UF 15-year male and female hybrid phantoms. The following is a list of overall assumptions and assumed bone surrogates made in this study:

1) Shafts of long bones have a *MVF* of 1.0 (no trabecular structures within the medullary cavities);

2) Rib *MVF* is assigned to the wrists/hands, patellae, and ankles/feet;

3) *SVF* and *CBVF* for the patella, wrist/hands, ankles/feet were determined by the in-vivo segmentation of the 18-year male cadaver;

4) Cellularity factors for the upper and lower half of the15-year male and female femur and humerus were partitioned in a gradient style into proximal, upper shaft, lower shaft, and distal, such that the linear average between proximal/upper shaft, and lower shaft/distal targeted the ICRP 70 reference cellularity for upper half and lower half (e.g. 55% proximal, 35% upper shaft, 20% lower shaft, and 0% distal);

5) Medullary marrow volume fraction values for the upper shaft and lower shaft are assumed to be identical to that for whole segmented shaft from the in-vivo scans;

6) All volume fractions obtained by image segmentation are assumed to contain *MST* because these tissues can not be realized independently in the image.

The following subsections are shortened due to the previous detailed analysis of skeletal tissue derivations in Chapter 2. Also, it should be noted that the tissue derivations below are considered the first iteration. Once this has been completed using the original image-based data, a second iteration must be done to match ICRP 89 total mineral bone 3700 g for the 15-year female and 4050 g for the 15-year male, excluding *MST*. This mineral bone matching is done by uniformly increasing or decreasing the original image-based *CBVF* from the 18-year male cadaver segmentation.

Miscellaneous skeletal tissues

As defined in ICRP Publication 89, miscellaneous skeletal tissues (*MST*) consist of blood vessels and periosteum, but exclude periarticular tissue and blood. Limitations on image contrast and spatial resolution do not allow for any visual delineation of miscellaneous skeletal tissues in the 18 year-old male CT dataset. Consequently, the reference volume of 15-year male and female *MST* given in Table 9.2.15 of ICRP Publication 89 (male – 150.49 cm^3 or 155 g / 1.03 g cm^{-1}, female – 142.16 cm^3 or 145 g / 1.02 g cm^{-1}) was first distributed by bone site based solely on fractional homogeneous skeletal volumes (male – 4943.17 cm^3, female – 4543.68 cm^3) as shown in Chapter 2, Eq. 2-1. *MST* masses were calculated using the gender-specific soft tissue density of 1.03 g cm^{-3} for the male and 1.03 g cm^{-3} for the female given in ICRU Publication 46 (ICRU 1992). Once total *MST* volumes were assigned to each phantom skeletal site, x, they were further partitioned into *MST* regions assigned to active marrow (AM^*), inactive marrow (IM^*), mineral bone (MB^*), trabecular bone (TB^*), and cortical bone (CB^*), respectively, also according to their relative volumes.[4]

[4] The asterisks for the variables denote their inclusion of constituent miscellaneous skeletal tissue volumes. Variables with no asterisk denote their ICRP 89 reference values which are exclusive of miscellaneous skeletal tissues.

$$V^{x}_{MST-AM} = \left(V^{x}_{MST}\right)\left(SVF^{x}\right)\left(MVF^{x}\right)\left(CF^{x}\right) \quad (4\text{-}1)$$

$$V^{x}_{MST-IM} = \left(V^{x}_{MST}\right)\left(SVF^{x}\right)\left(MVF^{x}\right)\left(1-CF^{x}\right)$$

$$V^{x}_{MST\text{-}MB} = \left(V^{x}_{MST}\right)\left(\frac{V^{x}_{MB*}}{V^{x}_{HB*}}\right)$$

$$V^{x}_{MST-CB} = \left(V^{x}_{MST-MB}\right)\left(\frac{V^{x}_{CB*}}{V^{x}_{MB*}}\right)$$

$$V^{x}_{MST-TB} = \left(V^{x}_{MST-MB}\right)\left(\frac{V^{x}_{TB*}}{V^{x}_{MB*}}\right)$$

The derivation of site-specific tissue volumes are given below.

Marrow masses and volumes

Active bone marrow volumes in the 15-year male and female are derived using the same method in Chapter 2, Eq. 2-3. Inactive bone marrow volumes are obtained by replacing the *CF* term with *(1-CF)* in Eq. 2-3 in Chapter 2. Long bones in the 15-year phantoms were partitioned as was done with the newborn phantom. These subdivisions are necessary in the 15-year phantoms due to the varying cellularity gradient across the long bone regions. In this study, homogeneous bone volumes are taken directly from the 15-year male and female hybrid phantoms of Lee *et al.* (2008). The bone site-specific *TAM* and *TAM** masses were calculated using Eq. 2-4 in Chapter 2, along with the ICRU Report 46 mass densities for active marrow (ρ_{AM} = 1.03 g cm^{-3}) and gender-specific soft tissue ($\rho_{ST-MALE}$ = 1.03 g cm^{-3}, $\rho_{ST-FEMALE}$ = 1.02 g cm^{-3}) (ICRU 1992). For mass calculations in inactive marrow, a density, ρ_{AM}, of 0.98 g cm^{-3} and the calculated volume of *IM* were used in place of the active marrow terms in Eq. 2-4 in Chapter 2.

Trabecular bone and cortical bone masses and volumes

ICRP Publication 70, Table 10, provides cortical bone and trabecular bone percentages by bone site, but only for the adult. Instead of determining 15-year male and female cortical and trabecular bone volumes based on these adult partitions of mineral bone, values of *CBVF* and *TBVF* were determined via image segmentation of the 18-year male cadaver CT images and autopsy microCT images, respectively. The mass and volumes for both cortical bone and trabecular bone were determined using the identical formulation in Eq. 2-5 through Eq. 2-8 in Chapter 2. However, the ρ_{CB} is the ICRP 89 density for 15-year cortical bone (1.80 g cm^{-3}), and it is assumed that 15-year trabecular bone has an identical mass density to 15-year cortical bone.

S/V ratios for the 15-year male and female skeleton

The cortical bone surface-to-volume (S/V) ratio is defined as the ratio of the Haversian canal surface area to the volume of ossified cortical bone, and is defined for dry bone (exclusive of periosteum and blood vessels). However, the trabecular bone S/V ratio is defined as the ratio of trabecular surface area to the volume of trabecular bone, and is also defined for dry bone. Reference values for S/V ratios of cortical bone and trabecular bone are presented in ICRP 70, Tables 11 and 12, respectively. ICRP Publication 89 suggests that a nominal reference value of 3 mm^2 mm^{-3} be used for cortical bone at skeletal sites not indicated in their Table 11. Similarly, a default value of 18 mm^2 mm^{-3} is given for the trabecular bone S/V ratio. In the present study, an *EGSnrc* subroutine was written to calculate (1) the total number of trabecular bone voxels and (2) the number of trabecular bone voxel surfaces adjacent to bone marrow voxels present in each 18-year male thresholded microCT-imaged skeletal site. The number of trabecular bone volume voxels was multiplied its unit volume to estimate the cumulative trabecular bone volume, while the number of bone voxel surfaces at the bone-marrow interface were multiplied by their unit

area to estimate the total trabecular bone surface area. Dividing the trabecular bone surface area by the trabecular bone volume gives the S/V ratios for each imaged skeletal site. For bone sites with multiple microstructures, a linear average was assumed for the overall reported value.

Homogeneous spongiosa masses, volumes, densities, and elemental compositions

Volumes, masses, and densities of the 15-year male and female homogeneous spongiosa are calculated with the same methodology as reported in Eq. 2-9 through 2-11 in Chapter 2, but with an *IM* terms included in the expressions:

$$V^{x}_{spongiosa*} = V^{x}_{TAM*} + V^{x}_{TIM*} + V^{x}_{TB*} = V^{x}_{TAM} + V^{x}_{TIM} + V^{x}_{TB} + V^{x}_{MST\text{-}TAM} + V^{x}_{MST\text{-}TIM} + V^{x}_{MST\text{-}TB}$$

$$V^{x}_{spongiosa} = V^{x}_{TAM} + V^{x}_{TIM} + V^{x}_{TB} \qquad (4\text{-}2)$$

$$m^{x}_{spongiosa*} = m^{x}_{TAM*} + m^{x}_{TIM*} + m^{x}_{TB*} = m^{x}_{TAM} + m^{x}_{TIM} + m^{x}_{TB} + m^{x}_{MST\text{-}TAM} + m^{x}_{MST\text{-}TIM} + m^{x}_{MST\text{-}TB}$$

$$m^{x}_{spongiosa} = m^{x}_{TAM} + m^{x}_{TIM} + m^{x}_{TB}$$

It should be noted that the shafts of long bones in the newborn are assumed to contain only medullary marrow, and are thus devoid of trabecular bone and not included in the calculation of spongiosa volumes, masses, or densities. Once homogeneous spongiosa volumes were calculated, 15-year male and female site-specific spongiosa densities for each bone site, x, as shown in Chapter 2, Eq. 2-10. The 15-year male and female site-specific spongiosa elemental compositions in percent by mass, $w^{x,k}_{spongiosa*}$, were calculated as similarly to Eq. 2-11 in Chapter 2, but with the inclusion of *IM*:

$$w^{x,k}_{spongiosa*} = \left[\frac{\left(w^{k}_{TAM*}\right)\left(m^{x}_{TAM*}\right) + \left(w^{k}_{TIM*}\right)\left(m^{x}_{TIM*}\right) + \left(w^{k}_{TB*}\right)\left(m^{x}_{TB*}\right)}{m^{x}_{spongiosa*}} \right] \qquad (4\text{-}3),$$

where *k* is the elemental index and *w* is the mass percentage. There are no age-dependent reference elemental composition data for trabecular bone, and thus, for these calculations, it was

assumed the 15-year male and female elemental compositions of trabecular bone were the same as that for cortical bone given in Table 13.4 of ICRP Publication 89. The elemental compositions of active and inactive marrow were taken to be that given in Table 13.4 in ICRP 89, independent of age and sex. The elemental compositions for *MST* were taken to be that of the male and female, gender-specific, values for ICRU-44 male and female average soft tissues as given in Table A1 of ICRU 46 (ICRU 1992).

Shallow marrow masses and volumes

As discussed in Bolch *et al.* (2007) and Gossner *et al.* (2000, 3003), the surrogate target regions defining the location of the osteoprogenitor cells are (1) a 50-μm layer of marrow surrounding the surfaces of bone trabeculae in regions of spongiosa, and (2) a 50-μm layer of marrow adjacent to cortical bone / medullary cavity boundary in the shafts of the long bones. These two tissue regions are defined as *shallow active marrow* (AM_{50}) and *shallow inactive marrow* (IM_{50}), which include both the shallow marrow from the trabecular regions and the medullary marrow, ,and are reported as a sum of total *shallow marrow* (TM_{50}) for the total target region in the 15-year male and female. Again, a summary of all terms is given in the Glossary due to the extensive list of tissue definitions.

To assess the shallow marrow volumes and masses, values of *shallow marrow volume fraction* (*SMVF*) were obtained from Monte Carlo sampling of 3D point locations within thresholded microCT images of 18-year male spongiosa. The *SMVF* is defined as the fraction of spongiosa volume assigned to total bone marrow localized within 50 μm of bone trabeculae surfaces. As such, volumes and masses of TAM_{50}* for bone site x are obtained as:

$$V^{x}_{TAM_{50}*} = \left(V^{x}_{spongiosa*}\right)\left(SMVF^{x}\right)\left(CF^{x}\right)$$

$$V^{x}_{TIM_{50}*} = \left(V^{x}_{spongiosa*}\right)\left(SMVF^{x}\right)\left(1-CF^{x}\right) \qquad (4\text{-}4)$$

$$m^x_{TAM_{50}*} = \left(V^x_{spongiosa*}\right)\left(SMVF^x\right)\left(CF^x\right)\left(\rho_{AM}\right) = \left(V^x_{TM_{50}*}\right)\left(CF^x\right)\left(\rho_{AM}\right)$$

$$m^x_{TIM_{50}*} = \left(V^x_{spongiosa*}\right)\left(SMVF^x\right)\left(1-CF^x\right)\left(\rho_{IM}\right) = \left(V^x_{TM_{50}*}\right)\left(1-CF^x\right)\left(\rho_{IM}\right)$$

To assess volumes and masses of CM_{50}* or the sum of CIM_{50}* and CAM_{50}*, the derived methods in Chapter 2, Eq. 2-13 and Eq. 2-14 were used. Cortical shallow marrow volume and active (CAM_{50}*) and inactive (CIM_{50}*) marrow masses were defined as:

$$V^x_{CM_{50}*} = \left(V^x_{medullary\ marrow*}\right)\left(SMVF^x_{shaft}\right)$$

$$m^x_{CAM_{50}*} = \left(V^x_{medullary\ marrow*}\right)\left(SMVF^x_{shaft}\right)\left(CF^x\right)\left(\rho_{AM}\right) = \left(V^x_{CM_{50}*}\right)\left(CF^x\right)\left(\rho_{AM}\right) \quad (4\text{-}5)$$

$$m^x_{CIM_{50}*} = \left(V^x_{medullary\ marrow*}\right)\left(SMVF^x_{shaft}\right)\left(1-CF^x\right)\left(\rho_{IM}\right) = \left(V^x_{CM_{50}*}\right)\left(1-CF^x\right)\left(\rho_{IM}\right)$$

Homogeneous skeleton masses, volumes, densities, and elemental compositions

In this study, as was done in Chapter 2 for the newborn, we have taken the non-cartilaginous homogeneous skeleton of the UF hybrid 15-year male and female phantoms and sub-divided it into explicit regions of trabecular spongiosa, cortical bone, and for the long bones, medullary marrow. Homogenized skeleton volumes, masses, densities, and elemental compositions were computed using the derivations in Eq. 2-16 through Eq. 2-18 from Chapter 2, but with the inclusion of *TIM* or *CIM* contributions to the spongiosa and long bones, respectively.

Electron Dosimetry Modeling for the 15-Year Female Hybrid Phantom

In this study, electron dosimetry was performed for the 15-year female only. The transport methodology with *PIRT*, *PIRTCartilage* and *PIRTCartilageLongBone* and homogeneous bone segmentation are described in Chapter 3, and were applied to the computations involving the 15 year-old female skeletal model. The 18-year male microCT skeletal images were used as a surrogate for the 15-year skeleton, as discussed in the aforementioned sections. Any

microstructure surrogate assignments were also previously identified. Electron energy deposition to cartilage (*CAR*) in the spine, ribs, and sternum is still reported as a surrogate target for the chondrocytes due to probabilistic incidence of chondrosarcoma. However, *CAR* sources are not performed during dosimetry analysis because the ossification process has been completed in the 15 year-old skeleton. Dosimetry results for the gender independent, skeletal site-dependent ICRP reference cellularities for the 15 year-old female were determined based on a linear averaged between the results at transported cellularities. There are significant differences in volume for the spongiosa, cortical bone, and medullary marrow between then male and female phantoms, but the same microstructure image sets would be used for the male dosimetry. Future studies are necessary to analyze the impact on marrow dosimetry regarding the overall electron escape fraction due to the larger volumes seen in the 15-year male skeletal model compared with the female.

Long bones require a separate modeling due to the variation in cellularity for the proximal, upper shaft, lower shaft, and distal regions. The modeling was performed such that the appropriate cellularity could be entered for the upper and lower shafts. For the 100%-10% cellularity cases, the same cellularity was placed in each region. For example, 50% cellularity was placed in the proximal, upper shaft, lower shaft, and distal regions for a 50% cellularity case run. Given the ICRP reference cellularity of 0% for the tibia, fibula, ulna, and radius, the reference *AF* and *SAF* data for an *AM* source did not need to be computed. Unlike the tibia, fibula, ulna and radius, the humerus and femur vary in ICRP reference cellularity between each of the four long bone regions. Therefore, the upper half and lower half of the humerus and femur were run separately with the ICRP reference cellularities in place and appropriate

microstructures. The results were mathematically combined to emulate the results from a full long bone model.

Results and Discussion

Homogeneous 15-Year Male and Female Skeletal Models

The 15 year-old male and female skeletal models were developed from whole-cadaver CT image segmentation, polygon mesh or NURBS surface modeling, and hybrid phantom voxelization. Details of the latter are given in Lee *et al.* (2008). The voxel resolution chosen for each whole-body phantom was 0.1122 cm x 0.1122 cm x 0.1122 cm and 0.0997 cm x 0.0997 cm x 0.0997 cm for the male and female, respectively, based on reference skin thickness.

The site-specific homogeneous bone volumes, inclusive and exclusive of bone-associated cartilage, are shown in Table 4-1 for both the 15-year male and female skeletal models. The polygon mesh total homogeneous skeletal model volumes were approximately 1% and less than 1% different compared to ICRP reference 15-year male and female, respectively. The volume of total segmented skeletal tissue (including all bone-associated cartilage) is 4806.20 cm^3 and 5191.64 cm^3 for the 15-year female and male skeletons, respectively. It should be noted that the reported cranium volume does not include teeth, and was therefore not included in the dosimetry model. The teeth were thus treated as a separate tissue structure of the phantom.

Based on a volume-weighted average of ICRP reference densities for the constituent skeletal tissues (1.03 g cm^{-3} for active marrow, 0.98 g cm^{-3} for inactive marrow, 1.80 g cm^{-3} for mineral bone, and 1.03 g cm^{-3} for miscellaneous skeletal tissues), a value of 1.36 g cm^{-3} is estimated as the skeletal-averaged non-cartilaginous homogenous bone density for the 15-year male and female skeletons. This is less than the 1.41 g cm^{-3} reported for the newborn in Chapter 2 due to the large amounts of *IM* present in the 15 year-old skeletons. Utilizing the homogeneous skeletal density, total non-cartilaginous skeletal masses of 6180.02 g and 6743.09

g were realized in the hybrid-NURBS/PM 15-year female and male phantoms, respectively. These values are thus -0.7% and -0.3% different from the ICRP reference total skeletal masses of 6225 g and 6765 g for the 15-year female and male, respectively. The total bone-associated cartilage masses for the hybrid-NURBS/PM 15-year female and male phantoms were 162.08 g and 152.33 g, respectively, which are -82% and -87% different from the reference masses of 920 g and 1140 g. Total cartilage volumes were not matched to ICRP reference value due to limited contrast resolution for the articular cartilage regions of the long bones and hyaline cartilage regions of the ears, larynx, trachea, extrapulmonary bronchi, and external nose. Only cartilage in the intervertebral disc, sternum, and ribs were directly segmented. However, an additional 26.75 g in the 15-year female and 30.68 g in the 15-year male is included for non-bone associated cartilage (external nose, trachea, larynx, extrapulmonary bronchi, and ears) based on the assumed distributions used in the newborn. The total 15-year male skeleton, excluding contributions from cartilage is approximately 8% larger, by volume, compared to the 15 year-old female. However, this percentage can vary by as much as 45% less in the 15-year female sternum to as little as 11% less in the 15-year thoracic vertebrae. It should be noted that female cervical vertebrae, lumbar vertebrae, sacrum, lower femur shaft, ribs, clavicles, os coxae, and scapula are larger, by volume, compared with the male by as little as 8% or as much as 27%.

Construction of the Heterogeneous 15-Year Male and Female Skeletal Models

Once the UF homogeneous 15-year male and female skeletons were constructed to match ICRP reference masses to within a 1% tolerance, the constituent skeletal tissues of active marrow, inactive marrow, trabecular bone, cortical bone, and *MST* were distributed across individual bone sites. Similar to the newborn in Chapter 2, cortical bone and spongiosa volume fractions were obtained following complete segmentation of each ex-vivo CT scanned skeletal site, but from the 18-year male. Marrow and trabecular bone volume fractions, from the 18-year

male microCT scanned harvested skeletal specimens, were then obtained through the image segmentation methods described in Chapter 2, and originated in Rajon *et al.* (2006). These volumes fractions are reported in Table 4-2. Column 1 and Column 4 are the original segmented values from the 18 year-old male of the *SVF*, *CBVF*, *MVF*, and *TBVF*. These values were used as the starting point for all subsequent calculations of skeletal tissues by bone site.

As discussed in the methods section, the calculations were performed as a first iteration with the original segmented values. It was determined that the ICRP reference total mineral bone would be the targeted value for development of the 15-year male and female skeletal. Consequently, the original microCT image analysis of the *MVF* and *TBVF* would be the final values used in the skeletal tissue calculations of trabecular bone and marrow. Compared with the original segmented 18-year male cadaver, the targeted 15-year female required a 2.1% uniform decrease in the *CBVF*, while the targeted 15-year male require a 2.7% uniform decrease. Therefore, all reported skeletal tissue values for both the 15 year-old male and female are based on the final iterative values of *SVF*/*CBVF* to match ICRP reference total mineral bone. The 15-year male has between 0.7% and 6% (lumbar vertebrae) larger *CBVF* (or smaller *SVF*) compared with the iterated 15-year female. Footnotes at the bottom of Table 4-2 indicate the corresponding standard deviations of the linearly-averaged *MVF* values from multiple microCT images from the same bone site (e.g. lumbar vertebrae).

Miscellaneous skeletal tissue masses and volumes

Table 4-3 and Table 4-4 give mass and volume distributions of miscellaneous skeletal tissues dispersed throughout the 15-year female and male skeletons, respectively, by skeletal site and constituent tissue. Again, these masses were calculated based on the assumption that the *MST* volume for a particular skeletal site is proportional to that bone site's total tissue volume (exclusive of bone-associated cartilage). This assumption was applied given the lack of literature

data to the contrary. The *MST* volumes in the os coxae and cranium are the greatest as those skeletal sites are proportionally the largest in the 15-year male and female.

Marrow masses and volumes

AM, *IM*, *TMS* (total marrow), and *AM**, *IM**, and *TMS** volumes were calculated for every skeletal site as shown in Table 4-5 and Table 4-6 for the 15-year female and male, respectively. The calculated *AM* and IM masses were approximately +4% and -5% for the 15-year female, and -3% and +1% for the 15-year male compared to the ICRP reference masses for these tissues. Active marrow distributions from this study are in fairly good agreement to those given by the non-imaged based methods of Watchman *et al.* (2007). The largest difference between then results in Watchman *et al.* (2007) and the current study was in the os coxae with a 73 g difference for the 15-year female, and 46 g in the 15-year male ribs. However, these sites have relatively large amounts of active marrow, which reduce any significance between the mass differences. Similarly for the *IM*, the largest differences were seen in the ankles/feet with 87 g and 62 g in the female and male, respectively. Again, this skeletal site contains the largest amount of *IM* in the entire skeleton, thus the differences are not significant.

Table 4-7 lists the percent mass distribution of active marrow, including *MST*, by bone site for the 15-year female and male skeletons with comparisons to values given in Table 9.4 of ICRP Publication 89. The majority of skeletal sites in this study show absolute differences of less than 2% with values in ICRP Publication 89. The 15-year female os coxae and 15-year male ribs have the highest percent differences, namely 6.02%, -4.07%, respectively. Again, fairly good agreement compared with ICRP reference data.

Cartilage masses and volumes

A summary of 15-year female and male cartilage volumes are given in Table 4-8, along with calculated masses based on an ICRU Report 46 reference density of 1.10 g/cm^3. Only the

sternum contains a layer of unossified bone. This bone is the last skeletal site to fully ossify, typically 18 years of age (White 2000). Table 4-8 next lists three major cartilage sites that were manually segmented from the original CT images (costal, cranial, and intervertebral discs). Final bone-associated cartilage masses were calculated as 162.08 g (female) and 183.96 g (male), while total cartilage masses were calculated to be 187.83 g (female) and 214.64 g (male). The calculated total cartilage mass is 80% lower than the ICRP 89 reference value of 920 g (female) and 1140 g (male). The final column in Table 4-8 gives the percent mass distribution of cartilage by bone site. Costal cartilage connecting the ribs to the sternum accounts for the largest proportion of cartilage at 52% in the 15-year female and 55% in the male. As stated previously, cartilage mass and volume were not targeted to match ICRP reference due to limited contrast resolution.

Trabecular bone and cortical bone masses and volumes

Cortical and trabecular bone volumes and masses by skeletal site are listed in Table 4-9 and 4-10 for the 15-year female and male, respectively. Values of the 15-year female and male total trabecular bone mass (exclusive of *MST*) were calculated at 784.51 g and 869.43 g, approximately 6% and 7%, respectively, more than reported in ICRP Publication 89. For cortical bone, the calculated masses for the female and male are 1619.72 and 1766.99g, a difference of only 2% less than the ICRP reference cortical bone masses for both genders. ICRP 89 reference values of cortical bone and trabecular bone are based on an assumed 80% / 20% partition of total mineral bone. Based on imaging data, this partition is approximately the same for the 15-year male and female skeletal models. These results are in contrast to the 40% cortical bone and 60% trabecular found in the newborn analysis in Chapter 2. The site-specific distribution of total mineral bone (excluding teeth) mass is shown in Table 4-11 for both the female and male skeletons, which shows the agreement with the targeted ICRP reference total

skeletal mineral bone of 3700 g in the female and 4050 g in the male (2960 g CB + 740 g TB 15-year female; 3240 g CB + 810 g TB 15-year male). Compared to Watchman *et al.* (2007), the 15 year-old trabecular bone masses presented in this chapter can vary by bone site up to 8 times higher. In contrast, cortical bone masses can vary by bone site up to 3 times higher in the current study. In Watchman *et al.* (2007), this difference is noticeable in the inability to match total ICRP Publication 89 reference masses of trabecular bone by 15% less and fair agreement in cortical bone by only 4% more.

Table 4-12 shows a comparison between the image-based newborn in Chapter 2, 15-year female and male in this study, and the ICRP Publication 89 adult reference percentages of cortical and trabecular bone. The 15-year skeletons appear to be in good agreement between cortical and trabecular percentages compared with ICRP reference values. However, the cortical percentage in the adult reference cranium appears to be overestimated, and the vertebrae almost appear to be in opposite agreement between the cortical and trabecular percentages. The percentage of mineral bone associated with cortical regions in the 15-year female and male range from a low of 50% and 48%, respectively, in the lumbar spine to a high of 92% both male and female wrists/hands. It appears that mineral bone displays a more prominent appearance at birth in the form of bone trabeculae and then shifts to cortical bone as the bone matures. This ratio of CB:TB gradually shifts toward an adult 80:20 ratio as the skeleton matures during childhood and early adolescence.

Shallow active marrow data

Table 4-13 and Table 4-14 show a summary of the shallow marrow data for the 15-year female and male skeleton. All volumes and masses in this table include their *MST* contributions. Column 2 lists the shallow marrow volume fractions (percentage of spongiosa volume) for each skeletal site. For example, 14.76% of the spongiosa in the 15-year male cervical vertebrae was

computed as shallow marrow. The footnotes at the bottom of Table 4-13 and Table 4-14 denote the surrogate skeletal sites used where image data was not available, along with *SMVF* standard deviations for bone sites where linear averages were taken. The average measured shaft lengths are listed in column 2 of Table 4-15. The femur shaft length is the longest at 33.92 cm in the male and 28.75 cm in the female. In column 3 of Table 4-15, standard deviations were calculated based on the ten length measurements for each long bone shaft. Column 4 of Table 4-15 lists the calculated medullary marrow radius given in Chapter 2.

These values were then used in Eq. 2-14 in Chapter 2 to calculate the $SMVF_{shaft}$ for the long bone shafts, which are given in column 2 of Table 4-13 and Table 4-14. Column 3 of Table 4-13 and Table 4-14 list the percentage of total marrow space assigned to shallow marrow. On average, approximately 16% of the total marrow space in each bone site (excluding that in long-bone shafts) is shallow marrow (50 μm from the trabecular surfaces) compared to the 20% in the newborn, while between 1.5% and 5% of the total medullary cavity volume is shallow marrow compared with 4% and 14% in the newborn. By multiplying the *SMVF* (column 2) by the spongiosa volume, or medullary marrow volume in the case of long bones, volumes of shallow marrow for each bone site were calculated and are listed in column 4 of Table 4-13 and Table 4-14. Corresponding shallow marrow masses at 100% cellularity (necessary for specific absorbed fraction calculations) are then given in column 5 of Table 4-13 and Table 4-14. The reference shallow inactive and active marrow masses are provided in columns 7 and 8 in both Table 4-13 and Table 4-14. Shallow active marrow values were determined by multiplying the shallow marrow volumes (column 4) by the reference cellularity and reference active marrow density. Likewise, the shallow inactive marrow masses were determined by multiplying the shallow marrow volume (column 4) by 1-*CF* and the reference inactive marrow density. In column 9, the

total reference shallow marrow mass based on the sum of columns 7 and 8 are listed. The total reference mass of shallow marrow throughout the entire skeleton was calculated to be 352.42 g for the 15-year female and 395.34 g for the 15-year male as compared to 333.7 g for the female and 365.2 g for the male estimated by Watchman *et al.* (2007). The estimate provided in Watchman *et al.* (2007) is in fairly good agreement with the image-based shallow marrow data provided in this study, with only 6% less for the female and 8% less for the male in the Watchman *et al.* (2007) study. The last column in Table 4-13 and Table 4-14 show the percent distribution of shallow marrow by bone site. The least amount of shallow marrow is found in the shafts of the long bones, while the greatest is found within the os coxae. This means that the long bone shafts must have fairly large medullary cavities.

S/V ratios for 15-year male and female hybrid phantoms

Table 4-16 shows a comparison of the S/V ratios computed for the hybrid newborn phantom (column 2), the gender-independent hybrid 15 year-old (column 3), the ICRP reference 15-year (column 4), and ICRP reference adult 44-year (column 5). The S/V ratio for all long bone shafts is equal to 0.0 $mm^2 mm^{-3}$ because these regions of the long bones do not contain bone trabeculae. Column 6 lists the ratios between then S/V values for the UF hybrid 15-year skeleton and the ICRP reference 15-year skeletal model. The 15-year in this study can have S/V ratios as low as half up to as much as twice the values reported for the ICRP reference 15-year. The largest difference is seen in the mandible and the largest is seen in the tibia. Compared with the ICRP adult S/V ratios, the image-based data from this study of the 15-year model are in fairly good agreement. This could be due to the fact that the imaging data was taken from an adult, 18-year male cadaver.

Homogeneous spongiosa masses, volumes, densities, and elemental compositions

Table 4-17 gives a summary of the 15-year female and male hybrid spongiosa masses, volumes and densities including *MST* for each of the 34 skeletal sites analyzed in this study. Table 4-17 also gives the summed spongiosa mass and volume data for the total skeleton, along with a volumetrically-weighted average spongiosa density for both female and male 15-year skeletal models. It appears that the majority of the 15-year female (487.01 g) and male (440.76 g) spongiosa resides in the os coxae, compared with the cranium for the hybrid newborn in Chapter 2. Similarly, the least amount of spongiosa mass is found in the distal ulna and proximal radius. The total skeleton spongiosa mass and volume were calculated as 3065.38 g and 2709.78 cm^3 for the 15-year female, and 3316.72 g and 2925.46 cm^3 for the 15-year male skeletons, respectively. Compared with the ICRP 89 reference spongiosa masses of 3037.84 g for the female (sum of 974.09 g of *TAM*, 1250.98 g of *TIM*, 72.77 g of *MST*, and 740.0 g of *TB*), and 3259.93 g for the male (sum of 1048.04 g of *TAM*, 1324.98 g of *TIM*, 76.91 g of *MST*, and 810.0 g of *TB*), the calculated 15-year female and male spongiosa sum is less than 1% and 2% higher, respectively.[5] Similar calculations can be performed with the spongiosa volumes and tissue constituent densities to show that the calculated 15-year female and male spongiosa sum across the skeleton is less than 1% different that the ICRP 89 reference spongiosa volumes. This almost perfect agreement is directly related to the matched trabecular bone percentage of 20% in both the image-based data used for the 15-year hybrid and the ICRP reference 15-year skeletons. The agreement in the *AM* and *IM* marrow masses between the hybrid and reference skeletal models also contributes to the agreement in spongiosa.

[5] Reference spongiosa masses exclude contributions in the long bone shafts since this is not considered spongiosa.

In Table 4-17, the 15-year female and male skeletal-averaged spongiosa density is estimated to be 1.13 g cm^{-3} and 1.12 g cm^{-3}, respectively. The male is slightly lower than the female due to larger amounts of *IM* in the male. In ICRU Report 46, Table A1, the only reference spongiosa density listed is that for the adult, namely 1.18 g cm^{-3}. For both the male and female 15 year-old, skeletal site-dependent spongiosa densities range from a low of 1.06 g cm^{-3} in the sacrum to a high of 1.25 g cm^{-3} in the cranium (largest proportion of trabecular bone). Despite the density range, the calculated skeletal-averaged spongiosa densities are in good agreement, only 4% for the female and 5% for the male lower, compared with the adult reference spongiosa density.

Table A1 of ICRU Report 46 lists reference elemental compositions of trabecular spongiosa, but only for the adult, and only for a fixed mixture of 33% cortical bone, and 67% marrow, which itself is comprised of 50% *IM* and 50% *AM* (all percentages by mass). For comparison, the UF hybrid 15-year male and female contain a mixture of 55% cortical bone and 45% marrow, comprised of 56% *IM* and 44% *AM*. As shown in Table 4-18 (female) and Table 4-19 (male), the spongiosa elemental compositions including *MST* vary significantly between skeletal sites for some elements. For example, the mass percentage of carbon in the 15-year female cranium spongiosa is about 35%, whereas approximately 63% is found the shafts of the long bones. Similarly, the shafts of the long bones does not contain any trabecular bone, therefore no Ca is present, compared to about 9% in the cranium. The total skeleton-averaged spongiosa elemental compositions for the 15-year male and female are fairly represented by the adult reference spongiosa elemental compositions in ICRU 46.

Homogeneous skeleton masses, volumes, densities, and elemental compositions

The homogeneous skeleton masses and volumes including *MST* were calculated and are listed in Table 4-20 for both the female and male 15 year-old adolescent. The data of Table 4-20

excludes cartilage mass and volume contributions to each bone site. Due to the length of this text, the data for homogeneous bone data including cartilage was not presented, but can be easily computed. Compared with the manually segmented NURBS/polygon mesh 15-year male and female phantoms, the derived total homogenous skeletal volume and mass are matched, which provides validation of the methods presented in this study.

The increased densities of homogeneous bone excluding cartilage compared to that in spongiosa regions is attributed to the contribution of cortical bone in the former. Density differences between site-specific homogeneous bones are similarly explained. The volumetric-weighted skeletal averaged homogeneous bone density is 1.35 g cm^{-3} for both the male and female. As seen for bone site-specific spongiosa densities, homogeneous bone densities vary considerably across the newborn skeleton (1.2 g cm^{-3} to 1.6 g cm^{-3}). Choosing a density specific to a given skeletal site of interest could provide additional improvements in the accuracy of dose estimates.

Homogeneous bone elemental compositions excluding cartilage for the 15-year female and male were computed, and are shown in Table 4-21 and Table 4-22, respectively. Elemental data vary considerably across the skeleton. The ICRP reference data and calculated data appear to be in reasonably good agreement, except for the oxygen content, which is approximately 20% less than reference in absolute difference. Improved agreement is seen when the cartilage component is considered in the elemental composition of total homogeneous bone.

15-Year Female Image Data for the Skeletal Macrostructure and Microstructure

The voxel resolution and voxel array size for the 15-year female skeletal macrostructure and 18-year male microstructure are shown in the first set of columns in Table 4-23. Due to computer memory limitations large bone sites such as the ribs and os coxae were voxelized at 0.06 cm and 0.05 cm, respectively, while a small bone site such as the clavicle was voxelized at

0.018 cm. However, even at the lowest resolution of 0.06 cm, differences less than 1% were achieved between the voxel volumes and polygon mesh volumes for the spongiosa and cortical bone tissues. Figure 4-1 A and Figure 4-1B illustrate the original polygon mesh and voxelized os coxae, respectively for the female (left) and male (right), while Figure 4-1 C and Figure 4-1 D illustrate the original and voxelized femur. The last three sets of columns in Table 4-23 are for the skeletal microstructure data obtained after filtering and thresholding the selected ROI for each bone sample. The largest ROI was selected for each microimage in order to obtain the best representative sample of spongiosa for transport. Voxel dimensions, marrow volume fractions (*MVF*), and trabecular bone volume fractions (*TBVF*) are all shown. Multiple regions were imaged for the cranium, lumbar vertebra, thoracic vertebra, cervical vertebra, proximal femur, and ribs. The average *MVF* and *TBVF* are indicated in Table 4-23 with the corresponding standard deviation. There are skeletal sites listed in the table which do not have a corresponding microimage due to the inability to obtain a sample from these skeletal regions during the bone harvest. As indicated in previously, surrogates for bone sites without microimages were assigned. These surrogates were then used for the microstructure image input into *PIRTCartilage* and *PIRTCartilageLongBone*. Finally, as indicated in Table 4-23, both the *MVF*/*TBVF* values for the 30 μm scan and 60 μm re-sampled images are shown. Most relative differences between the 30 μm and 60 μm samples are less than 1%. Therefore, no statistical difference can be seen between the original 30 μm and re-sampled 60 μm images.

Bone-Site Dependent Specific Absorbed Fraction Data for the UF Hybrid 15-Year Female Phantom

Tabular data for the 15-year female specific absorbed fractions are in Appendix H. The corresponding figures for the tabular data are in Appendices I – L. Specific absorbed fractions are calculated based on Chapter 3, Eq. 3-3. As previously mentioned, multiple sample sites from

the cranium, ribs, lumbar vertebra, thoracic vertebra, femur, humerus, tibia, fibula, ulna, radius and cervical vertebra were transported. Average specific absorbed fraction data was obtained based on the methods in Chapter 3, Eq. 3-3 though Eq. 3-11. Likewise, data for the *CBV* sources were linearly averaged.

Each of the 20 bone sites is listed as a set of two or three tables: *AM* targets, TM_{50} targets, and *CAR* targets (only for intervertebral discs in the vertebrae, ribs, and sternum) for all bone tissue sources. Cellularity dependence for the specific absorbed fractions is only found when the electron source is in *AM* and at low to intermediate electron energies. In the case of cellularity-independent specific absorbed fractions for the *TBV*, *TBS*, and *CBV* electron sources, only input microstructures at 100% cellularity were run. However, for the *IM* source, 50% cellularity was arbitrarily chosen for each case run, as was done in Chapter 3 for the newborn. The following sections discuss the specific absorbed fraction results for the three targets: *AM*, TM_{50} and *CAR* (intervertebral disc and costal cartilage targets only).

Specific absorbed fractions for an active marrow target from a source in active marrow

Specific absorbed fractions for electron sources in *AM* irradiating *AM* targets are shown in Appendix I based on the tabular data in Appendix H. Similar to the newborn in Chapter 3, this source-target combination exhibits a monotonically decreasing function for both the absorbed fraction and specific absorbed fraction quantities. As the electron energy increases, the electrons will eventually escape out of spongiosa, only depositing a fraction of the initial energy to marrow. The absorbed fraction approaches unity for an electron energy 10 keV and below. Therefore, the corresponding specific absorbed fraction at low electron energies is proportional to the inverse target tissue mass. If the mass of the target tissue, *AM*, is held constant at 100% cellularity, then a decrease in the fractional cellularity will increase the overall specific absorbed fraction ratio. Once the electron energy has reached approximately 150 keV to 1.5 MeV, as

compared to the newborn energies of 500 keV to 1 MeV, depending on the bone site, each curve collapses and becomes cellularity independent. This convergence is achieved once the electron energy has reached the point where a sufficient number of marrow cavities have been crossed and the electron range exceeds the dimensions of the spongiosa region. For low to intermediate electron energies, it is important to asses the accuracy of a marrow cellularity measurement in a patient given a factor of 10 difference in the specific absorbed fraction quantity in the most extreme case. The largest amount of energy deposition to *AM* from an *AM* source occurs in the os coxae compared to the newborn cranium, and least amount in the mandible as compared to the patella in the newborn, directly proportional to the amount of active marrow in these bone regions. *SAF* results at the ICRP reference cellularity are shown in the tables of Appendix H. Again, a linear average of the *SAF* data at the transported cellularities was performed to compute the *SAF* results at the ICRP reference cellularity.

As described in the methods section of this chapter, the long bones were run with the same cellularity across all regions for the incremental cellularity case runs. Both proximal and distal microstructure image data is available for these bone sites, but the transport code does not currently accept two microstructures due to memory constraints. Similarly to other bone sites, two sets of *AF* data were computed. The first set was based on the proximal microstructure being placed in both proximal and distal spongiosa regions, and the second set was based on the distal microstructure being placed in the proximal and distal spongiosa regions. Similar to the methods in Chapter 3, for the incremental cellularity data, the averaged specific absorbed fractions were computed based on the mass fractional source distributions. However, the fractional source distributions for the proximal microstructure were based on the mass of the proximal and upper shaft source mass compared to the whole long bone source mass. Similarly,

the fractional source distribution of the distal microstructure was based on the mass of the distal and lower shaft source mass compared to the entire mass of the source in the long bone. Consequently, the averaged absorbed fraction data has a higher weighting toward the higher fractional source mass.

A separate case run was performed for the ICRP reference long bones due to cellularity variations across the proximal, shaft, and distal regions. However, for the tibia, fibula, ulna and radius, the reference *AM* mass is 0.0 g. Therefore, the ICRP reference *SAF* for an *AM* target from an *AM* source is 0.0. The humerus and femur have different cellularity values for each region (55% proximal, 35% upper shaft, 20% lower shaft, and 0% distal). Therefore, the upper half (proximal and upper shaft) and lower half (lower haft and distal) were run separately for the two cases. Averaged results were again based on the fractional source contributions, but of the reference masses for the ICRP cellularity. Unfortunately, by running upper and lower half of the femur and humerus separately, cross-fire between then shaft regions is not neglected. A simple analysis was performed running the upper (with proximal microstructure) and lower (with distal microstructure) half of the humerus for a 100% cellularity case for an *AM*, *TBV*, *TBS*, and *CBV* source to *AM* target. *AF* results from these two runs were then mathematically averaged as discussed above. These results were then compared with the averaged AF results from a full long bone run at 100% cellularity with the averaged proximal and distal microstructures. Neglecting cross-fire for an *AM* source creates approximately 9.5% difference for a 10 MeV electron. This is the worst case scenario, as the lower half of the long bone does not contain as much *AM* source mass as in the upper half. For a *CBV* source, neglecting cortical bone cross fire between shaft regions into AM causes up to a 9% difference at low to intermediate electron energies. Again, this is the maximum difference that would be seen, since ICRP reference

cellularity in the shafts is less than 100%. For the *TBV* and *TBS* sources, less than 5% difference is seen due to the fact that these sources are exclusively contained in the proximal and distal ends. Based on the CSDA range of approximately 10 cm, a 10 MeV electron in soft tissue will not cross the 9.8 cm shaft length unless the particles are starting close to the proximal/distal/shaft interface.

Specific absorbed fractions for an active marrow target from all other bone sources

Similarly to Appendix I, the specific absorbed fraction figures in Appendix J are for *AM* targets, but from an *IM*, *TBS*, *TBV*, or *CBV* source. As shown in Figure 3-2 in Chapter 3, the specific absorbed fractions for these sources are cellularity independent. As such, these sources were run at 100% cellularity, except in the case of the *IM* source, which was run at an arbitrarily chosen 50% cellularity. As previously discussed, for a *TBS* source, 50% of the time electrons are emitted toward the marrow cavity, and 50% of the time electrons are emitted toward the trabecular bone. Therefore, the specific absorbed fraction for a *TBS* source to *AM* target is 50% the product of the inverse target tissue mass at 100% cellularity and the *CF* at low electron energies, or 50% of the specific absorbed fraction value for an *AM* source to *AM* target at the ICRP 15-year female site-specific reference cellularity. The addition of the *CF* term in the denominator explains the larger difference in the 15-year female SAF data between the ICRP reference *AM* source and *TBS* source to *AM* target compared with the newborn. Finally, similarly to the *AM* source and target cellularity independence at high electron energies, the *TBS*, *TBV*, and *IM* sources begin to converge at electron energies between 420 keV and 3 MeV. Therefore, source independence occurs at these energies because the electrons have traveled through a large enough number of marrow cavities and space to effectively results in the same energy deposition.

Energy deposition from an *IM* and *TBV* source continues to increase as electron energy increases until the electron energy reaches the point of electron escape out of spongiosa, as shown in the figures by the mound-shaped trend. A similar response is seen in the *CBV* source. Electrons with enough energy will escape the cortical bone region and deposit energy into spongiosa, then exit the spongiosa once the energy corresponding to the spongiosa thickness has been reached, which causes a decrease in the energy deposition. Therefore, the lower the electron energy corresponding to the maximum energy deposition for a *CBV* source, the thinner the cortical bone region. At a peak energy deposition of 4.0 MeV, the femur has the thickest cortical bone, probably as a result of the thick cortical shaft region, compared to 2.0 MeV peak for the newborn femur. Similarly, the thinnest cortical bone can be found in the vertebrae, at a peak energy of 1.5 MeV, compared to the newborn patella at 0.5 MeV. Table 4-24 lists measured bone site-specific cortical bone thicknesses for the UF hybrid 15-year female phantom. These were estimated using the measurement tool in *Rhinoceros*™. For the *CBV* source, the dosimetry results exactly correlate with measured cortical bone thickness. For an *IM* source the peak energy deposition occurs at a constant 80 keV to100 keV. This corresponds to the maximum distance an electron travels to reach the spongiosa boundary. For a *TBV* source, the thickness of bone trabeculae, marrow cavity size, and *AM* mass in combination determine the electron energy where maximum energy deposition occurs.

Specific absorbed fractions for a shallow marrow target from all bone sources

As reported for the newborn in Chapter 3, results for the 50-μm target region definition are reported as total shallow marrow or TM_{50}. Appendix K illustrates the specific absorbed fractions from a source in *AM* at reference cellularity, *IM*, *TBV*, *CBV*, and *TBS* to target TM_{50}. As with previous results, these sources are cellularity independent, and therefore run at 100% cellularity, except for the *IM* source, which was run with 50% cellularity, as shown in Figure 4-2 A through

Figure 4-2 D. Source independence occurs for the *IM* (at 50% cellularity), *and AM* (at ICRP reference cellularity) sources, but not for the *TBS* source as was seen in the newborn. As was shown in Eq. 3-8 ad Eq. 3-9 in Chapter 3, the *AF* and *SAF* data for an *AM* source to TM_{50} target is proportional to the *SMVF* and ratio of the *SMVF* and TM_{50} target mass, respectively. For the newborn, the *SMVF* was approximately 50% for most bone sites. Therefore, since the AF data for the *TBS* source to TM_{50} target is also approximately 50% at low energies, the *TBS* source also becomes source independent and converges with the *AM* and *IM* sources. However, for the 15-year female, the *SMVF* values are less than 50% (range between 5% - 22%), which means the *IM* and *AM* sources will have source convergence, but at a value less than the *TBS* source. For example, the lumbar vertebra, cranium, and sacrum have a *SMVF* of approximately 0.14, 0.20, and 0.08, respectively. After dividing by the shallow marrow mass for each bone site, the values become 0.005, 0.004, and 0.008, respectively. The specific absorbed fraction results, as reported in Appendix H for 1 keV are approximately 0.005, 0.006, and 0.008, respectively. The other skeletal sites follow this same pattern of cellularity independence

For a *TBV* source, the source independence occurs between 150 keV and 1.5 MeV, depending on the bone site, compared with 200 keV to 700 keV for the newborn in Chapter 3. The electron must have enough energy to exit the trabecular bone volume. Consequently, as with previous discussion, the convergence occurs at the electron energy for which the source particle has traversed enough marrow cavities to effectively deposit the same energy whether the particle began in *TBV, TBS, AM*, or *IM*.

Specific absorbed fractions for a cartilage target from all bone sources

Similar to the newborn, cellularity independence is shown for the AM source in Figure 4-3 A through Figure 4-3 D. Unlike the newborn, where every bone contains an ossification center surrounded by cartilage, the 15-year female is completely ossified except the sternum.

Therefore, only *CAR* targets in the intervertebral discs, sternum, and costal regions are considered. Appendix L illustrates the specific absorbed fraction results by bone site for sources starting in *AM* (at reference cellularity) *IM*, *TBS*, *TBV*, or *CBV* sources depositing energy in the *CAR* target. Electron sources in *AM* (ICRP reference cellularity), *TBS*, *IM*, and *TBV* are source independent for the specific absorbed faction quantities. Electrons need enough energy to traverse the entire spongiosa and cortical bone regions to deposit any energy in the target cartilage region, regardless of the particle source.

The *CBV* source converges with sources in cervical vertebrae and rib spongiosa, *AM*, *IM*, *TBS*, and *TBV*. As previously discussed, there reaches a point where the electron energy is source is high enough that regardless of the source, the same amount of energy is going to be deposited. However, for the thoracic vertebrae and lumbar vertebrae the sources in spongiosa deposit more electron energy into a *CAR* target. This is due to the fact that these bones are not completely surrounded by a cartilage layer like in the newborn. The vertebrae are completely ossified by 15 years of age and do not contain a uniform cartilage layer. More energy deposition occurs from sources in spongiosa at higher energies due to cross-fire, which is why the energy deposition from spongiosa exceeds the *CBV* at higher energies. Contributions of cross-fire for a CBV source occur at the intermediate electron energies. Convergence is expected to occur when the electron energy from sources in spongiosa significantly exceed the overall dimensions of the spine to avoid cross-fire dependence. The cervical spine converges due to the relative size compared with the thoracic and lumbar spine regions. The sternum appears to needs higher electron energy for convergence to occur.

Skeletal-Averaged Absorbed Fraction Comparisons for the UF Hybrid 15-Year Female Phantom and the 2003 15-Year Model

The current Stabin and Siegel (2003) model does not contain absorbed fraction data by skeletal site. Instead, skeletal-averaged absorbed fraction data based on skeletal tissue masses tied to the ORNL stylized phantom are reported. Calculations of the skeletal-averaged absorbed fraction values are based on the formulations in Chapter 3. Values of $f_{s,i}$ are listed in Table 4-25, along with the ICRP reference cellularity by bone site for the 15-year female. Tabular data of the skeletal-averaged absorbed fraction data for the 15-year female are listed in Table 4-26. Figures 4-4 A–D illustrate the tabular data found in Table 4-26. For a *TBS* source to *AM* target, the *PIRT* skeletal-averaged absorbed fraction data are approximately 2% to 5% less than the 2003 model up to 100 keV. Between 100 keV and 1 MeV, there is approximately 4% to 15% difference between the two models. After 1 MeV, electron escape dominates the physics, and by 10 MeV the infinite 2003 model overestimates the energy deposition to *AM* by almost 4.0 times, assuming the infinite results for the 4 MeV can be extended to 10 MeV. Similarly, the 2003 *TBV* source for the 15 year-old overestimates between approximately 5% to 20% in the low to intermediate electron energy range due to the microstructural differences. Overestimations in the 2003 model due to the macrostructure occur after 500 keV, up to 3.98 times at 10 MeV. For an *AM* source, the divergence begins at approximately 15 keV to 1 MeV. Underestimations due to using 2D chord distributions from 9-year microstructural data for a 15 year-old in the 2003 model can be as high as 12%. At electron energies above 1 MeV, the models diverge due to the *PIRT* modeling of electron escape from the macrostructure compared to the infinite transport modeling in the 2003 model. For comparison, newborn divergence due to electron escape begins at 400 keV due to smaller bones. As before, extending the 2003 results out to 10 MeV can show up to 3.5 times more energy deposition that in the *PIRT* model compared to 17.5 times in the

newborn. In the 2003 model, energy deposition from a *CBV* source to *AM* target is zero. However, the skeletal-averaged *PIRT* model shows up to 6% energy deposition at 2 MeV, compared with 11% at 800 keV for the newborn. Tabular results for TM_{50} targets are reported, but are not compared with the 2003 model. As with the newborn, a fair comparison cannot be made between the two models because a 10-μm endosteal layer of active marrow was utilized in the 2003 model, while a 50-μm shallow marrow target region of the summed active and inactive marrow was used in *PIRT*.

The current 2003 model uses overall cortical and trabecular bone percentages of 80%/20%, respectively. These percentages were confirmed in the study for the 15-year male and female. Assuming a uniform mineral bone source (cortical bone plus trabecular bone), Figure 4-5 compares the skeletal-averaged absorbed fraction results between the 2003 model and *PIRT* model using a weighted cortical/trabecular bone percentage of 80%/20%. The 2003 model underestimates the energy deposition from electron sources in *MB* to targets in *AM* up to 25% for electron energies up to 4 MeV. Once electron escape is accounted for, the 2003 model overestimates the skeletal-averaged absorbed fraction by 1.65 times at 10 MeV. All differences are due to both the exclusion of cortical bone as a source and differences in the trabecular microstructure used in the 2003 model.

Conclusions

In this study, comprehensive skeletal tissue models were developed for the UF hybrid reference 15-year male and female. The model includes bone-specific masses and volumes of all relevant tissue components including active marrow, inactive marrow endosteal tissues, trabecular bone, cortical bone, miscellaneous skeletal tissues, and cartilage. Site-specific and skeletal-averaged tissue densities and elemental compositions are also derived. Model data sources included CT images of whole-cadaver 18-year male skeleton, along with the

corresponding microCT images of the 18-year male bone specimens. In this study, the 18-year image sets served as surrogate data for the 15-year male and female skeleton.

The site-specific distribution of active and inactive marrow compare reasonably well with that given for the reference 15-year male and female in ICRP Publication 89. In ICRP Publication 89, 15-year total mineral bone is partitioned as 20% trabecular and 80% cortical – values accepted as averaged across the adult skeleton. In the present model, analysis of 18-year whole-cadaver CT images and microCT images reveal the same percentage. These values, however, vary from 50% cortical and 50% trabecular to 90% cortical and 10% trabecular across the 15-year male and female skeletons, and thus a single skeletal-averaged value can be misleading when looking at a particular skeletal region. The 15-year male and female skeletal tissue model permits a sub-segmentation of the homogeneous bones in the UF hybrid 15-year male and female phantom into specific regions of cortical bone, spongiosa, and medullary marrow.

Similarly to the newborn, the results in this chapter show the importance of source-target combinations in terms of cellularity independence and source independence as a function of electron energy for specific absorbed fraction data. *IM*, *TBV*, *CBV*, and *TBS* sources to *AM* targets are all cellularity independent. Depending on the bone site, source independence from *IM*, *TBV*, and *TBS* sources to *AM* and TM_{50} targets occurs at high electron energies. Cellularity independence also exists for an *AM* source to TM_{50} targets. Convergence of the various cellularity curves from *AM* sources to *AM* targets, depending on the bone site, occurs between 150 keV and 1.5 MeV. Results also show relative thickness of spongiosa and cortical bone based on the energy for peak deposition. Therefore, it is often useful to analyze skeletal site-

specific data variations, especially when exposing a certain region of the body to radiation (e.g. CAP exam).

When comparing skeletal-averaged absorbed fraction data for an *AM*, *IM*, *TBV*, or *TBS* source to any target, the differences between then *PIRT* and 2003 models differ at low to intermediate electron energies due to microstructural differences between the 18-year 3D model in this study and the 9-year 2D chords used in the 2003 model, and consistently overestimates at energies greater than 4 MeV due to electron escape. Microstructural differences between the newborn and the 2003 model are not as significant because 1.7-year data was used. Electron escape becomes significant after 1 MeV for the 15-year female, compared with 400 keV for the newborn due to the size differences. Future studies will analyze any significant differences in electron escape between the 15-year male and female skeletal macrostructures.

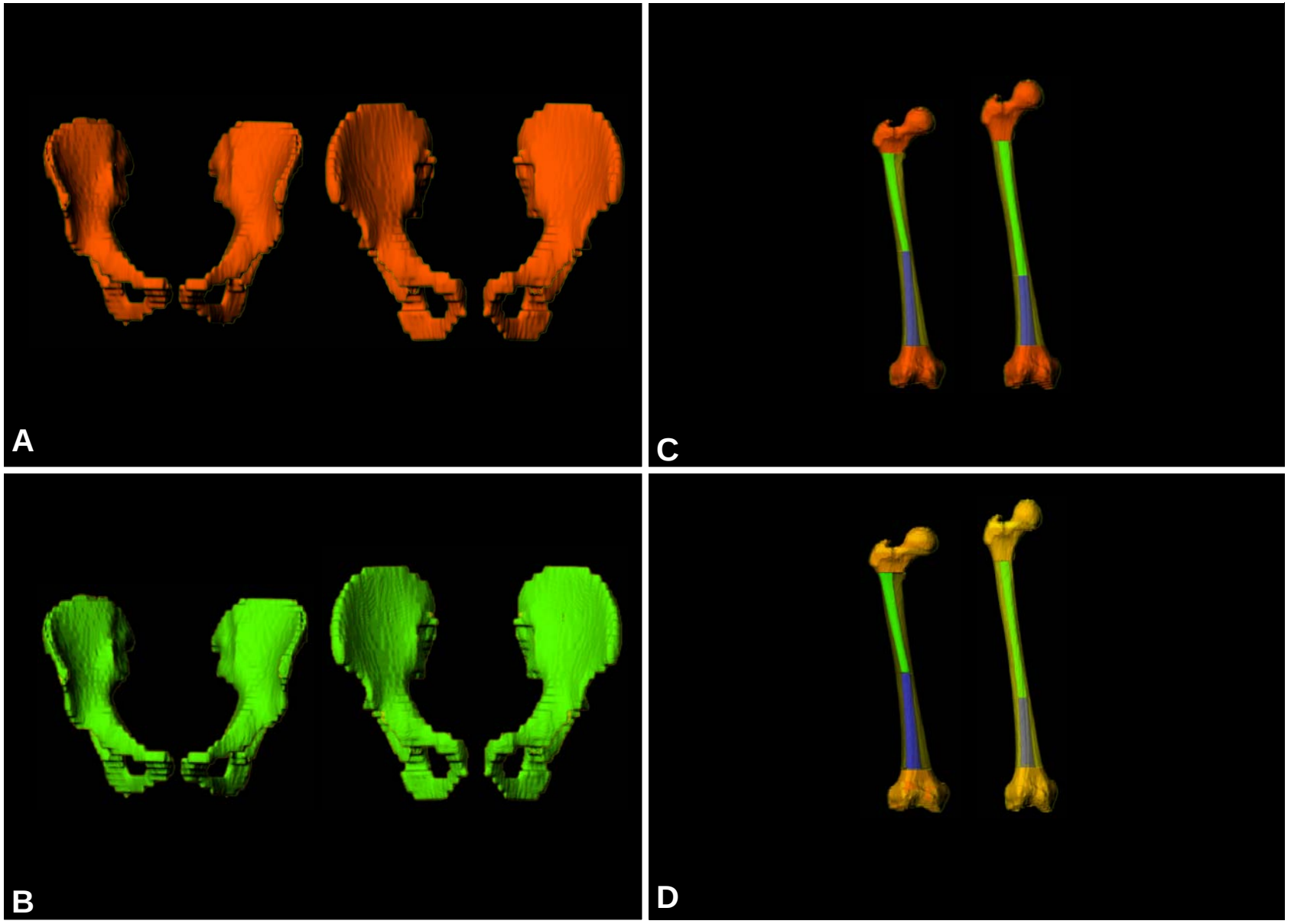

Figure 4-1. Comparison between the original rendered polygon mesh and segmented voxelized 15-year male (right) and 15-year female (left) (A) polygon mesh os coxae, (B) voxelized os coxae, (C) polygon mesh femur, and (D) voxelized femur.

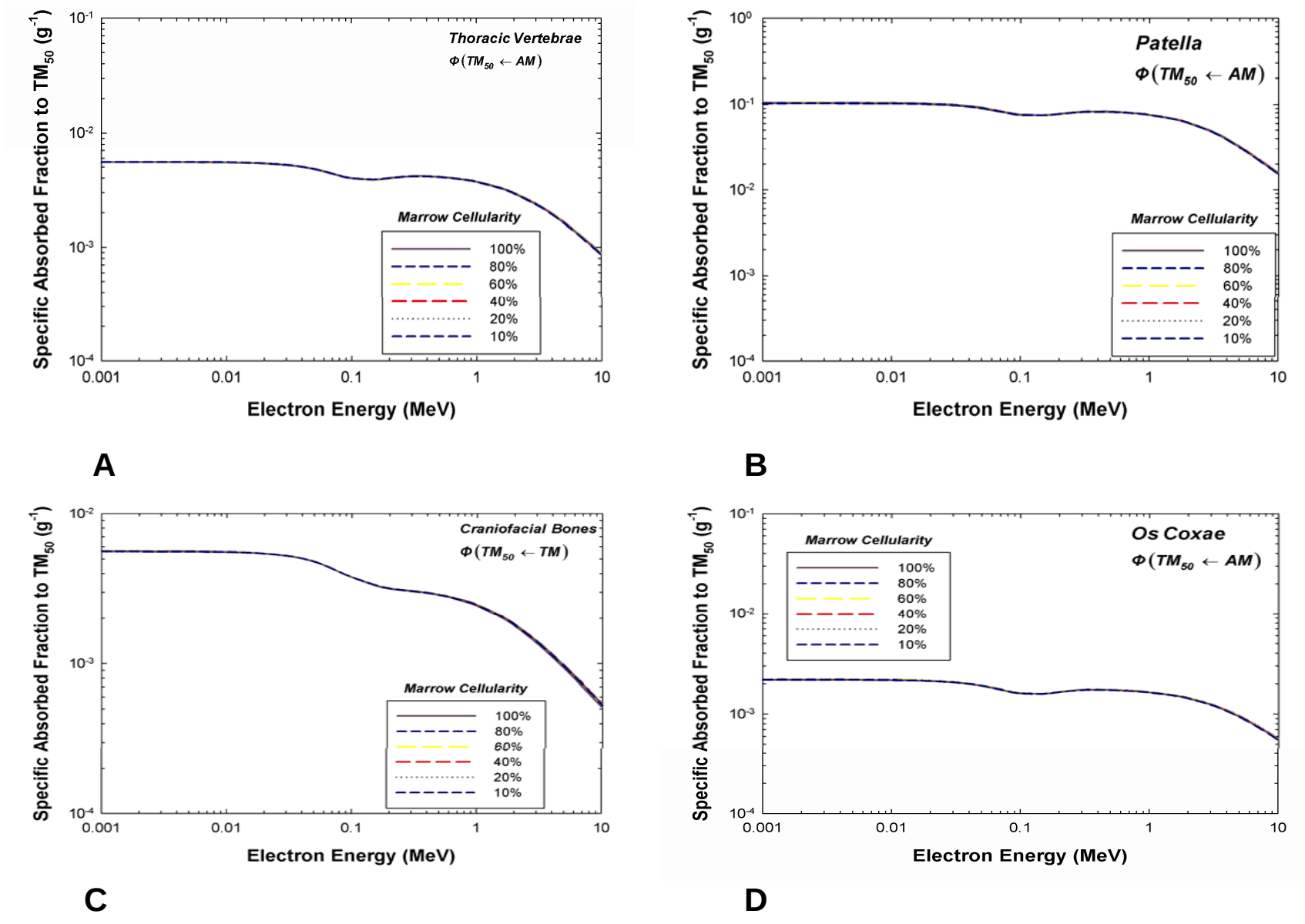

Figure 4-2. 15-year female specific absorbed fraction data from an *AM* source to a TM_{50} target at various cellularities for the (A) thoracic vertebrae, (B) patella, (C) craniofacial bones, and (D) os coxae.

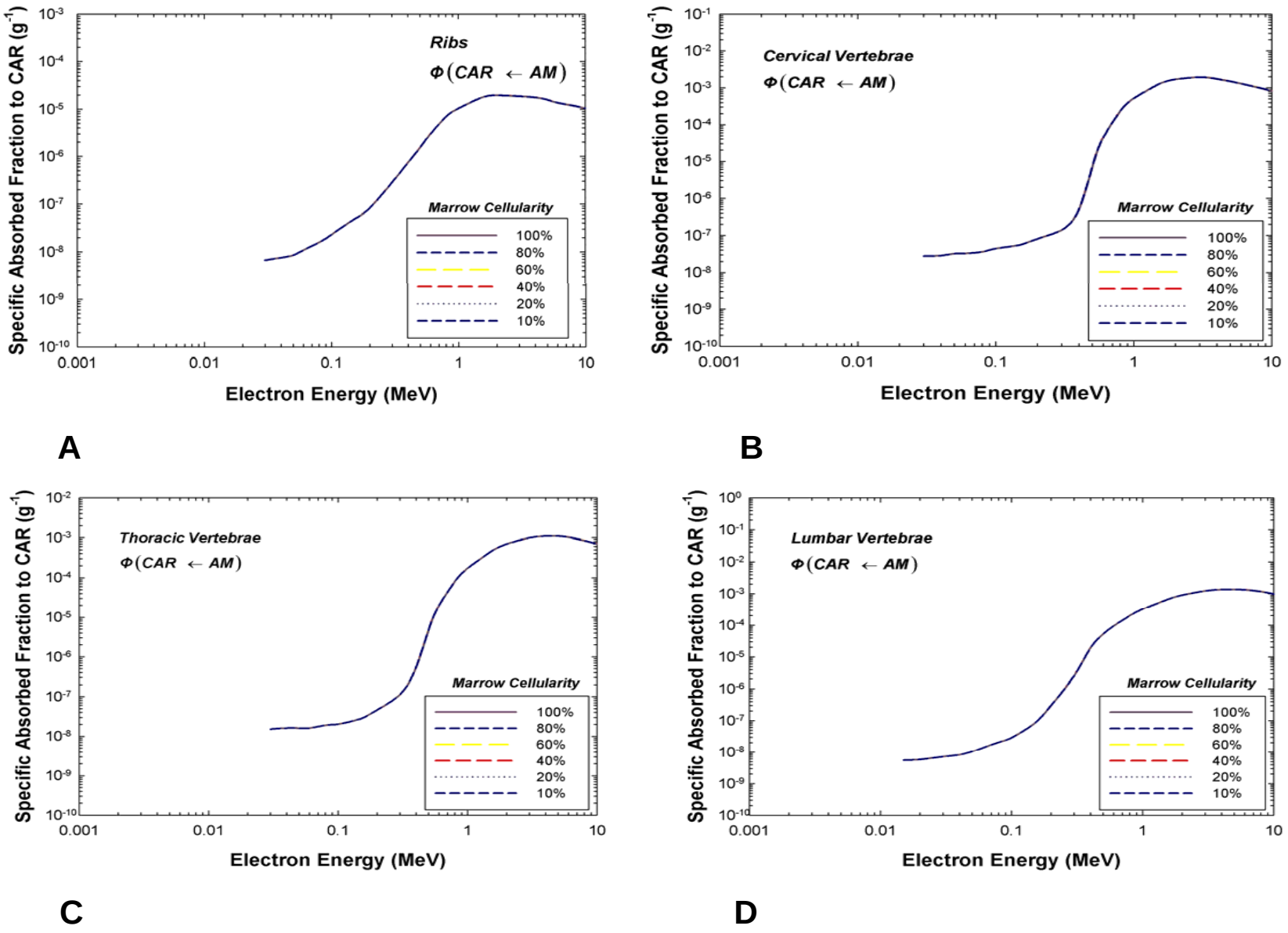

Figure 4-3. 15-year female specific absorbed fraction data from an *AM* source to a CAR target at various cellularities for the A) ribs, B) cervical vertebrae, C) thoracic vertebrae, and D) lumbar vertebrae.

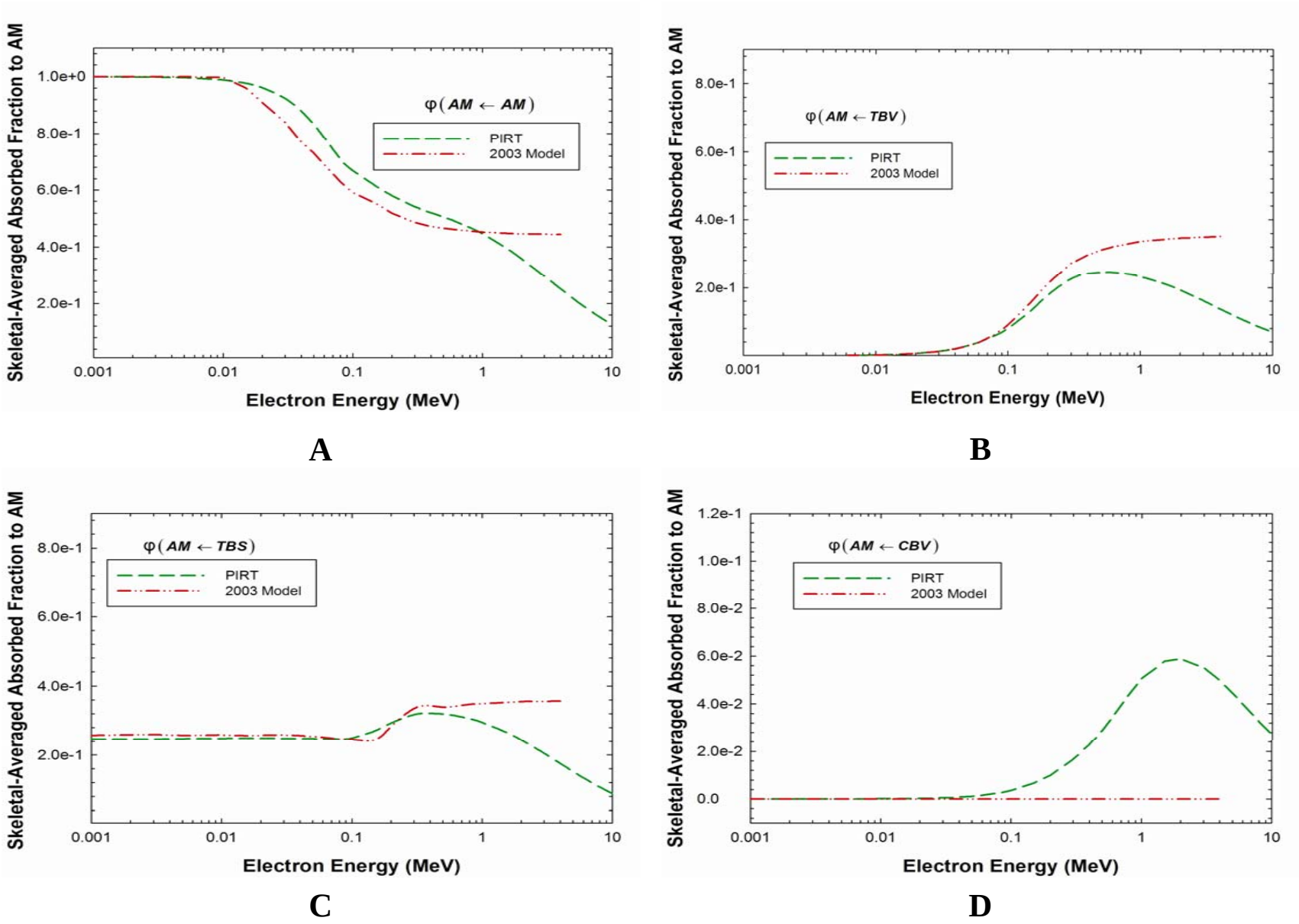

Figure 4-4. Comparison between the 2003 and *PIRT* 15 year-old female skeletal-averaged absorbed fraction data to an *AM* target at ICRP reference cellularity for the A) *AM* source, B) *TBV* source, C) *TBS* source, and D) *CBV* source.

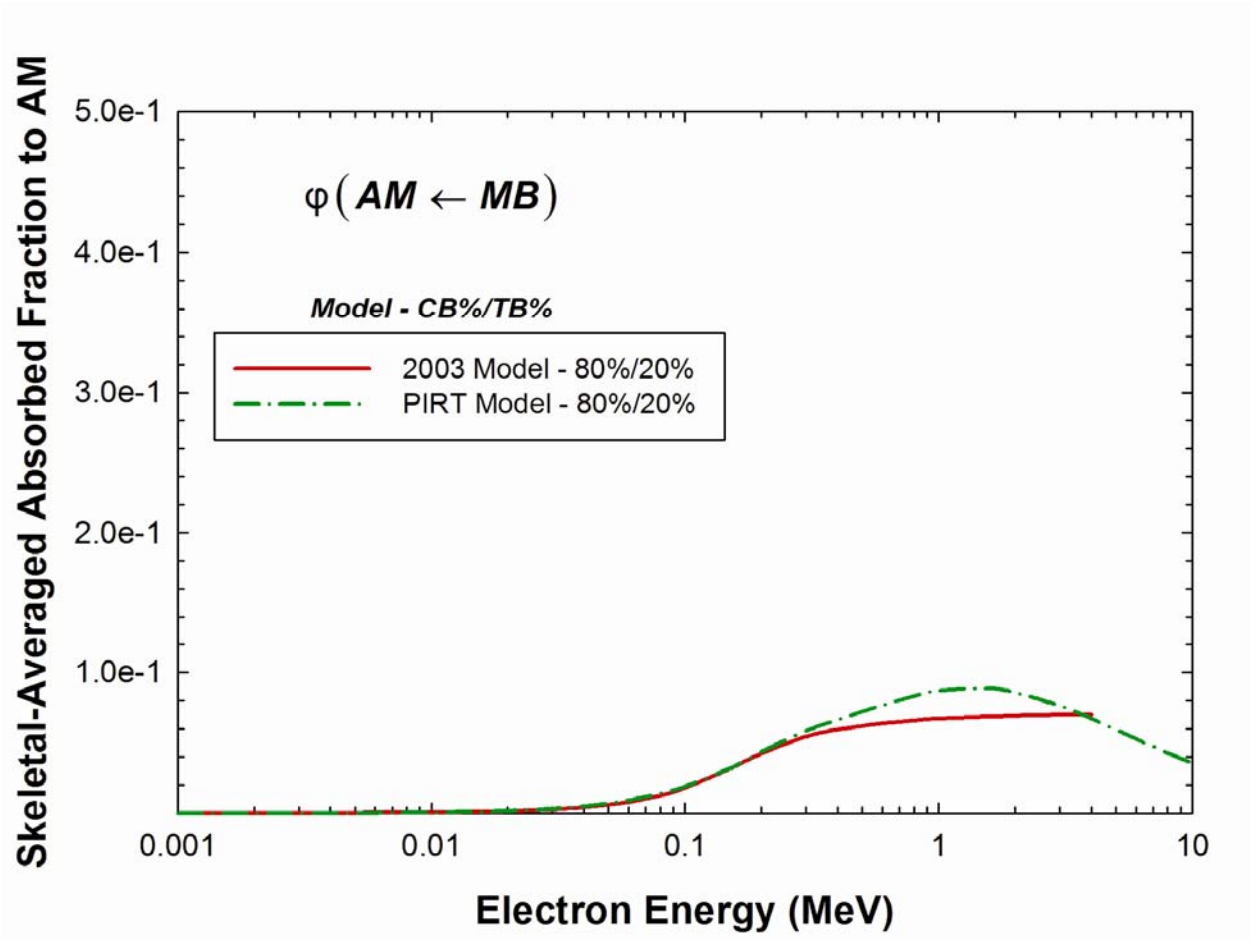

Figure 4-5. Comparison between the 2003 and *PIRT* 15 year-old female skeletal-averaged absorbed fraction data to an *AM* target at ICRP reference cellularity from the mineral bone (*MB*) source at 80% cortical and 20% trabecular bone.

Table 4-1. Bone volumes given in the hybrid-NURBS/PM models and in the reconstructed hybrid-voxel models of the 15-year female (left) and male (right) skeletons for (1) the combined tissues of cortical bone and trabecular spongiosa, (2) outer layers of bone-associated cartilage, and (3) total volume of all tissues.

	Polygon Mesh/NURBS Volumes - Female			Polygon Mesh/NURBS Volumes - Male		
Skeletal Site	**Cortical Bone + Spongiosa (cm^3)**	**Cartilage Bone-Associated (cm^3)**	**[1]Total Homogeneous Bone (cm^3)**	**Cortical Bone + Spongiosa (cm^3)**	**Cartilage Bone-Associated (cm^3)**	**[1]Total Homogeneous Bone (cm^3)**
Cranium	521.74	0.00	521.74	635.40	0.00	635.40
Mandible	46.74	0.00	46.74	59.01	0.00	59.01
[1]Cervical	75.77	0.00	79.63	60.47	0.00	63.38
[1]Thoracic	226.16	0.00	254.69	250.64	0.00	283.41
[1]Lumbar	237.23	0.00	263.97	216.64	0.00	240.13
[1]Sternum	31.41	32.17	63.58	45.21	28.49	73.70
[1,2]Ribs	266.19	0.00	322.24	244.50	0.00	295.32
Scapulae	198.99	0.00	198.99	144.73	0.00	144.73
Clavicles	52.13	0.00	52.13	39.89	0.00	39.89
Os coxae	564.83	0.00	564.83	507.30	0.00	507.30
Sacrum	165.40	0.00	165.40	135.42	0.00	135.42
Humeri, Proximal	124.31	0.00	124.31	156.31	0.00	156.31
Humeri, Upper Shaft	63.58	0.00	63.58	78.56	0.00	78.56
Humeri, Lower Shaft	55.49	0.00	55.49	69.79	0.00	69.79
Humeri, Distal	75.07	0.00	75.07	94.85	0.00	94.85
Radii, Proximal	11.64	0.00	11.64	15.34	0.00	15.34
Radii, Shaft	42.43	0.00	42.43	47.71	0.00	47.71
Radii, Distal	21.25	0.00	21.25	28.03	0.00	28.03
Ulnae, Proximal	39.98	0.00	39.98	51.38	0.00	51.38
Ulnae, Shaft	50.45	0.00	50.45	58.23	0.00	58.23
Ulnae, Distal	7.27	0.00	7.27	9.54	0.00	9.54
Wrists and Hands	102.51	0.00	102.51	124.46	0.00	124.46
Femora, Proximal	177.45	0.00	177.45	231.67	0.00	231.67
Femora, Upper Shaft	126.58	0.00	126.58	172.52	0.00	172.52
Femora, Lower Shaft	143.03	0.00	143.03	131.36	0.00	131.36
Femora, Distal	240.98	0.00	240.98	270.05	0.00	270.05
Patellae	25.32	0.00	25.32	31.29	0.00	31.29
Tibiae, Proximal	190.51	0.00	190.51	219.28	0.00	219.28
Tibiae, Shaft	167.83	0.00	167.83	201.16	0.00	201.16
Tibiae, Distal	69.17	0.00	69.17	80.32	0.00	80.32
Fibulae, Proximal	15.75	0.00	15.75	20.03	0.00	20.03
Fibulae, Shaft	24.78	0.00	24.78	34.18	0.00	34.18
Fibulae, Distal	15.17	0.00	15.17	19.32	0.00	19.32
Ankles and Feet	366.55	0.00	366.55	458.56	0.00	458.56
Cranial Cartilage	N/A	0.00	0.00	N/A	0.00	0.00
Costal Cartilage	N/A	56.06	56.06	N/A	50.82	50.82
CV Intervertebral Discs	N/A	3.86	3.86	N/A	2.91	2.91
TV Intervertebral Discs	N/A	28.53	28.53	N/A	32.77	32.77
LV Intervertebral Discs	N/A	26.73	26.73	N/A	23.49	23.49
Total Skeleton (cm^3)	4543.68	147.34	4806.20	4943.17	138.48	5191.64
Mass(g)	6180.02	162.08	6367.85	6743.09	152.33	6926.10
Reference Mass (g)	6225.00	920.00	7145.00	6765.00	1140.00	7905.00
Ratio	0.99	0.18	0.89	0.99676	0.13362	0.88

[1]Total bone includes contributions of costal, intervertebral disc cartilage, bone-associated sternal, and all non-bone associated estimates.

[2]This volume is NURBS, while all others are polygon mesh

Table 4-2. Comparison of the 18-year segmented and iterated 15-year male and female bone tissue volume fractions by bone site.

	18-Year Old Male		15-Year Female		15-Year Male		18-Year Old Male	
Skeletal Site	**SVF - Segmented**	**CBVF - Segmented**	**SVF - Iterated**	**CBVF - Iterated**	**SVF - Iterated**	**CBVF - Iterated**	**MVF**	**BVF**
[1]Cranium	0.5006	0.4994	0.5221	0.4779	0.5279	0.4721	0.6807	0.3193
Mandible	0.4189	0.5811	0.4404	0.5596	0.4462	0.5538	0.7173	0.2827
[2]Cervical	0.6649	0.3351	0.6864	0.3136	0.6922	0.3078	0.8400	0.1601
[3]Thoracic	0.7728	0.2272	0.7943	0.2057	0.8001	0.1999	0.8720	0.1280
[4]Lumbar	0.8823	0.1177	0.9038	0.0962	0.9096	0.0904	0.8940	0.1060
Sternum	0.7023	0.2977	0.7238	0.2762	0.7296	0.2704	0.9066	0.0934
[5]Ribs	0.5910	0.4090	0.6125	0.3875	0.6183	0.3817	0.8792	0.1208
Right Scapula	0.4985	0.5015	0.5200	0.4800	0.5258	0.4742	0.6935	0.3065
Right Clavicle	0.3742	0.6258	0.3957	0.6043	0.4015	0.5985	0.8243	0.1757
[6]Os coxae	0.7677	0.2323	0.7892	0.2108	0.7950	0.2050	0.8949	0.1051
Sacrum	0.6890	0.3110	0.7105	0.2895	0.7163	0.2837	0.9437	0.0563
Humerii, Right Proximal	0.8221	0.1779	0.8436	0.1564	0.8494	0.1506	0.8448	0.1552
[7]Humerii, Upper Shaft	0.1979	0.8021	0.2194	0.7806	0.2252	0.7748	1.0000	0.0000
[7]Humerii, Lower Shaft	0.1979	0.8021	0.2194	0.7806	0.2252	0.7748	1.0000	0.0000
Humerii, Right Distal	0.5684	0.4316	0.5899	0.4101	0.5957	0.4043	0.7847	0.2153
Radii, Right Proximal	0.6043	0.3957	0.6258	0.3742	0.6316	0.3684	0.7939	0.2061
Radii, Shaft	0.1105	0.8895	0.1320	0.8680	0.1378	0.8622	1.0000	0.0000
Radii, Right Distal	0.7225	0.2775	0.7440	0.2560	0.7498	0.2502	0.8035	0.1965
Ulna, Right Proximal	0.6676	0.3324	0.6891	0.3109	0.6949	0.3051	0.7462	0.2538
Ulna, Shaft	0.1163	0.8837	0.1378	0.8622	0.1436	0.8564	1.0000	0.0000
Ulna, Right Distal	0.6516	0.3484	0.6731	0.3269	0.6789	0.3211	0.8140	0.1860
[8]Wrist and Hands	0.3940	0.6060	0.4155	0.5845	0.4213	0.5787	0.8792	0.1208
[9]Femora, Proximal	0.7728	0.2272	0.7943	0.2057	0.8001	0.1999	0.7936	0.2064
[7]Femora, Upper Shaft	0.2343	0.7657	0.2558	0.7442	0.2616	0.7384	1.0000	0.0000
[7]Femora, Lower Shaft	0.2343	0.7657	0.2558	0.7442	0.2616	0.7384	1.0000	0.0000
Femora, Distal	0.8345	0.1655	0.8560	0.1440	0.8618	0.1382	0.7221	0.2779
[8]Patella	0.5951	0.4049	0.6166	0.3834	0.6224	0.3776	0.8792	0.1208
Tibia, Proximal	0.7194	0.2806	0.7409	0.2591	0.7467	0.2533	0.9050	0.0950
Tibia, Shaft	0.2672	0.7328	0.2887	0.7113	0.2945	0.7055	1.0000	0.0000
Tibia, Distal	0.8135	0.1865	0.8350	0.1650	0.8408	0.1592	0.8146	0.1854
Fibula, Proximal	0.6282	0.3718	0.6497	0.3503	0.6555	0.3445	0.8485	0.1515
Fibula, Shaft	0.2115	0.7885	0.2330	0.7670	0.2387	0.7613	1.0000	0.0000
Fibula, Distal	0.6130	0.3870	0.6345	0.3655	0.6403	0.3597	0.7349	0.2651
[8]Ankles and Feet	0.7114	0.2886	0.7329	0.2671	0.7387	0.2613	0.8792	0.1208

[1]The MVF is a inear average between occipital, frontal, parietal (+/- 2.06%)

[2]The MVF is a linear average between C_3 and C_6 (+/- 2.23%)

[3]The MVF is a linear average between T_1, T_3, T_6, T_9, and T_{12} (+/- 1.74%)

[4]The MVF is a linear average between L_1,L_2, L_3, L_4, and L_5 (+/- 2.01%)

[5]The MVF is a linear average between the upper (rib-1), middle (rib-6), and lower right (rib-12) rib (+/- 3.04%)

[6]The MVF was calculated from the right ilium

[7]The SVF for the upper shaft was segmented and assumed to be the same for the lower shaft

[8]The MVF for the rib was used as a surrogate

[9]The MVF is a linear average of the right and left head and neck (+/- 3.46%)

Table 4-3. Masses and volumes of site-specific miscellaneous skeletal tissue in the 15-year female phantom. *MST* – miscellaneous skeletal tissue, *MB* – mineral bone, *AM* – active marrow, *IM* – inactive marrow, *CB* – cortical bone, *TB* – trabecular bone.

Skeletal Site	Total MST Volume (cm^3)	Total MST Mass (g)	MST In MB Volume (cm^3)	MST In MB Mass (g)	MST In AM Volume (cm^3)	MST In AM Mass (g)	MST In IM Volume (cm^3)	MST In IM Mass (g)	MST In CB Volume (cm^3)	MST In CB Mass (g)	MST In TB Volume (cm^3)	MST In TB Mass (g)
Cranium	16.32	16.65	10.52	10.73	3.19	3.25	2.61	2.66	7.80	7.96	2.72	2.78
Mandible	1.46	1.49	1.00	1.02	0.25	0.26	0.21	0.21	0.82	0.83	0.18	0.19
Cervical	2.37	2.42	1.00	1.02	1.03	1.05	0.34	0.35	0.74	0.76	0.26	0.27
Thoracic	7.08	7.22	2.17	2.22	3.68	3.75	1.23	1.25	1.46	1.48	0.72	0.73
Lumbar	7.42	7.57	1.43	1.45	4.50	4.59	1.50	1.53	0.71	0.73	0.71	0.73
Sternum	0.98	1.00	0.34	0.34	0.48	0.49	0.16	0.16	0.27	0.28	0.07	0.07
Ribs	8.33	8.49	3.84	3.92	3.36	3.43	1.12	1.14	3.23	3.29	0.62	0.63
Scapulae	6.23	6.35	3.98	4.06	1.23	1.26	1.01	1.03	2.99	3.05	0.99	1.01
Clavicles	1.63	1.66	1.10	1.12	0.28	0.29	0.25	0.26	0.99	1.01	0.11	0.12
Os coxae	17.67	18.03	5.19	5.29	7.99	8.15	4.49	4.58	3.72	3.80	1.47	1.50
Sacrum	5.17	5.28	1.71	1.74	2.22	2.26	1.25	1.27	1.50	1.53	0.21	0.21
Humeri, Proximal	3.89	3.97	1.12	1.14	1.52	1.55	1.25	1.27	0.61	0.62	0.51	0.52
Humeri, Upper Shaft	1.99	2.03	1.55	1.58	0.15	0.16	0.28	0.29	1.55	1.58	0.00	0.00
Humeri, Lower Shaft	1.74	1.77	1.36	1.38	0.08	0.08	0.30	0.31	1.36	1.38	0.00	0.00
Humeri, Distal	2.35	2.40	1.26	1.29	0.00	0.00	1.09	1.11	0.96	0.98	0.30	0.30
Radii, Proximal	0.36	0.37	0.18	0.19	0.00	0.00	0.18	0.18	0.14	0.14	0.05	0.05
Radii, Shaft	1.33	1.35	1.15	1.18	0.00	0.00	0.18	0.18	1.15	1.18	0.00	0.00
Radii, Distal	0.66	0.68	0.27	0.27	0.00	0.00	0.40	0.41	0.17	0.17	0.10	0.10
Ulnae, Proximal	1.25	1.28	0.61	0.62	0.00	0.00	0.64	0.66	0.39	0.40	0.22	0.22
Ulnae, Shaft	1.58	1.61	1.36	1.39	0.00	0.00	0.22	0.22	1.36	1.39	0.00	0.00
Ulnae, Distal	0.23	0.23	0.10	0.10	0.00	0.00	0.12	0.13	0.07	0.08	0.03	0.03
Wrists and Hands	3.21	3.27	2.04	2.08	0.00	0.00	1.17	1.20	1.87	1.91	0.16	0.16
Femora, Proximal	5.55	5.66	2.05	2.09	1.92	1.96	1.57	1.61	1.14	1.16	0.91	0.93
Femora, Upper Shaft	3.96	4.04	2.95	3.01	0.35	0.36	0.66	0.67	2.95	3.01	0.00	0.00
Femora, Lower Shaft	4.48	4.56	3.33	3.40	0.23	0.23	0.92	0.93	3.33	3.40	0.00	0.00
Femora, Distal	7.54	7.69	2.88	2.94	0.00	0.00	4.66	4.75	1.09	1.11	1.79	1.83
Patellae	0.79	0.81	0.36	0.37	0.00	0.00	0.43	0.44	0.30	0.31	0.06	0.06
Tibiae, Proximal	5.96	6.08	1.96	2.00	0.00	0.00	4.00	4.08	1.54	1.58	0.42	0.43
Tibiae, Shaft	5.25	5.36	3.73	3.81	0.00	0.00	1.52	1.55	3.73	3.81	0.00	0.00
Tibiae, Distal	2.16	2.21	0.69	0.71	0.00	0.00	1.47	1.50	0.36	0.36	0.34	0.34
Fibulae, Proximal	0.49	0.50	0.22	0.23	0.00	0.00	0.27	0.28	0.17	0.18	0.05	0.05
Fibulae, Shaft	0.78	0.79	0.59	0.61	0.00	0.00	0.18	0.18	0.59	0.61	0.00	0.00
Fibulae, Distal	0.47	0.48	0.25	0.26	0.00	0.00	0.22	0.23	0.17	0.18	0.08	0.08
Ankles and Feet	11.47	11.70	4.08	4.16	0.00	0.00	7.39	7.54	3.06	3.12	1.02	1.04
Total Skeleton	142.16	145.00	66.39	67.72	32.48	33.13	43.29	44.16	52.31	53.36	14.08	14.36
ICRP 89 Reference	142.16	145.00										
Ratio	1.00	1.00										

Table 4-4. Masses and volumes of site-specific miscellaneous skeletal tissue in the 15-year male phantom. *MST* – miscellaneous skeletal tissue, *MB* – mineral bone, *AM* – active marrow, *IM* – inactive marrow, *CB* – cortical bone, *TB* – trabecular bone.

Skeletal Site	Total MST Volume (cm^3)	Total MST Mass (g)	MST In MB Volume (cm^3)	MST In MB Mass (g)	MST In AM Volume (cm^3)	MST In AM Mass (g)	MST In IM Volume (cm^3)	MST In IM Mass (g)	MST In CB Volume (cm^3)	MST In CB Mass (g)	MST In TB Volume (cm^3)	MST In TB Mass (g)
Cranium	19.34	19.92	12.39	12.76	3.82	3.94	3.13	3.22	9.13	9.41	3.26	3.36
Mandible	1.80	1.85	1.22	1.26	0.32	0.33	0.26	0.27	0.99	1.02	0.23	0.23
Cervical	1.84	1.90	0.77	0.79	0.80	0.83	0.27	0.28	0.57	0.58	0.20	0.21
Thoracic	7.63	7.86	2.31	2.38	3.99	4.11	1.33	1.37	1.53	1.57	0.78	0.80
Lumbar	6.60	6.79	1.23	1.27	4.02	4.14	1.34	1.38	0.60	0.61	0.64	0.66
Sternum	1.38	1.42	0.47	0.48	0.68	0.70	0.23	0.23	0.37	0.38	0.09	0.10
Ribs	7.44	7.67	3.40	3.50	3.03	3.13	1.01	1.04	2.84	2.93	0.56	0.57
Scapulae	4.41	4.54	2.80	2.88	0.88	0.91	0.72	0.74	2.09	2.15	0.71	0.73
Clavicles	1.21	1.25	0.81	0.84	0.21	0.22	0.19	0.19	0.73	0.75	0.09	0.09
Os coxae	15.44	15.91	4.46	4.59	7.03	7.24	3.96	4.07	3.17	3.26	1.29	1.33
Sacrum	4.12	4.25	1.34	1.38	1.78	1.84	1.00	1.03	1.17	1.20	0.17	0.17
Humeri, Proximal	4.76	4.90	1.34	1.38	1.88	1.93	1.54	1.58	0.72	0.74	0.63	0.65
Humeri, Upper Shaft	2.39	2.46	1.85	1.91	0.19	0.19	0.35	0.36	1.85	1.91	0.00	0.00
Humeri, Lower Shaft	2.12	2.19	1.65	1.70	0.10	0.10	0.38	0.39	1.65	1.70	0.00	0.00
Humeri, Distal	2.89	2.97	1.54	1.58	0.00	0.00	1.35	1.39	1.17	1.20	0.37	0.38
Radii, Proximal	0.47	0.48	0.23	0.24	0.00	0.00	0.23	0.24	0.17	0.18	0.06	0.06
Radii, Shaft	1.45	1.50	1.25	1.29	0.00	0.00	0.20	0.21	1.25	1.29	0.00	0.00
Radii, Distal	0.85	0.88	0.34	0.35	0.00	0.00	0.51	0.53	0.21	0.22	0.13	0.13
Ulnae, Proximal	1.56	1.61	0.75	0.78	0.00	0.00	0.81	0.84	0.48	0.49	0.28	0.28
Ulnae, Shaft	1.77	1.83	1.52	1.56	0.00	0.00	0.25	0.26	1.52	1.56	0.00	0.00
Ulnae, Distal	0.29	0.30	0.13	0.13	0.00	0.00	0.16	0.17	0.09	0.10	0.04	0.04
Wrists and Hands	3.79	3.90	2.39	2.46	0.00	0.00	1.40	1.45	2.19	2.26	0.19	0.20
Femora, Proximal	7.05	7.26	2.57	2.65	2.46	2.54	2.02	2.08	1.41	1.45	1.16	1.20
Femora, Upper Shaft	5.25	5.41	3.88	3.99	0.48	0.50	0.89	0.92	3.88	3.99	0.00	0.00
Femora, Lower Shaft	4.00	4.12	2.95	3.04	0.21	0.22	0.84	0.86	2.95	3.04	0.00	0.00
Femora, Distal	8.22	8.47	3.10	3.20	0.00	0.00	5.12	5.27	1.14	1.17	1.97	2.03
Patellae	0.95	0.98	0.43	0.44	0.00	0.00	0.52	0.54	0.36	0.37	0.07	0.07
Tibiae, Proximal	6.68	6.88	2.16	2.23	0.00	0.00	4.51	4.65	1.69	1.74	0.47	0.49
Tibiae, Shaft	6.12	6.31	4.32	4.45	0.00	0.00	1.80	1.86	4.32	4.45	0.00	0.00
Tibiae, Distal	2.45	2.52	0.77	0.79	0.00	0.00	1.67	1.73	0.39	0.40	0.38	0.39
Fibulae, Proximal	0.61	0.63	0.27	0.28	0.00	0.00	0.34	0.35	0.21	0.22	0.06	0.06
Fibulae, Shaft	1.04	1.07	0.79	0.82	0.00	0.00	0.25	0.26	0.79	0.82	0.00	0.00
Fibulae, Distal	0.59	0.61	0.31	0.32	0.00	0.00	0.28	0.29	0.21	0.22	0.10	0.10
Ankles and Feet	13.96	14.38	4.89	5.04	0.00	0.00	9.07	9.34	3.65	3.76	1.25	1.28
Total Skeleton	150.49	155.00	70.65	72.77	31.90	32.86	47.94	49.37	55.48	57.15	15.17	15.62
ICRP 89 Reference	150.49	155.00										
Ratio	1.00	1.00										

Table 4-5. Site-specific active marrow volumes and masses of skeletal tissues in the 15-year female hybrid phantom including and then excluding contributions from miscellaneous skeletal tissues.

	Excluding MST						Including MST					
Skeletal Site	**TAM Volume (cm^3)**	**TAM Mass (g)**	**TIM Volume (cm^3)**	**TIM Mass (g)**	**TMS Volume (cm^3)**	**TMS Mass (g)**	**TAM* Volume (cm^3)**	**TAM* Mass (g)**	**TIM* Volume (cm^3)**	**TIM* Mass (g)**	**TMS* Volume (cm^3)**	**TMS* Mass (g)**
Cranium	98.79	101.75	80.82	79.21	179.61	180.96	101.98	105.00	83.44	81.87	185.41	186.87
Mandible	7.87	8.10	6.44	6.31	14.30	14.41	8.12	8.36	6.64	6.52	14.76	14.88
Cervical	31.74	32.69	10.58	10.37	42.32	43.06	32.76	33.74	10.92	10.72	43.69	44.45
Thoracic	113.82	117.23	37.94	37.18	151.76	154.41	117.49	120.98	39.16	38.43	156.66	159.41
Lumbar	139.26	143.43	46.42	45.49	185.68	188.92	143.75	148.02	47.92	47.02	191.67	195.04
Sternum	14.98	15.42	4.99	4.89	19.97	20.32	15.46	15.92	5.15	5.06	20.61	20.97
Ribs	104.14	107.27	34.71	34.02	138.86	141.29	107.51	110.70	35.84	35.16	143.34	145.86
Scapulae	38.24	39.38	31.28	30.66	69.52	70.04	39.47	40.64	32.29	31.69	71.76	72.33
Clavicles	8.56	8.82	7.91	7.75	16.47	16.57	8.84	9.10	8.16	8.01	17.00	17.11
Os coxae	247.33	254.75	139.12	136.34	386.45	391.09	255.32	262.90	143.62	140.92	398.93	403.82
Sacrum	68.75	70.82	38.67	37.90	107.43	108.72	70.97	73.08	39.92	39.17	110.90	112.26
Humeri, Proximal	47.20	48.61	38.62	37.84	85.82	86.46	48.72	50.17	39.86	39.12	88.59	89.29
Humeri, Upper Shaft	4.73	4.87	8.78	8.61	13.51	13.48	4.88	5.03	9.07	8.90	13.95	13.93
Humeri, Lower Shaft	2.36	2.43	9.43	9.25	11.79	11.68	2.43	2.51	9.74	9.56	12.17	12.06
Humeri, Distal	0.00	0.00	33.67	32.99	33.67	32.99	0.00	0.00	34.75	34.10	34.75	34.10
Radii, Proximal	0.00	0.00	5.60	5.49	5.60	5.49	0.00	0.00	5.79	5.68	5.79	5.68
Radii, Shaft	0.00	0.00	5.43	5.32	5.43	5.32	0.00	0.00	5.60	5.50	5.60	5.50
Radii, Distal	0.00	0.00	12.30	12.06	12.30	12.06	0.00	0.00	12.70	12.46	12.70	12.46
Ulnae, Proximal	0.00	0.00	19.91	19.51	19.91	19.51	0.00	0.00	20.56	20.17	20.56	20.17
Ulnae, Shaft	0.00	0.00	6.73	6.60	6.73	6.60	0.00	0.00	6.95	6.82	6.95	6.82
Ulnae, Distal	0.00	0.00	3.86	3.78	3.86	3.78	0.00	0.00	3.98	3.91	3.98	3.91
Wrists and Hands	0.00	0.00	36.28	35.55	36.28	35.55	0.00	0.00	37.45	36.75	37.45	36.75
Femora, Proximal	59.60	61.39	48.76	47.79	108.36	109.17	61.52	63.35	50.34	49.39	111.86	112.74
Femora, Upper Shaft	10.98	11.31	20.39	19.98	31.37	31.29	11.33	11.67	21.05	20.65	32.38	32.32
Femora, Lower Shaft	7.09	7.30	28.36	27.79	35.45	35.09	7.32	7.54	29.27	28.72	36.59	36.26
Femora, Distal	0.00	0.00	144.30	141.41	144.30	141.41	0.00	0.00	148.96	146.17	148.96	146.17
Patellae	0.00	0.00	13.30	13.03	13.30	13.03	0.00	0.00	13.73	13.47	13.73	13.47
Tibiae, Proximal	0.00	0.00	123.75	121.28	123.75	121.28	0.00	0.00	127.75	125.35	127.75	125.35
Tibiae, Shaft	0.00	0.00	46.93	46.00	46.93	46.00	0.00	0.00	48.45	47.54	48.45	47.54
Tibiae, Distal	0.00	0.00	45.58	44.67	45.58	44.67	0.00	0.00	47.05	46.17	47.05	46.17
Fibulae, Proximal	0.00	0.00	8.41	8.24	8.41	8.24	0.00	0.00	8.68	8.52	8.68	8.52
Fibulae, Shaft	0.00	0.00	5.59	5.48	5.59	5.48	0.00	0.00	5.77	5.66	5.77	5.66
Fibulae, Distal	0.00	0.00	6.85	6.72	6.85	6.72	0.00	0.00	7.07	6.94	7.07	6.94
Ankles and Feet	0.00	0.00	228.81	224.23	228.81	224.23	0.00	0.00	236.20	231.77	236.20	231.77
Total	1005.42	1035.58	1340.55	1313.74	2345.97	2349.32	1037.90	1068.71	1383.84	1357.90	2421.74	2426.60
ICRP 89 Reference Values	970.87	1000.00	1408.16	1380.00	2379.04	2380.00	1003.35	1033.13	1451.45	1424.16	2454.81	2457.28
Ratio	1.04	1.04	0.95	0.95	0.99	0.99	1.03	1.03	0.95	0.95	0.99	0.99

Table 4-6. Site-specific active marrow volumes and masses of skeletal tissues in the 15-year male hybrid phantom including and then excluding contributions from miscellaneous skeletal tissues.

	Excluding MST						Including MST					
Skeletal Site	**TAM Volume (cm^3)**	**TAM Mass (g)**	**TIM Volume (cm^3)**	**TIM Mass (g)**	**TMS Volume (cm^3)**	**TMS Mass (g)**	**TAM* Volume (cm^3)**	**TAM* Mass (g)**	**TIM* Volume (cm^3)**	**TIM* Mass (g)**	**TMS* Volume (cm^3)**	**TMS* Mass (g)**
Cranium	121.75	125.40	99.61	97.62	221.36	223.02	125.57	129.34	102.74	100.84	228.31	230.18
Mandible	10.07	10.37	8.24	8.08	18.31	18.45	10.39	10.70	8.50	8.34	18.89	19.04
Cervical	25.57	26.33	8.52	8.35	34.09	34.68	26.37	27.16	8.79	8.63	35.16	35.79
Thoracic	127.16	130.98	42.39	41.54	169.55	172.52	131.16	135.09	43.72	42.91	174.88	178.00
Lumbar	128.09	131.93	42.70	41.84	170.79	173.78	132.11	136.08	44.04	43.22	176.15	179.30
Sternum	21.75	22.40	7.25	7.10	29.00	29.51	22.43	23.10	7.48	7.34	29.91	30.44
Ribs	96.65	99.55	32.22	31.57	128.87	131.12	99.68	102.67	33.23	32.61	132.91	135.29
Scapulae	28.14	28.99	23.03	22.57	51.17	51.55	29.03	29.90	23.75	23.31	52.78	53.21
Clavicles	6.65	6.85	6.15	6.02	12.80	12.87	6.86	7.07	6.34	6.22	13.20	13.29
Os coxae	223.96	230.68	125.98	123.46	349.94	354.14	230.99	237.92	129.93	127.53	360.93	365.46
Sacrum	56.80	58.50	31.95	31.31	88.75	89.81	58.58	60.34	32.95	32.34	91.53	92.68
Humeri, Proximal	59.81	61.60	48.93	47.95	108.74	109.56	61.68	63.54	50.47	49.54	112.15	113.07
Humeri, Upper Shaft	6.00	6.18	11.15	10.93	17.15	17.11	6.19	6.38	11.50	11.29	17.69	17.67
Humeri, Lower Shaft	3.05	3.14	12.19	11.95	15.24	15.09	3.14	3.24	12.57	12.34	15.72	15.58
Humeri, Distal	0.00	0.00	42.99	42.13	42.99	42.13	0.00	0.00	44.34	43.52	44.34	43.52
Radii, Proximal	0.00	0.00	7.46	7.31	7.46	7.31	0.00	0.00	7.69	7.55	7.69	7.55
Radii, Shaft	0.00	0.00	6.37	6.25	6.37	6.25	0.00	0.00	6.57	6.45	6.57	6.45
Radii, Distal	0.00	0.00	16.37	16.05	16.37	16.05	0.00	0.00	16.89	16.58	16.89	16.58
Ulnae, Proximal	0.00	0.00	25.83	25.31	25.83	25.31	0.00	0.00	26.64	26.15	26.64	26.15
Ulnae, Shaft	0.00	0.00	8.11	7.94	8.11	7.94	0.00	0.00	8.36	8.21	8.36	8.21
Ulnae, Distal	0.00	0.00	5.11	5.01	5.11	5.01	0.00	0.00	5.27	5.18	5.27	5.18
Wrists and Hands	0.00	0.00	44.70	43.81	44.70	43.81	0.00	0.00	46.11	45.25	46.11	45.25
Femora, Proximal	78.44	80.80	64.18	62.90	142.63	143.69	80.91	83.33	66.20	64.97	147.10	148.31
Femora, Upper Shaft	15.32	15.78	28.44	27.87	43.76	43.65	15.80	16.27	29.34	28.79	45.13	45.06
Femora, Lower Shaft	6.66	6.86	26.65	26.12	33.32	32.99	6.87	7.08	27.49	26.98	34.36	34.06
Femora, Distal	0.00	0.00	162.94	159.69	162.94	159.69	0.00	0.00	168.06	164.96	168.06	164.96
Patellae	0.00	0.00	16.60	16.27	16.60	16.27	0.00	0.00	17.12	16.81	17.12	16.81
Tibiae, Proximal	0.00	0.00	143.67	140.80	143.67	140.80	0.00	0.00	148.19	145.45	148.19	145.45
Tibiae, Shaft	0.00	0.00	57.44	56.29	57.44	56.29	0.00	0.00	59.24	58.14	59.24	58.14
Tibiae, Distal	0.00	0.00	53.34	52.27	53.34	52.27	0.00	0.00	55.02	54.00	55.02	54.00
Fibulae, Proximal	0.00	0.00	10.80	10.59	10.80	10.59	0.00	0.00	11.14	10.94	11.14	10.94
Fibulae, Shaft	0.00	0.00	7.91	7.75	7.91	7.75	0.00	0.00	8.16	8.01	8.16	8.01
Fibulae, Distal	0.00	0.00	8.82	8.64	8.82	8.64	0.00	0.00	9.09	8.92	9.09	8.92
Ankles and Feet	0.00	0.00	288.75	282.98	288.75	282.98	0.00	0.00	297.82	292.32	297.82	292.32
Total	1015.88	1046.35	1526.81	1496.27	2542.68	2542.62	1047.78	1079.21	1574.74	1545.64	2622.52	2624.86
ICRP 89 Reference Values	1048.54	1080.00	1510.20	1480.00	2558.75	2560.00	1080.45	1112.86	1558.14	1529.37	2638.59	2642.23
Ratio	0.97	0.97	1.01	1.01	0.99	0.99	0.97	0.97	1.01	1.01	0.99	0.99

*Denotes inclusion of associated miscellaneous skeletal tissue volumes and masses

Table 4-7. Comparison of site-specific active marrow distribution between the UF 15-year female (left) and male (right) hybrid phantoms and reference values given in ICRP Publication 89.

	Female				Male			
Skeletal Site	**NURBS/Polygon Mesh (%)**	**ICRP 89, Table 9.4 (%)**	**Difference (abs. %)**	**Ratio NURBS/ICRP**	**NURBS/Polygon Mesh (%)**	**ICRP 89, Table 9.4 (%)**	**Difference (abs. %)**	**Ratio NURBS/ICRP**
Cranium	9.83	9.19	0.63	1.07	11.98	9.19	2.79	1.30
Mandible	0.78	0.90	-0.12	0.87	0.99	0.90	0.09	1.10
Cervical	3.16	3.30	-0.14	0.96	2.52	3.30	-0.78	0.76
Thoracic	11.32	13.69	-2.37	0.83	12.52	13.69	-1.17	0.91
Lumbar	13.85	10.49	3.36	1.32	12.61	10.49	2.12	1.20
Sternum	1.49	2.70	-1.21	0.55	2.14	2.70	-0.56	0.79
Ribs	10.36	13.59	-3.23	0.76	9.51	13.59	-4.07	0.70
Scapulae	3.80	3.30	0.51	1.15	2.77	3.30	-0.53	0.84
Clavicles	0.85	1.00	-0.15	0.85	0.66	1.00	-0.34	0.66
Os coxae	24.60	18.48	6.12	1.33	22.05	18.48	3.56	1.19
Sacrum	6.84	8.39	-1.55	0.81	5.59	8.39	-2.80	0.67
Humeri, Proximal	4.69	3.10	2.07	1.67	5.89	3.10	3.38	2.09
Humeri, Upper Shaft	0.47				0.59			
Humeri, Lower Shaft	0.23	0.70	-0.46	0.34	0.30	0.70	-0.40	0.43
Humeri, Distal	0.00				0.00			
Radii, Proximal	0.00				0.00			
Radii, Shaft	0.00	0.00	0.00	1.00	0.00	0.00	0.00	1.00
Radii, Distal	0.00				0.00			
Ulnae, Proximal	0.00				0.00			
Ulnae, Shaft	0.00	0.00	0.00	1.00	0.00	0.00	0.00	1.00
Ulnae, Distal	0.00				0.00			
Wrists and Hands	0.00	0.00	0.00	1.00	0.00	0.00	0.00	1.00
Femora, Proximal	5.93	9.19	-2.17	0.76	7.72	9.19	0.04	1.00
Femora, Upper Shaft	1.09				1.51			
Femora, Lower Shaft	0.71	2.00	-1.29	0.35	0.66	2.00	-1.34	0.33
Femora, Distal	0.00				0.00			
Patellae	0.00	0.00	0.00	1.00	0.00	0.00	0.00	1.00
Tibiae, Proximal	0.00				0.00			
Tibiae, Shaft	0.00	0.00	0.00	1.00	0.00	0.00	0.00	1.00
Tibiae, Distal	0.00				0.00			
Fibulae, Proximal	0.00				0.00			
Fibulae, Shaft	0.00	0.00	0.00	1.00	0.00	0.00	0.00	1.00
Fibulae, Distal	0.00				0.00			
Ankles and Feet	0.00	0.00	0.00	1.00	0.00	0.00	0.00	1.00
Total	100.00	100.00	0.00		100.00	100.00	0.00	

Table 4-8. Masses, volumes, and percent distribution of cartilage by bone site in the UF 15-year female (left) and male (right) phantoms.

	Female			Male		
Skeletal Site	**Cartilage Volume (cm^3)**	**Cartilage Mass (g)**	**% Distribution**	**Cartilage Volume (cm^3)**	**Cartilage Mass (g)**	**% Distribution**
Cranium	0.00	0.00	0.00	0.00	0.00	0.00
Mandible	0.00	0.00	0.00	0.00	0.00	0.00
Cervical	0.00	0.00	0.00	0.00	0.00	0.00
Thoracic	0.00	0.00	0.00	0.00	0.00	0.00
Lumbar	0.00	0.00	0.00	0.00	0.00	0.00
Sternum	32.17	35.39	18.84	28.49	31.33	14.60
Ribs	0.00	0.00	0.00	0.00	0.00	0.00
Scapulae	0.00	0.00	0.00	0.00	0.00	0.00
Clavicles	0.00	0.00	0.00	0.00	0.00	0.00
Os coxae	0.00	0.00	0.00	0.00	0.00	0.00
Sacrum	0.00	0.00	0.00	0.00	0.00	0.00
Humeri, Proximal	0.00	0.00	0.00	0.00	0.00	0.00
Humeri, Upper Shaft	0.00	0.00	0.00	0.00	0.00	0.00
Humeri, Lower Shaft	0.00	0.00	0.00	0.00	0.00	0.00
Humeri, Distal	0.00	0.00	0.00	0.00	0.00	0.00
Radii, Proximal	0.00	0.00	0.00	0.00	0.00	0.00
Radii, Shaft	0.00	0.00	0.00	0.00	0.00	0.00
Radii, Distal	0.00	0.00	0.00	0.00	0.00	0.00
Ulnae, Proximal	0.00	0.00	0.00	0.00	0.00	0.00
Ulnae, Shaft	0.00	0.00	0.00	0.00	0.00	0.00
Ulnae, Distal	0.00	0.00	0.00	0.00	0.00	0.00
Wrists and Hands	0.00	0.00	0.00	0.00	0.00	0.00
Femora, Proximal	0.00	0.00	0.00	0.00	0.00	0.00
Femora, Upper Shaft	0.00	0.00	0.00	0.00	0.00	0.00
Femora, Lower Shaft	0.00	0.00	0.00	0.00	0.00	0.00
Femora, Distal	0.00	0.00	0.00	0.00	0.00	0.00
Patellae	0.00	0.00	0.00	0.00	0.00	0.00
Tibiae, Proximal	0.00	0.00	0.00	0.00	0.00	0.00
Tibiae, Shaft	0.00	0.00	0.00	0.00	0.00	0.00
Tibiae, Distal	0.00	0.00	0.00	0.00	0.00	0.00
Fibulae, Proximal	0.00	0.00	0.00	0.00	0.00	0.00
Fibulae, Shaft	0.00	0.00	0.00	0.00	0.00	0.00
Fibulae, Distal	0.00	0.00	0.00	0.00	0.00	0.00
Ankles and Feet	0.00	0.00	0.00	0.00	0.00	0.00
Cranial Cartilage	0.00	0.00	0.00	0.00	0.00	0.00
Costal Cartilage	56.06	61.66	32.83	79.58	87.54	40.78
CV Intervertebral Discs	3.86	4.24	2.26	2.91	3.20	1.49
TV Intervertebral Discs	28.53	31.38	16.71	32.77	36.05	16.79
LV Intervertebral Discs	26.73	29.40	15.65	23.49	25.84	12.04
[1]External Nose	1.47	1.61	0.86	1.92	2.11	0.99
[2]Ears	8.36	9.20	4.90	8.36	9.20	4.29
[3]Extrapulmonary Bronchi	3.7	4.10	2.18	3.75	4.13	1.92
[3]Larynx	7.04	7.74	4.12	10.34	11.37	5.30
[3]Trachea	2.82	3.10	1.65	3.52	3.87	1.80
Total Skeleton (Only Bone-Associated Cartilage)	147.34	162.08	100.00	167.24	183.96	100.00
Total Skeleton (All Cartilage)	170.76	187.83		195.13	214.64	
ICRP 89 Reference	836.36	920.00		1036.36	1140.00	
Ratio (All Cartilage)	0.20	0.20		0.19	0.19	

[1] 33.3333% of total NURBS volume contains cartilage

[2] 100% of NURBS volume contains cartilage

[3] 50% of NURBS volume contains cartilage

Table 4-9. Site-specific trabecular and cortical bone volumes and mass including and excluding *MST* in the 15-year female hybrid phantom.

	Including MST				Excluding MST			
Skeletal Site	**Trabecular Bone* Volume (cm^3)**	**Trabecular Bone* Mass (g)**	**Cortical Bone* Volume (cm^3)**	**Cortical Bone* Mass (g)**	**Trabecular Bone Volume (cm^3)**	**Trabecular Bone Mass (g)**	**Cortical Bone Volume (cm^3)**	**Cortical Bone Mass (g)**
Cranium	86.99	154.45	249.34	442.73	84.26	151.68	241.54	434.77
Mandible	5.82	10.33	26.15	46.44	5.64	10.15	25.34	45.60
Cervical	8.32	14.78	23.76	42.19	8.06	14.51	23.02	41.43
Thoracic	22.99	40.82	46.51	82.59	22.27	40.09	45.06	81.11
Lumbar	22.74	40.37	22.83	40.53	22.02	39.64	22.11	39.80
Sternum	2.12	3.77	8.67	15.40	2.06	3.70	8.40	15.13
Ribs	19.69	34.96	103.15	183.16	19.07	34.33	99.92	179.86
Scapulae	31.72	56.32	95.51	169.59	30.72	55.30	92.52	166.54
Clavicles	3.62	6.44	31.50	55.94	3.51	6.32	30.52	54.93
Os coxae	46.85	83.19	119.05	211.38	45.39	81.70	115.32	207.58
Sacrum	6.62	11.75	47.89	85.03	6.41	11.54	46.39	83.51
Humeri, Proximal	16.27	28.90	19.45	34.53	15.77	28.38	18.84	33.91
Humeri, Upper Shaft	0.00	0.00	49.63	88.12	0.00	0.00	48.08	86.54
Humeri, Lower Shaft	0.00	0.00	43.31	76.90	0.00	0.00	41.96	75.52
Humeri, Distal	9.54	16.93	30.79	54.66	9.24	16.63	29.82	53.68
Radii, Proximal	1.50	2.67	4.36	7.74	1.45	2.62	4.22	7.60
Radii, Shaft	0.00	0.00	36.83	65.39	0.00	0.00	35.67	64.21
Radii, Distal	3.11	5.52	5.44	9.66	3.01	5.42	5.27	9.49
Ulnae, Proximal	6.99	12.41	12.43	22.07	6.77	12.19	12.04	21.67
Ulnae, Shaft	0.00	0.00	43.50	77.23	0.00	0.00	42.14	75.84
Ulnae, Distal	0.91	1.62	2.37	4.22	0.88	1.59	2.30	4.14
Wrists and Hands	5.14	9.13	59.91	106.38	4.98	8.97	58.04	104.46
Femora, Proximal	29.10	51.66	36.49	64.80	28.19	50.74	35.35	63.63
Femora, Upper Shaft	0.00	0.00	94.20	167.26	0.00	0.00	91.25	164.25
Femora, Lower Shaft	0.00	0.00	106.44	189.00	0.00	0.00	103.11	185.60
Femora, Distal	57.33	101.79	34.69	61.60	55.53	99.96	33.60	60.49
Patellae	1.89	3.35	9.71	17.23	1.83	3.29	9.40	16.92
Tibiae, Proximal	13.41	23.81	49.36	87.64	12.99	23.38	47.81	86.06
Tibiae, Shaft	0.00	0.00	119.38	211.96	0.00	0.00	115.64	208.15
Tibiae, Distal	10.71	19.01	11.41	20.26	10.37	18.67	11.06	19.90
Fibulae, Proximal	1.55	2.75	5.52	9.79	1.50	2.70	5.34	9.62
Fibulae, Shaft	0.00	0.00	19.01	33.75	0.00	0.00	18.41	33.14
Fibulae, Distal	2.55	4.53	5.54	9.84	2.47	4.45	5.37	9.67
Ankles and Feet	32.44	57.61	97.91	173.85	31.43	56.57	94.85	170.73
Total Skeleton	449.92	798.87	1672.03	2968.85	435.84	784.51	1619.72	2915.49
ICRP 89 Reference	N/A	N/A	N/A	N/A	411.11	740.00	1644.44	2960.00
Ratio	N/A	N/A	N/A	N/A	1.06	1.06	0.98	0.98

*Denotes inclusion of associated miscellaneous skeletal tissue volumes and masses

Table 4-10. Site-specific trabecular and cortical bone volumes and mass including and excluding *MST* in the newborn 15-year male phantom.

	Including MST				Excluding MST			
Skeletal Site	**Trabecular Bone* Volume (cm^3)**	**Trabecular Bone* Mass (g)**	**Cortical Bone* Volume (cm^3)**	**Cortical Bone* Mass (g)**	**Trabecular Bone Volume (cm^3)**	**Trabecular Bone Mass (g)**	**Cortical Bone Volume (cm^3)**	**Cortical Bone Mass (g)**
Cranium	107.11	190.29	299.98	532.93	103.85	186.93	290.85	523.53
Mandible	7.44	13.22	32.68	58.06	7.22	12.99	31.69	57.04
Cervical	6.70	11.90	18.61	33.06	6.50	11.69	18.04	32.48
Thoracic	25.67	45.60	50.10	89.00	24.88	44.79	48.57	87.43
Lumbar	20.89	37.12	19.59	34.80	20.26	36.47	18.99	34.19
Sternum	3.08	5.47	12.22	21.72	2.99	5.38	11.85	21.33
Ribs	18.26	32.43	93.33	165.81	17.70	31.86	90.49	162.89
Scapulae	23.33	41.44	68.63	121.92	22.61	40.71	66.54	119.77
Clavicles	2.81	5.00	23.87	42.41	2.73	4.91	23.14	41.66
Os coxae	42.39	75.31	103.99	184.74	41.10	73.98	100.82	181.48
Sacrum	5.46	9.70	38.43	68.26	5.29	9.53	37.26	67.06
Humeri, Proximal	20.60	36.60	23.55	41.83	19.98	35.96	22.83	41.09
Humeri, Upper Shaft	0.00	0.00	60.87	108.14	0.00	0.00	59.02	106.23
Humeri, Lower Shaft	0.00	0.00	54.08	96.07	0.00	0.00	52.43	94.37
Humeri, Distal	12.17	21.61	38.35	68.12	11.79	21.23	37.18	66.92
Radii, Proximal	2.00	3.55	5.65	10.04	1.94	3.49	5.48	9.86
Radii, Shaft	0.00	0.00	41.14	73.08	0.00	0.00	39.89	71.79
Radii, Distal	4.13	7.34	7.02	12.46	4.00	7.21	6.80	12.24
Ulnae, Proximal	9.06	16.10	15.68	27.85	8.79	15.81	15.20	27.36
Ulnae, Shaft	0.00	0.00	49.87	88.60	0.00	0.00	48.35	87.04
Ulnae, Distal	1.21	2.14	3.06	5.44	1.17	2.10	2.97	5.35
Wrists and Hands	6.33	11.25	72.02	127.95	6.14	11.05	69.83	125.69
Femora, Proximal	38.26	67.98	46.30	82.26	37.10	66.78	44.89	80.81
Femora, Upper Shaft	0.00	0.00	127.39	226.31	0.00	0.00	123.51	222.32
Femora, Lower Shaft	0.00	0.00	96.99	172.32	0.00	0.00	94.04	169.27
Femora, Distal	64.68	114.90	37.31	66.29	62.71	112.88	36.18	65.12
Patellae	2.35	4.18	11.81	20.99	2.28	4.10	11.45	20.62
Tibiae, Proximal	15.56	27.64	55.54	98.67	15.08	27.15	53.85	96.93
Tibiae, Shaft	0.00	0.00	141.92	252.14	0.00	0.00	137.60	247.69
Tibiae, Distal	12.52	22.24	12.79	22.72	12.14	21.85	12.40	22.32
Fibulae, Proximal	1.99	3.53	6.90	12.26	1.93	3.47	6.69	12.04
Fibulae, Shaft	0.00	0.00	26.02	46.23	0.00	0.00	25.23	45.42
Fibulae, Distal	3.28	5.83	6.95	12.35	3.18	5.72	6.74	12.13
Ankles and Feet	40.91	72.67	119.83	212.89	39.66	71.39	116.18	209.13
Total Skeleton	498.18	885.05	1822.47	3237.72	483.02	869.43	1766.99	3180.57
ICRP 89 Reference	N/A	N/A	N/A	N/A	450.00	810.00	1800.00	3240.00
Ratio	N/A	N/A	N/A	N/A	1.07	1.07	0.98	0.98

*Denotes inclusion of associated miscellaneous skeletal tissue volumes and masses

Table 4-11. Site-specific total mineral bone volumes and mass including and excluding *MST* in the 15-year female (left) and male (right) hybrid phantoms.

	Female				Male			
Skeletal Site	**Total Mineral Bone Volume (cm^3)**	**Total Mineral Bone Mass (g)**	**Total Mineral Bone* Volume (cm^3)**	**Total Mineral Bone* Mass (g)**	**Total Mineral Bone Volume (cm^3)**	**Total Mineral Bone Mass (g)**	**Total Mineral Bone* Volume (cm^3)**	**Total Mineral Bone* Mass (g)**
Cranium	325.80	586.45	336.33	597.18	394.70	710.46	407.09	723.22
Mandible	30.97	55.75	31.97	56.77	38.91	70.03	40.13	71.29
Cervical	31.08	55.94	32.08	56.97	24.54	44.17	25.31	44.96
Thoracic	67.33	121.20	69.51	123.41	73.46	132.22	75.76	134.59
Lumbar	44.14	79.45	45.56	80.90	39.25	70.66	40.49	71.92
Sternum	10.46	18.83	10.80	19.17	14.84	26.71	15.31	27.19
Ribs	119.00	214.20	122.84	218.12	108.19	194.75	111.59	198.24
Scapulae	123.25	221.84	127.23	225.90	89.15	160.48	91.95	163.36
Clavicles	34.03	61.25	35.13	62.37	25.87	46.57	26.69	47.41
Os coxae	160.71	289.28	165.90	294.57	141.92	255.45	146.37	260.04
Sacrum	52.80	95.04	54.51	96.78	42.55	76.59	43.89	77.97
Humeri, Proximal	34.60	62.29	35.72	63.43	42.81	77.05	44.15	78.44
Humeri, Upper Shaft	48.08	86.54	49.63	88.12	59.02	106.23	60.87	108.14
Humeri, Lower Shaft	41.96	75.52	43.31	76.90	52.43	94.37	54.08	96.07
Humeri, Distal	39.06	70.31	40.32	71.59	48.97	88.15	50.51	89.73
Radii, Proximal	5.68	10.22	5.86	10.40	7.42	13.35	7.65	13.59
Radii, Shaft	35.67	64.21	36.83	65.39	39.89	71.79	41.14	73.08
Radii, Distal	8.28	14.90	8.55	15.18	10.81	19.45	11.15	19.80
Ulnae, Proximal	18.81	33.86	19.42	34.48	23.98	43.17	24.74	43.95
Ulnae, Shaft	42.14	75.84	43.50	77.23	48.35	87.04	49.87	88.60
Ulnae, Distal	3.18	5.73	3.28	5.83	4.14	7.45	4.27	7.58
Wrists and Hands	63.02	113.43	65.05	115.51	75.97	136.74	78.35	139.20
Femora, Proximal	63.54	114.37	65.59	116.46	81.99	147.59	84.57	150.24
Femora, Upper Shaft	91.25	164.25	94.20	167.26	123.51	222.32	127.39	226.31
Femora, Lower Shaft	103.11	185.60	106.44	189.00	94.04	169.27	96.99	172.32
Femora, Distal	89.14	160.45	92.02	163.39	98.88	177.99	101.99	181.19
Patellae	11.23	20.21	11.59	20.58	13.73	24.72	14.16	25.16
Tibiae, Proximal	60.80	109.44	62.77	111.45	68.93	124.07	71.09	126.30
Tibiae, Shaft	115.64	208.15	119.38	211.96	137.60	247.69	141.92	252.14
Tibiae, Distal	21.43	38.57	22.12	39.28	24.54	44.17	25.31	44.96
Fibulae, Proximal	6.84	12.32	7.07	12.55	8.62	15.52	8.89	15.79
Fibulae, Shaft	18.41	33.14	19.01	33.75	25.23	45.42	26.02	46.23
Fibulae, Distal	7.84	14.12	8.10	14.37	9.92	17.85	10.23	18.17
Ankles and Feet	126.28	227.30	130.35	231.46	155.84	280.52	160.74	285.56
Total Skeleton	2055.56	3700.00	2121.94	3767.72	2250.00	4050.00	2320.65	4122.77
ICRP 89 Reference	2055.56	3700.00	2121.94	3767.72	2250.00	4050.00	2320.65	4122.77
Ratio	1.00	1.00	1.00	1.00	1.00	1.00	1.00	1.00

*Denotes inclusion of associated miscellaneous skeletal tissue volumes and masses

Table 4-12. Percentages of total mineral bone attributed to cortical bone and to trabecular bone by skeletal site in the newborn, 15-year female and male hybrid phantoms compared to the ICRP adult reference values.

	Newborn		15 Y Female		15 Y Male		Adult	
Skeletal Site	**Cortical**	**Trabecular**	**Cortical**	**Trabecular**	**Cortical**	**Trabecular**	**Cortical**	**Trabecular**
Cranium	0.27	0.73	0.74	0.26	0.74	0.26	0.95	0.05
Mandible	0.41	0.59	0.82	0.18	0.81	0.19	0.95	0.05
Cervical	0.47	0.53	0.74	0.26	0.74	0.26	0.25	0.75
Thoracic	0.57	0.43	0.67	0.33	0.66	0.34	0.25	0.75
Lumbar	0.39	0.61	0.50	0.50	0.48	0.52	0.34	0.66
Sternum	0.37	0.63	0.80	0.20	0.80	0.20	0.94	0.06
Ribs	0.41	0.59	0.84	0.16	0.84	0.16	0.94	0.06
Scapula	0.54	0.46	0.75	0.25	0.75	0.25	0.94	0.06
Clavicles	0.54	0.46	0.90	0.10	0.89	0.11	0.94	0.06
Os coxae	0.61	0.39	0.72	0.28	0.71	0.29	0.90	0.10
Sacrum	0.39	0.61	0.88	0.12	0.88	0.12	0.75	0.25
Humeri, upper half	0.50	0.50	0.81	0.19	0.80	0.20	0.90	0.10
Humeri, lower half	0.55	0.45	0.89	0.11	0.88	0.12	0.90	0.10
Radii	0.57	0.43	0.91	0.09	0.90	0.10	0.87	0.13
Ulna	0.57	0.43	0.88	0.12	0.87	0.13	0.87	0.13
Wrist and Hands	0.38	0.62	0.92	0.08	0.92	0.08	0.95	0.05
Femora, upper half	0.54	0.46	0.82	0.18	0.82	0.18	0.77	0.23
Femora, lower half	0.68	0.32	0.71	0.29	0.67	0.33	0.77	0.23
Patella	0.38	0.62	0.84	0.16	0.83	0.17	0.77	0.23
Tibia	0.55	0.45	0.88	0.12	0.88	0.12	0.83	0.17
Fibula	0.60	0.40	0.88	0.12	0.88	0.12	0.89	0.11
Ankles and Feet	0.38	0.62	0.75	0.25	0.75	0.25	0.65	0.35

Table 4-13. Distribution of shallow marrow by skeletal site in the 15-year female hybrid phantom.

Bone Site	Shallow Marrow* SMVF (% of SV)	Shallow Marrow* (% of MV)	Shallow Marrow* Volume (cm^3)	Shallow Marrow* Mass (g) @100%	Shallow Marrow Cellularity (%)	Shallow Inactive Marrow* Mass (g)	Shallow Active Marrow* Mass (g)	Shallow Marrow* Mass (g) @ Ref. Cell.	Shallow Marrow* % of total
[1]Cranium	13.84%	20.33%	37.70	38.83	55	16.63	21.36	37.98	10.78%
Mandible	14.21%	19.81%	2.92	3.01	55	1.29	1.66	2.95	0.84%
[2]Cervical	14.76%	17.57%	7.68	7.91	75	1.88	5.93	7.81	2.22%
[3]Thoracic	13.27%	15.22%	23.85	24.56	75	5.84	18.42	24.27	6.89%
[4]Lumbar	12.20%	13.64%	26.15	26.94	75	6.41	20.20	26.61	7.55%
Sternum	12.63%	13.93%	2.87	2.96	75	0.70	2.22	2.92	0.83%
[5]Ribs	12.01%	13.66%	19.57	20.16	75	4.80	15.12	19.92	5.65%
Right Scapula	11.87%	17.11%	12.28	12.65	55	5.42	6.96	12.37	3.51%
Right Clavicle	10.43%	12.66%	2.15	2.22	53	0.99	1.17	2.17	0.61%
[6]Os coxae	12.78%	14.29%	56.99	58.70	64	20.11	37.57	57.67	16.37%
Sacrum	7.15%	7.58%	8.40	8.65	64	2.96	5.54	8.50	2.41%
Humerii, Right Proximal	13.28%	15.73%	13.93	14.35	55	6.14	7.89	14.04	3.98%
[7]Humerii, Upper Shaft	2.09%	2.09%	0.29	0.30	35	0.19	0.10	0.29	0.08%
[7]Humerii, Lower Shaft	2.26%	2.26%	0.27	0.28	20	0.22	0.06	0.27	0.08%
Humerii, Right Distal	13.57%	17.30%	6.01	6.19	0	5.89	0.00	5.89	1.67%
Radii, Right Proximal	13.54%	17.05%	0.99	1.02	0	0.97	0.00	0.97	0.27%
Radii, Shaft	4.39%	4.39%	0.25	0.25	0	0.24	0.00	0.24	0.07%
Radii, Right Distal	13.57%	16.89%	2.15	2.21	0	2.10	0.00	2.10	0.60%
Ulna, Right Proximal	15.16%	20.32%	4.18	4.30	0	4.09	0.00	4.09	1.16%
Ulna, Shaft	3.93%	3.93%	0.27	0.28	0	0.27	0.00	0.27	0.08%
Ulna, Right Distal	16.04%	19.71%	0.78	0.81	0	0.77	0.00	0.77	0.22%
[8]Wrist and Hands	12.01%	13.66%	5.11	5.27	0	5.01	0.00	5.01	1.42%
[9]Femora, Proximal	15.33%	19.31%	21.60	22.25	55	9.53	12.24	21.76	6.18%
[7]Femora, Upper Shaft	1.68%	1.68%	0.54	0.56	35	0.35	0.20	0.54	0.15%
[7]Femora, Lower Shaft	1.55%	1.55%	0.57	0.58	20	0.44	0.12	0.56	0.16%
Femora, Distal	15.64%	21.66%	32.26	33.23	0	31.62	0.00	31.62	8.97%
[8]Patella	12.01%	13.66%	1.87	1.93	0	1.84	0.00	1.84	0.52%
Tibia, Proximal	10.73%	11.85%	15.14	15.60	0	14.84	0.00	14.84	4.21%
Tibia, Shaft	1.75%	1.75%	0.85	0.87	0	0.83	0.00	0.83	0.24%
Tibia, Distal	15.14%	18.59%	8.75	9.01	0	8.57	0.00	8.57	2.43%
Fibula, Proximal	13.14%	15.48%	1.34	1.38	0	1.32	0.00	1.32	0.37%
Fibula, Shaft	5.02%	5.02%	0.29	0.30	0	0.28	0.00	0.28	0.08%
Fibula, Distal	16.32%	22.20%	1.57	1.62	0	1.54	0.00	1.54	0.44%
[8]Ankles and Feet	12.01%	13.66%	32.25	33.22	0	31.61	0.00	31.61	8.97%
Total Skeleton	-	-	351.85	362.40	-	195.67	156.75	352.42	100.00%

[1]The MVF is a inear average between occipital, frontal, parietal (+/- 2.06%)

[2]The MVF is a linear average between C_3 and C_6 (+/- 2.23%)

[3]The MVF is a linear average between T_1, T_3, T_6, T_9, and T_{12} (+/- 1.74%)

[4]The MVF is a linear average between L_1,L_2, L_3, L_4, and L_5 (+/- 2.01%)

[5]The MVF is a linear average between the upper (rib-1), middle (rib-6), and lower right (rib-12) rib (+/- 3.04%)

[6]The MVF was calculated from the right ilium

[7]The SVF for the upper shaft was segmented and assumed to be the same for the lower shaft

[8]The MVF for the rib was used as a surrogate

[9]The MVF is a linear average of the right and left head and neck (+/- 3.46%)

Table 4-14. Distribution of shallow marrow by skeletal site in the 15-year male hybrid phantom.

Bone Site	Shallow Marrow* SMVF (% of SV)	Shallow Marrow* (% of MV)	Shallow Marrow* Volume (cm^3)	Shallow Marrow* Mass (g) @ 100%	Shallow Marrow Cellularity (%)	Shallow Inactive Marrow* Mass (g)	Shallow Active Marrow* Mass (g)	Shallow Marrow* Mass (g) @ Ref. Cell.	Shallow Marrow* % of total
[1]Cranium	13.84%	20.33%	46.42	47.81	55	21.52	26.30	47.81	12.09%
Mandible	14.21%	19.81%	3.74	3.85	55	1.73	2.12	3.85	0.97%
[2]Cervical	14.76%	17.57%	6.18	6.36	75	1.59	4.77	6.36	1.61%
[3]Thoracic	13.27%	15.22%	26.62	27.42	75	6.85	20.56	27.42	6.94%
[4]Lumbar	12.20%	13.64%	24.03	24.75	75	6.19	18.57	24.75	6.26%
Sternum	12.63%	13.93%	4.17	4.29	75	1.07	3.22	4.29	1.09%
[5]Ribs	12.01%	13.66%	18.15	18.69	75	4.67	14.02	18.69	4.73%
Right Scapula	11.87%	17.11%	9.03	9.30	55	4.19	5.12	9.30	2.35%
Right Clavicle	10.43%	12.66%	1.67	1.72	53	0.81	0.91	1.72	0.44%
[6]Os coxae	12.78%	14.29%	51.56	53.11	64	19.12	33.99	53.11	13.43%
Sacrum	7.15%	7.58%	6.93	7.14	64	2.57	4.57	7.14	1.81%
Humerii, Right Proximal	13.28%	15.73%	17.64	18.17	55	8.17	9.99	18.17	4.60%
[7]Humerii, Upper Shaft	1.89%	1.89%	0.33	0.34	35	0.22	0.12	0.34	0.09%
[7]Humerii, Lower Shaft	2.07%	2.07%	0.33	0.34	20	0.27	0.07	0.34	0.08%
Humerii, Right Distal	13.57%	17.30%	7.67	7.90	0	7.90	0.00	7.90	2.00%
Radii, Right Proximal	13.54%	17.05%	1.31	1.35	0	1.35	0.00	1.35	0.34%
Radii, Shaft	4.07%	4.07%	0.27	0.28	0	0.28	0.00	0.28	0.07%
Radii, Right Distal	13.57%	16.89%	2.85	2.94	0	2.94	0.00	2.94	0.74%
Ulna, Right Proximal	15.16%	20.32%	5.41	5.58	0	5.58	0.00	5.58	1.41%
Ulna, Shaft	3.61%	3.61%	0.30	0.31	0	0.31	0.00	0.31	0.08%
Ulna, Right Distal	16.04%	19.71%	1.04	1.07	0	1.07	0.00	1.07	0.27%
[8]Wrist and Hands	12.01%	13.66%	6.30	6.48	0	6.48	0.00	6.48	1.64%
[9]Femora, Proximal	15.33%	19.31%	28.41	29.26	55	13.17	16.09	29.26	7.40%
[7]Femora, Upper Shaft	1.44%	1.44%	0.65	0.67	35	0.44	0.23	0.67	0.17%
[7]Femora, Lower Shaft	1.64%	1.64%	0.56	0.58	20	0.47	0.12	0.58	0.15%
Femora, Distal	15.64%	21.66%	36.40	37.49	0	37.49	0.00	37.49	9.48%
[8]Patella	12.01%	13.66%	2.34	2.41	0	2.41	0.00	2.41	0.61%
Tibia, Proximal	10.73%	11.85%	17.56	18.09	0	18.09	0.00	18.09	4.58%
Tibia, Shaft	1.60%	1.60%	0.95	0.98	0	0.98	0.00	0.98	0.25%
Tibia, Distal	15.14%	18.59%	10.23	10.53	0	10.53	0.00	10.53	2.66%
Fibula, Proximal	13.14%	15.48%	1.72	1.78	0	1.78	0.00	1.78	0.45%
Fibula, Shaft	4.29%	4.29%	0.35	0.36	0	0.36	0.00	0.36	0.09%
Fibula, Distal	16.32%	22.20%	2.02	2.08	0	2.08	0.00	2.08	0.53%
[8]Ankles and Feet	12.01%	13.66%	40.67	41.89	0	41.89	0.00	41.89	10.60%
Total Skeleton	-	-	383.82	395.34	-	234.56	160.77	395.34	100.00%

[1]The MVF is a inear average between occipital, frontal, parietal (+/- 2.06%)

[2]The MVF is a linear average between C_3 and C_6 (+/- 2.23%)

[3]The MVF is a linear average between T_1, T_3, T_6, T_9, and T_{12} (+/- 1.74%)

[4]The MVF is a linear average between L_1,L_2, L_3, L_4, and L_5 (+/- 2.01%)

[5]The MVF is a linear average between the upper (rib-1), middle (rib-6), and lower right (rib-12) rib (+/- 3.04%)

[6]The MVF was calculated from the right ilium

[7]The SVF for the upper shaft was segmented and assumed to be the same for the lower shaft

[8]The MVF for the rib was used as a surrogate

[9]The MVF is a linear average of the right and left head and neck (+/- 3.46%)

Table 4-15. Lengths and radii of the medullary cavities within the long bones of the 15-year female (left) and male (right) hybrid phantoms.

	Measured Height (cm) Medullary Marrow		Measured Height Std. Dev. (cm)		Calculated Radius (cm) Medullary Marrow	
Bone site	**Female**	**Male**	**Female**	**Male**	**Female**	**Male**
Humerii, Upper Shaft	9.76	10.18	0.10	0.10	0.48	0.53
Humerii, Lower Shaft	9.99	10.85	0.12	0.03	0.44	0.48
Radii, Shaft	17.53	17.73	0.16	0.13	0.23	0.24
Ulna, Shaft	17.44	17.67	0.03	0.17	0.25	0.27
Femora, Upper Shaft	14.64	17.04	0.06	0.13	0.59	0.69
Femora, Lower Shaft	14.11	16.88	0.05	0.05	0.64	0.61
Tibia, Shaft	23.74	24.37	0.05	0.11	0.57	0.62
Fibula, Shaft	23.76	24.42	0.05	0.07	0.20	0.23

Table 4-16. Comparison of trabecular bone surface-to-volume (S/V) ratios (mm^2 mm^{-3}) by skeletal site and age.

Skeletal Site	mm^2/mm^3 [a]Hybrid Newborn	mm^2/mm^3 [b]15-year	mm^2/mm^3 [c]ICRP 15-year	mm^2/mm^3 [c]ICRP-Adult	Ratio 15-year hybrid/ 15-year reference
Cranium	3.8	12.6	7.1	7.8	1.77
Mandible	29.7	14.0	7.1	7.8	1.98
Cervical	14.3	26.0	21.9	18.0	1.19
Thoracic	13.8	28.1	21.9	18.0	1.28
Lumbar	17.9	31.3	22.8	19.7	1.38
Sternum	31.0	34.2	19.2	18.5	1.79
Ribs	29.7	24.2	19.2	18.5	1.26
Scapulae	25.3	10.1	21.4	18.5	0.47
Clavicles	25.3	15.4	21.4	18.5	0.72
Os coxae	25.3	31.2	20.0	17.2	1.56
Sacrum	17.9	31.6	21.3	19.7	1.49
Humeri, Proximal	17.9	23.8	18.0	18.0	0.66
Humeri, Upper Shaft	0.0	0.0			
Humeri, Lower Shaft	0.0	0.0	18.0	18.0	0.58
Humeri, Distal	17.9	20.7			
Radii, Proximal	17.9	19.7			
Radii, Shaft	0.0	0.0	18.0	18.0	0.72
Radii, Distal	17.9	19.0			
Ulnae, Proximal	17.9	16.9			
Ulnae, Shaft	0.0	0.0	18.0	18.0	0.73
Ulnae, Distal	17.9	22.3			
Wrists and Hands	17.9	24.2	18.0	18.0	1.35
Femora, Proximal	17.9	21.6	17.9	17.3	0.61
Femora, Upper Shaft	0.0	0.0			
Femora, Lower Shaft	0.0	0.0	17.9	17.3	0.44
Femora, Distal	17.9	15.9			
Patellae	17.9	24.2	18.0	18.0	1.35
Tibiae, Proximal	17.9	29.7			
Tibiae, Shaft	0.0	0.0	18.0	18.0	0.94
Tibiae, Distal	17.9	21.3			
Fibulae, Proximal	17.9	23.4			
Fibulae, Shaft	0.0	0.0	18.0	18.0	0.74
Fibulae, Distal	17.9	16.7			
Ankles and Feet	17.9	24.2	18.0	18.0	1.35

[a]Refer to Chapter 2 for detailed analysis.

[b]18-year male specimens serve as surrogate for 15-year male and female; see text for detailed microstructure data.

[c]values from Beddoe (1976).

Table 4-17. Site-specific homogeneous spongiosa mass, volume, and density data, including *MST*, in the 15-year female (left) and male (right) hybrid phantoms.

	Homogeneous* Spongiosa Mass (g)		Homogeneous* Spongiosa Volume (cm^3)		Homogeneous* Spongiosa Density (g/cm^3)	
Skeletal Site	**Female**	**Male**	**Female**	**Male**	**Female**	**Male**
Cranium	341.33	420.47	272.40	335.42	1.25	1.25
Mandible	25.21	32.27	20.58	26.33	1.22	1.23
Cervical	59.23	47.69	52.01	41.86	1.14	1.14
Thoracic	200.24	223.60	179.65	200.54	1.11	1.11
Lumbar	235.41	216.42	214.41	197.05	1.10	1.10
Sternum	24.75	35.92	22.74	32.99	1.09	1.09
Ribs	180.82	167.72	163.03	151.17	1.11	1.11
Scapulae	128.65	94.65	103.48	76.10	1.24	1.24
Clavicles	23.55	18.29	20.63	16.01	1.14	1.14
Os coxae	487.01	440.76	445.79	403.32	1.09	1.09
Sacrum	124.00	102.38	117.51	97.00	1.06	1.06
Humeri, Proximal	118.18	149.68	104.86	132.76	1.13	1.13
Humeri, Distal	51.03	65.13	44.29	56.50	1.15	1.15
Radii, Proximal	8.34	11.10	7.29	9.69	1.14	1.15
Radii, Distal	17.98	23.91	15.81	21.02	1.14	1.14
Ulnae, Proximal	32.58	42.25	27.55	35.70	1.18	1.18
Ulnae, Distal	5.52	7.32	4.89	6.48	1.13	1.13
Wrists and Hands	45.88	56.50	42.60	52.44	1.08	1.08
Femora, Proximal	164.41	216.29	140.96	185.37	1.17	1.17
Femora, Distal	247.96	279.86	206.29	232.74	1.20	1.20
Patellae	16.82	20.98	15.61	19.47	1.08	1.08
Tibiae, Proximal	149.16	173.08	141.16	163.74	1.06	1.06
Tibiae, Distal	65.18	76.24	57.76	67.54	1.13	1.13
Fibulae, Proximal	11.27	14.47	10.23	13.13	1.10	1.10
Fibulae, Distal	11.47	14.75	9.63	12.37	1.19	1.19
Ankles and Feet	289.38	364.99	268.64	338.72	1.08	1.08
Total Skeleton	3065.38	3316.72	2709.78	2925.46		
Volume Weighted Average Density					1.13	1.12
ICRP 89 Reference	3037.84	3259.93	2717.65	2907.62		
Ratio	0.99	0.98	1.00	0.99		
ICRU 46 Adult Density					1.18	1.18
Ratio					0.96	0.95

*Denotes inclusion of associated miscellaneous skeletal tissue volumes and masses

Table 4-18. Site-specific homogeneous spongiosa elemental composition (% by mass) in the 15-year female hybrid phantom.

	Element											
Skeletal Site	H	C	N	O	Ca	Na	Mg	P	S	Cl	K	Fe
Cranium	7.76	35.20	3.15	39.93	9.11	0.14	0.15	4.31	0.22	0.00	0.01	0.03
Mandible	8.06	36.67	3.06	39.50	8.25	0.14	0.14	3.92	0.22	0.00	0.01	0.03
Cervical	9.04	38.92	3.12	40.88	5.02	0.12	0.16	2.46	0.21	0.00	0.01	0.06
Thoracic	9.35	40.30	3.05	40.61	4.10	0.12	0.16	2.04	0.20	0.00	0.01	0.06
Lumbar	9.57	41.28	3.00	40.41	3.45	0.12	0.16	1.75	0.20	0.00	0.01	0.06
Sternum	9.70	41.86	2.97	40.30	3.07	0.11	0.15	1.57	0.20	0.00	0.01	0.06
Ribs	9.42	40.62	3.03	40.54	3.89	0.12	0.16	1.95	0.20	0.00	0.01	0.06
Scapulae	7.86	35.71	3.12	39.78	8.81	0.14	0.15	4.17	0.22	0.00	0.01	0.03
Clavicles	9.03	41.88	2.72	37.70	5.50	0.13	0.13	2.66	0.19	0.00	0.01	0.04
Os coxae	9.66	43.29	2.77	38.61	3.44	0.12	0.14	1.73	0.19	0.00	0.01	0.05
Sacrum	10.19	45.77	2.63	37.99	1.91	0.11	0.13	1.03	0.18	0.00	0.01	0.06
Humeri, Proximal	9.21	42.39	2.72	37.86	4.92	0.12	0.13	2.40	0.19	0.00	0.01	0.04
[1]Humeri, Upper Shaft	11.12	55.30	1.70	31.39	0.00	0.10	0.07	0.14	0.14	0.00	0.01	0.03
[1]Humeri, Lower Shaft	11.27	58.71	1.30	28.31	0.00	0.10	0.04	0.12	0.12	0.00	0.01	0.02
Humeri, Distal	8.97	47.72	1.92	31.18	6.68	0.13	0.07	3.17	0.17	0.00	0.01	0.00
Radii, Proximal	9.06	48.29	1.88	30.92	6.43	0.13	0.06	3.05	0.17	0.00	0.01	0.00
[1]Radii, Shaft	11.47	63.33	0.76	24.13	0.00	0.10	0.00	0.10	0.10	0.00	0.01	0.00
Radii, Distal	9.16	48.90	1.83	30.64	6.18	0.13	0.06	2.93	0.16	0.00	0.01	0.00
Ulnae, Proximal	8.59	45.40	2.09	32.22	7.67	0.14	0.07	3.62	0.18	0.00	0.01	0.00
[1]Ulnae, Shaft	11.47	63.33	0.76	24.13	0.00	0.10	0.00	0.10	0.10	0.00	0.01	0.00
Ulnae, Distal	9.26	49.57	1.78	30.34	5.89	0.13	0.06	2.80	0.16	0.00	0.01	0.00
Wrists and Hands	9.97	53.96	1.45	28.36	4.01	0.12	0.04	1.94	0.14	0.00	0.01	0.00
Femora, Proximal	8.73	39.98	2.87	38.55	6.33	0.13	0.14	3.04	0.20	0.00	0.01	0.04
[1]Femora, Upper Shaft	11.12	55.30	1.70	31.39	0.00	0.10	0.07	0.14	0.14	0.00	0.01	0.03
[1]Femora, Lower Shaft	11.27	58.71	1.30	28.31	0.00	0.10	0.04	0.12	0.12	0.00	0.01	0.02
Femora, Distal	8.37	44.01	2.20	32.85	8.26	0.14	0.08	3.89	0.18	0.00	0.01	0.00
Patellae	9.97	53.96	1.45	28.36	4.01	0.12	0.04	1.94	0.14	0.00	0.01	0.00
Tibiae, Proximal	10.27	55.82	1.32	27.52	3.21	0.12	0.03	1.58	0.13	0.00	0.01	0.00
[1]Tibiae, Shaft	11.47	63.33	0.76	24.13	0.00	0.10	0.00	0.10	0.10	0.00	0.01	0.00
Tibiae, Distal	9.27	49.60	1.78	30.32	5.87	0.13	0.06	2.80	0.16	0.00	0.01	0.00
Fibulae, Proximal	9.63	51.84	1.61	29.32	4.92	0.12	0.05	2.36	0.15	0.00	0.01	0.00
[1]Fibulae, Shaft	11.47	63.33	0.76	24.13	0.00	0.10	0.00	0.10	0.10	0.00	0.01	0.00
Fibulae, Distal	8.49	44.75	2.14	32.52	7.95	0.14	0.08	3.75	0.18	0.00	0.01	0.00
Ankles and Feet	9.97	53.96	1.45	28.36	4.01	0.12	0.04	1.94	0.14	0.00	0.01	0.00
Total Skeleton Spongiosa	9.28	44.31	2.49	36.05	4.99	0.12	0.11	2.42	0.18	0.00	0.01	0.03

[1]Medullary marrow; contains marrow only

Table 4-19. Site-specific homogeneous spongiosa elemental composition (% by mass) in the 15-year male hybrid phantom.

	Element											
Skeletal Site	H	C	N	O	Ca	Na	Mg	P	S	Cl	K	Fe
Cranium	7.75	35.05	3.16	40.06	9.11	0.14	0.15	4.31	0.22	0.01	0.01	0.03
Mandible	8.05	36.53	3.07	39.63	8.25	0.14	0.14	3.92	0.22	0.01	0.01	0.03
Cervical	9.03	38.77	3.13	41.02	5.03	0.12	0.16	2.46	0.21	0.01	0.01	0.06
Thoracic	9.34	40.14	3.06	40.75	4.11	0.12	0.16	2.04	0.20	0.01	0.01	0.06
Lumbar	9.56	41.12	3.01	40.56	3.45	0.12	0.16	1.75	0.20	0.01	0.01	0.06
Sternum	9.69	41.69	2.98	40.45	3.07	0.11	0.15	1.57	0.20	0.01	0.01	0.06
Ribs	9.42	40.46	3.04	40.69	3.89	0.12	0.16	1.95	0.20	0.01	0.01	0.06
Scapulae	7.86	35.56	3.13	39.91	8.82	0.14	0.15	4.18	0.22	0.01	0.01	0.03
Clavicles	9.03	41.72	2.73	37.84	5.50	0.13	0.13	2.66	0.20	0.01	0.01	0.04
Os coxae	9.66	43.13	2.77	38.76	3.44	0.12	0.14	1.73	0.19	0.01	0.01	0.05
Sacrum	10.18	45.60	2.64	38.14	1.91	0.11	0.13	1.04	0.18	0.01	0.01	0.06
Humeri, Proximal	9.21	42.23	2.73	38.00	4.92	0.12	0.13	2.40	0.19	0.01	0.01	0.04
[1]Humeri, Upper Shaft	11.12	55.13	1.71	31.55	0.00	0.10	0.07	0.14	0.14	0.01	0.01	0.04
[1]Humeri, Lower Shaft	11.27	58.54	1.31	28.46	0.00	0.10	0.04	0.12	0.13	0.01	0.01	0.02
Humeri, Distal	8.96	47.57	1.93	31.31	6.68	0.13	0.07	3.17	0.17	0.01	0.01	0.00
Radii, Proximal	9.05	48.14	1.89	31.06	6.44	0.13	0.06	3.05	0.17	0.01	0.01	0.00
[1]Radii, Shaft	11.47	63.16	0.76	24.29	0.00	0.10	0.00	0.10	0.11	0.01	0.01	0.00
Radii, Distal	9.15	48.74	1.84	30.78	6.18	0.13	0.06	2.94	0.17	0.01	0.01	0.00
Ulnae, Proximal	8.59	45.25	2.10	32.36	7.67	0.14	0.07	3.62	0.18	0.01	0.01	0.00
[1]Ulnae, Shaft	11.47	63.16	0.76	24.29	0.00	0.10	0.00	0.10	0.11	0.01	0.01	0.00
Ulnae, Distal	9.26	49.41	1.79	30.48	5.89	0.13	0.06	2.80	0.16	0.01	0.01	0.00
Wrists and Hands	9.96	53.80	1.46	28.50	4.01	0.12	0.04	1.94	0.14	0.01	0.01	0.00
Femora, Proximal	8.72	39.82	2.87	38.69	6.33	0.13	0.14	3.04	0.20	0.01	0.01	0.04
[1]Femora, Upper Shaft	11.12	55.13	1.71	31.55	0.00	0.10	0.07	0.14	0.14	0.01	0.01	0.04
[1]Femora, Lower Shaft	11.27	58.54	1.31	28.46	0.00	0.10	0.04	0.12	0.13	0.01	0.01	0.02
Femora, Distal	8.37	43.87	2.20	32.98	8.27	0.14	0.08	3.89	0.19	0.01	0.01	0.00
Patellae	9.96	53.80	1.46	28.50	4.01	0.12	0.04	1.94	0.14	0.01	0.01	0.00
Tibiae, Proximal	10.26	55.66	1.32	27.67	3.22	0.12	0.03	1.58	0.14	0.01	0.01	0.00
[1]Tibiae, Shaft	11.47	63.16	0.76	24.29	0.00	0.10	0.00	0.10	0.11	0.01	0.01	0.00
Tibiae, Distal	9.27	49.45	1.79	30.46	5.88	0.13	0.06	2.80	0.16	0.01	0.01	0.00
Fibulae, Proximal	9.62	51.68	1.62	29.46	4.92	0.12	0.05	2.36	0.15	0.01	0.01	0.00
[1]Fibulae, Shaft	11.47	63.16	0.76	24.29	0.00	0.10	0.00	0.10	0.11	0.01	0.01	0.00
Fibulae, Distal	8.49	44.60	2.15	32.65	7.95	0.14	0.08	3.75	0.18	0.01	0.01	0.00
Ankles and Feet	9.96	53.80	1.46	28.50	4.01	0.12	0.04	1.94	0.14	0.01	0.01	0.00
Total Skeleton Spongiosa	9.27	44.48	2.45	35.80	5.08	0.12	0.11	2.46	0.18	0.01	0.01	0.03

[1]Medullary marrow; contains marrow only

Table 4-20. Site-specific homogenized bone masses, volumes, and densities (excluding cartilage).

	15-Year Female			15-Year Male		
Skeletal Site	**Homogeneous Bone Mass (g)**	**Homogeneous Bone Volume (cm3)**	**Homogeneous Bone Density (g/cm3)**	**Homogeneous Bone Mass (g)**	**Homogeneous Bone Volume (cm3)**	**Homogeneous Bone Density (g/cm3)**
Cranium	784.05	521.74	1.50	953.40	635.40	1.50
Mandible	71.65	46.74	1.53	90.33	59.01	1.53
Cervical	101.42	75.77	1.34	80.75	60.47	1.34
Thoracic	282.83	226.16	1.25	312.60	250.64	1.25
Lumbar	275.94	237.23	1.16	251.23	216.64	1.16
Sternum	40.15	31.41	1.28	57.64	45.21	1.27
Ribs	363.98	266.19	1.37	333.53	244.50	1.36
Scapulae	298.24	198.99	1.50	216.57	144.73	1.50
Clavicles	79.49	52.13	1.52	60.70	39.89	1.52
Os coxae	698.39	564.83	1.24	625.50	507.30	1.23
Sacrum	209.04	165.40	1.26	170.65	135.42	1.26
Humeri, Proximal	152.71	124.31	1.23	191.51	156.31	1.23
[1]Humeri, Upper Shaft	102.05	63.58	1.61	125.81	78.56	1.60
[1]Humeri, Lower Shaft	88.97	55.49	1.60	111.65	69.79	1.60
Humeri, Distal	105.69	75.07	1.41	133.25	94.85	1.40
Radii, Proximal	16.08	11.64	1.38	21.14	15.34	1.38
[1]Radii, Shaft	70.88	42.43	1.67	79.54	47.71	1.67
Radii, Distal	27.64	21.25	1.30	36.38	28.03	1.30
Ulnae, Proximal	54.65	39.98	1.37	70.10	51.38	1.36
[1]Ulnae, Shaft	84.05	50.45	1.67	96.81	58.23	1.66
Ulnae, Distal	9.74	7.27	1.34	12.76	9.54	1.34
Wrists and Hands	152.26	102.51	1.49	184.45	124.46	1.48
Femora, Proximal	229.21	177.45	1.29	298.55	231.67	1.29
[1]Femora, Upper Shaft	199.58	126.58	1.58	271.38	172.52	1.57
[1]Femora, Lower Shaft	225.26	143.03	1.57	206.38	131.36	1.57
Femora, Distal	309.55	240.98	1.28	346.15	270.05	1.28
Patellae	34.05	25.32	1.34	41.97	31.29	1.34
Tibiae, Proximal	236.80	190.51	1.24	271.75	219.28	1.24
[1]Tibiae, Shaft	259.51	167.83	1.55	310.28	201.16	1.54
Tibiae, Distal	85.45	69.17	1.24	98.96	80.32	1.23
Fibulae, Proximal	21.06	15.75	1.34	26.73	20.03	1.33
[1]Fibulae, Shaft	39.41	24.78	1.59	54.24	34.18	1.59
Fibulae, Distal	21.32	15.17	1.41	27.10	19.32	1.40
Ankles and Feet	463.23	366.55	1.26	577.87	458.56	1.26
Total Skeleton	6194.32	4543.68		6747.63	4943.17	
Volume Weighted Average Density			1.35			1.35
Original 15-Year Hybrid Phantom	6180.02	4543.68		6743.09	4943.17	
Ratio	1.00	1.00		1.00	1.00	

[1]Contains medullary marrow (no trabecular bone) and cortical bone only

Table 4-21. Site-specific homogeneous bone elemental composition (excluding cartilage) in the 15-year female hybrid phantom (% by mass).

	Element											
Skeletal Site	H	C	N	O	Ca	Na	Mg	P	S	Cl	K	Fe
Cranium	5.59	24.51	3.78	43.00	15.33	0.17	0.18	7.15	0.26	0.00	0.00	0.01
Mandible	5.38	23.46	3.84	43.31	15.95	0.18	0.18	7.43	0.27	0.00	0.00	0.01
Cervical	6.91	29.50	3.60	42.75	11.31	0.16	0.17	5.32	0.24	0.00	0.00	0.03
Thoracic	7.76	33.29	3.41	42.00	8.78	0.14	0.17	4.17	0.23	0.00	0.01	0.04
Lumbar	8.74	37.61	3.19	41.14	5.90	0.13	0.16	2.86	0.21	0.00	0.01	0.05
Sternum	7.48	32.04	3.47	42.24	9.61	0.15	0.17	4.55	0.23	0.00	0.00	0.04
Ribs	6.65	28.37	3.65	42.97	12.06	0.16	0.18	5.66	0.25	0.00	0.00	0.03
Scapulae	5.62	24.66	3.77	42.96	15.25	0.17	0.18	7.11	0.26	0.00	0.00	0.01
Clavicles	5.44	23.86	3.81	43.10	15.80	0.18	0.18	7.36	0.27	0.00	0.00	0.01
Os coxae	7.92	35.11	3.22	40.66	8.49	0.14	0.16	4.03	0.22	0.00	0.01	0.04
Sacrum	7.64	33.77	3.29	40.99	9.32	0.15	0.16	4.41	0.23	0.00	0.01	0.03
Humeri, Proximal	8.02	36.48	3.07	39.56	8.36	0.14	0.15	3.97	0.22	0.00	0.01	0.03
[1]Humeri, Upper Shaft	4.90	21.60	3.92	43.46	17.38	0.18	0.18	8.08	0.28	0.00	0.00	0.00
[1]Humeri, Lower Shaft	4.92	22.03	3.86	43.06	17.40	0.18	0.18	8.08	0.27	0.00	0.00	0.00
Humeri, Distal	6.36	31.46	3.13	38.52	13.64	0.17	0.13	6.36	0.24	0.00	0.00	0.00
Radii, Proximal	6.59	32.89	3.03	37.87	13.02	0.16	0.13	6.07	0.23	0.00	0.00	0.00
[1]Radii, Shaft	4.51	19.93	3.99	43.72	18.57	0.19	0.18	8.62	0.28	0.00	0.00	0.00
Radii, Distal	7.33	37.50	2.68	35.79	11.05	0.15	0.11	5.17	0.21	0.00	0.00	0.00
Ulnae, Proximal	6.71	33.64	2.97	37.53	12.70	0.16	0.12	5.93	0.23	0.00	0.00	0.00
[1]Ulnae, Shaft	4.53	20.10	3.98	43.65	18.50	0.19	0.18	8.58	0.28	0.00	0.00	0.00
Ulnae, Distal	6.95	35.15	2.86	36.85	12.06	0.16	0.12	5.63	0.22	0.00	0.00	0.00
Wrists and Hands	5.74	27.63	3.42	40.24	15.27	0.17	0.15	7.11	0.25	0.00	0.00	0.00
Femora, Proximal	7.37	33.28	3.26	40.48	10.23	0.15	0.15	4.82	0.23	0.00	0.00	0.03
[1]Femora, Upper Shaft	5.09	22.60	3.85	43.11	16.87	0.18	0.18	7.84	0.27	0.00	0.00	0.01
[1]Femora, Lower Shaft	5.10	23.11	3.79	42.62	16.89	0.18	0.17	7.85	0.27	0.00	0.00	0.00
Femora, Distal	7.49	38.50	2.61	35.34	10.63	0.15	0.10	4.97	0.21	0.00	0.00	0.00
Patellae	6.91	34.89	2.88	36.97	12.17	0.16	0.12	5.68	0.22	0.00	0.00	0.00
Tibiae, Proximal	7.92	41.19	2.41	34.13	9.47	0.15	0.09	4.45	0.20	0.00	0.01	0.00
[1]Tibiae, Shaft	5.31	24.90	3.62	41.48	16.44	0.18	0.16	7.64	0.26	0.00	0.00	0.00
Tibiae, Distal	8.00	41.70	2.37	33.89	9.25	0.15	0.09	4.35	0.19	0.00	0.01	0.00
Fibulae, Proximal	6.97	35.30	2.85	36.78	11.99	0.16	0.12	5.60	0.22	0.00	0.00	0.00
[1]Fibulae, Shaft	5.01	23.04	3.76	42.32	17.24	0.18	0.17	8.01	0.27	0.00	0.00	0.00
Fibulae, Distal	6.38	31.60	3.12	38.45	13.58	0.17	0.13	6.33	0.23	0.00	0.00	0.00
Ankles and Feet	7.70	39.82	2.51	34.74	10.06	0.15	0.10	4.71	0.20	0.00	0.01	0.00
Total Skeleton	6.71	30.87	3.34	40.52	12.25	0.16	0.15	5.73	0.24	0.00	0.00	0.02

[1]Contains medullary marrow (no trabecular bone) and cortical bone only

Table 4-22. Site-specific homogeneous bone elemental composition (excluding cartilage) in the 15-year male hybrid phantom (% by mass).

	Element											
Skeletal Site	H	C	N	O	Ca	Na	Mg	P	S	Cl	K	Fe
Cranium	5.61	24.50	3.78	43.08	15.28	0.17	0.18	7.12	0.27	0.00	0.00	0.01
Mandible	5.40	23.44	3.84	43.38	15.89	0.18	0.18	7.40	0.27	0.00	0.00	0.01
Cervical	6.94	29.51	3.60	42.84	11.21	0.15	0.17	5.28	0.25	0.00	0.00	0.03
Thoracic	7.80	33.32	3.40	42.10	8.67	0.14	0.17	4.12	0.23	0.01	0.01	0.04
Lumbar	8.78	37.66	3.18	41.24	5.77	0.13	0.16	2.80	0.21	0.01	0.01	0.05
Sternum	7.52	32.07	3.47	42.34	9.50	0.15	0.17	4.50	0.24	0.00	0.00	0.04
Ribs	6.68	28.38	3.65	43.06	11.97	0.16	0.18	5.62	0.25	0.00	0.00	0.03
Scapulae	5.64	24.64	3.77	43.04	15.19	0.17	0.17	7.08	0.27	0.00	0.00	0.01
Clavicles	5.46	23.87	3.81	43.17	15.73	0.18	0.18	7.33	0.27	0.00	0.00	0.01
Os coxae	7.96	35.16	3.22	40.74	8.37	0.14	0.16	3.98	0.22	0.01	0.01	0.04
Sacrum	7.68	33.83	3.29	41.07	9.20	0.14	0.16	4.36	0.23	0.00	0.00	0.03
Humeri, Proximal	8.05	36.54	3.07	39.63	8.25	0.14	0.14	3.92	0.22	0.01	0.01	0.03
[1]Humeri, Upper Shaft	4.93	21.64	3.91	43.51	17.31	0.18	0.18	8.04	0.28	0.00	0.00	0.00
[1]Humeri, Lower Shaft	4.94	22.08	3.86	43.09	17.33	0.18	0.17	8.05	0.28	0.00	0.00	0.00
Humeri, Distal	6.38	31.52	3.13	38.55	13.56	0.17	0.13	6.32	0.24	0.00	0.00	0.00
Radii, Proximal	6.61	32.95	3.02	37.90	12.94	0.16	0.13	6.04	0.23	0.00	0.00	0.00
[1]Radii, Shaft	4.53	19.98	3.99	43.75	18.50	0.19	0.18	8.59	0.28	0.00	0.00	0.00
Radii, Distal	7.36	37.58	2.67	35.81	10.96	0.15	0.11	5.13	0.21	0.00	0.00	0.00
Ulnae, Proximal	6.73	33.70	2.96	37.56	12.63	0.16	0.12	5.89	0.23	0.00	0.00	0.00
[1]Ulnae, Shaft	4.56	20.15	3.97	43.67	18.43	0.19	0.18	8.55	0.28	0.00	0.00	0.00
Ulnae, Distal	6.98	35.23	2.85	36.87	11.97	0.16	0.12	5.59	0.22	0.00	0.00	0.00
Wrists and Hands	5.77	27.70	3.41	40.27	15.20	0.17	0.15	7.07	0.25	0.00	0.00	0.00
Femora, Proximal	7.40	33.30	3.26	40.56	10.13	0.15	0.15	4.78	0.23	0.00	0.00	0.03
[1]Femora, Upper Shaft	5.11	22.64	3.85	43.15	16.79	0.18	0.18	7.81	0.27	0.00	0.00	0.01
[1]Femora, Lower Shaft	5.13	23.16	3.78	42.66	16.81	0.18	0.17	7.82	0.27	0.00	0.00	0.00
Femora, Distal	7.52	38.56	2.60	35.37	10.54	0.15	0.10	4.94	0.21	0.00	0.00	0.00
Patellae	6.94	34.99	2.87	36.98	12.07	0.16	0.12	5.64	0.22	0.00	0.00	0.00
Tibiae, Proximal	7.96	41.32	2.39	34.13	9.36	0.15	0.09	4.39	0.20	0.01	0.01	0.00
[1]Tibiae, Shaft	5.33	24.98	3.61	41.50	16.36	0.18	0.16	7.61	0.26	0.00	0.00	0.00
Tibiae, Distal	8.04	41.81	2.36	33.91	9.15	0.14	0.09	4.30	0.19	0.01	0.01	0.00
Fibulae, Proximal	7.01	35.39	2.84	36.80	11.90	0.16	0.12	5.56	0.22	0.00	0.00	0.00
[1]Fibulae, Shaft	5.03	23.11	3.75	42.34	17.16	0.18	0.17	7.97	0.27	0.00	0.00	0.00
Fibulae, Distal	6.40	31.65	3.12	38.49	13.51	0.17	0.13	6.30	0.24	0.00	0.00	0.00
Ankles and Feet	7.74	39.94	2.50	34.75	9.95	0.15	0.10	4.67	0.20	0.00	0.00	0.00
Total Skeleton	6.70	30.90	3.33	40.44	12.31	0.16	0.15	5.76	0.24	0.00	0.00	0.02

[1]Contains medullary marrow (no trabecular bone) and cortical bone only

Table 4-23. Macrostructure for the 15-year female and microstructure imaging data for the 18-year male skeleton.

	Macrostructure		Microstructure						Microstructure		Microstructure	
			Dimensions						*MVF*	*TBVF*	*MVF*	*TBVF*
	Voxel Size	Resolution	*60 Microns*			*30 Microns*			*60 Microns*		*30 Microns*	
	x y z	(cm)	*x*	*y*	*z*	*x*	*y*	*z*				
Cranium (Average)	408 x 516 x 459	0.035							0.6793 (+/- 0.022)	0.3207 (+/- 0.022)	0.6807 (+/- 0.020)	0.3193 (+/- 0.020)
- Occipital			39	407	147	78	815	294	0.6892	0.3108	0.6910	0.3090
- Frontal			16	209	349	33	419	699	0.6540	0.3460	0.6570	0.3430
- Parietal			19	409	246	39	818	493	0.6948	0.3052	0.6940	0.3060
Mandible	351 x 266 x 243	0.03							0.7184	0.2816	0.7173	0.2827
Sternum	223 x 345 x 807	0.02	97	454	426	195	909	852	0.9073	0.0927	0.9066	0.0934
Ribs (Average)	439 x 295 x 554	0.06							0.8788 (+/- 0.032)	0.1212 (+/- 0.032)	0.8792 (+/- 0.030)	0.1208 (+/- 0.030)
- Upper (Right Rib 1)			23	117	299	47	234	599	0.8442	0.1558	0.8462	0.1538
- Middle (Right Rib 6)			52	102	526	105	205	1052	0.9057	0.0943	0.9061	0.0939
- Lower (Right Rib 12)			38	82	367	77	165	735	0.8866	0.1134	0.8854	0.1146
Scapula (Right)	427 x 301 x 541	0.03	36	128	270	73	257	541	0.6940	0.3060	0.6935	0.3065
Clavicle (Right)	697 x 594 x 134	0.018	126	286	211	253	572	423	0.8221	0.1779	0.8243	0.1757
Vertebrae												
- Cervicle (Average)	366 x 324 x 552	0.02							0.8434 (+/-0.021)	0.1567 (+/- 0.021)	0.8400 (+/- 0.022)	0.1601 (+/- 0.022)
- 18Y C_3			150	208	155	301	417	310	0.8283	0.1717	0.8242	0.1758
- 18Y C_6			226	244	268	452	489	536	0.8584	0.1416	0.8557	0.1443
- Thoracic (Average)	219 x 288 x 926	0.03							0.8747 (+/- 0.018)	0.1253 (+/- 0.018)	0.8720 (+/- 0.018)	0.1280 (+/- 0.018)
- 18Y T_1			248	263	252	496	526	505	0.8523	0.1477	0.8502	0.1498
- 18Y T_3			242	261	271	484	523	543	0.8624	0.1376	0.8597	0.1403
- 18Y T_6			242	265	391	485	531	783	0.8761	0.1239	0.8735	0.1265
- 18Y T_9			314	341	369	629	682	739	0.8860	0.1140	0.8831	0.1169
- 18Y T_{12}			340	357	547	681	715	1094	0.8966	0.1034	0.8936	0.1064
- Lumbar Spine (Average)	271 x 323 x 541	0.03							0.8960 (+/- 0.020)	0.1040 (+/- 0.022)	0.8940 (+/- 0.020)	0.1060 (+/- 0.020)
- 18Y L_1			326	338	555	653	677	1111	0.9094	0.0906	0.9064	0.0936
- 18Y L_2			292	356	611	585	712	1222	0.9211	0.0789	0.9167	0.0833
- 18Y L_3			228	380	533	456	760	1066	0.9029	0.0971	0.9009	0.0991
- 18Y L_4			189	393	531	379	787	1062	0.8747	0.1253	0.8743	0.1257
- 18Y L_5			316	236	430	632	473	860	0.8720	0.1280	0.8715	0.1285
Pelvis												
- Os Coxae (Right Ilium)	499 x 287 x 399	0.05	44	476	528	89	952	1057	0.8955	0.1045	0.8949	0.1051
- Sacrum	333 x 307 x 363	0.03	190	116	314	381	233	629	0.9441	0.0559	0.9437	0.0563

Table 4-23. Continued.

	Macrostructure		Microstructure						Microstructure		Microstructure			
			Dimensions						MVF	TBVF	MVF	TBVF	Threshold	Threshold
	Voxel Size	Resolution	60 Microns			30 Microns			60 Microns		30 Microns		Actual	Used
	x y z	(cm)	x	y	z	x	y	z						
Femur (Right)	244 x 268 x 1047	0.04												
- Distal														
- Right			292	362	333	584	724	667	0.7180	0.2820	0.7221	0.2779	154.5	155
- Proximal									0.7886 (+/- 0.047)	0.2114 (+/- 0.047)	0.7891 (+/- 0.0470)	0.2109 (+/- 0.0470)		
- Head														
- Right			248	499	499	497	998	999	0.7553	0.2447	0.7559	0.2441	156.5	157
- Neck														
- Right			329	357	420	659	715	841	0.8220	0.1780	0.8223	0.1777	155.5	156
Fibula (Right)	145 x 128 x 1135	0.03												
- Distal														
- Right			276	180	282	552	361	565	0.7315	0.2685	0.7349	0.2651	156.5	157
- Proximal														
- Right			295	178	341	591	356	682	0.8459	0.1541	0.8485	0.1515	153.5	154
Tibia (Right)	275 x 184 x 1156	0.03												
- Distal														
- Right			416	394	260	833	789	521	0.8131	0.1869	0.8146	0.1854	155.5	156
- Proximal														
- Right			355	384	341	710	768	683	0.9060	0.0940	0.9050	0.0950	155.5	156
Humerus (Right)	292 x 154 x 789	0.04												
- Distal														
- Right			140	540	170	281	1081	340	0.7825	0.2175	0.7847	0.2153	156.5	157
- Proximal														
- Right			417	320	425	835	641	851	0.8462	0.1538	0.8448	0.1552	158.5	159
Radius (Right)	172 x 282 x 1176	0.02												
- Distal														
- Right			230	293	231	461	587	463	0.8030	0.1970	0.8035	0.1965	155.5	156
- Proximal														
- Right			105	498	107	544	141	434	0.7979	0.2021	0.7939	0.2061	161.5	162
Ulna (Right)	206 x 178 x 842	0.03												
- Distal														
- Right			121	339	135	242	679	270	0.8140	0.1860	0.814	0.186	155.5	156
- Proximal														
- Right			199	521	212	399	1042	424	0.7434	0.2566	0.7462	0.2538	156.5	157
Foot (Right)	298 x 807 x 284	0.03												
Hand (Right)	150 x 358 x 553	0.03												
Patella (Right)	445 x 188 x 367	0.01												

Table 4-24. Cortical bone thickness estimates in the 15-year female skeleton.

Bone	15Y Female Cortical Bone Thickness ESTIMATES (cm)
Cranium	0.13
Mandible	0.16
Cervical Vertebrae	0.08
Thoracic Vertebrae	0.07
Lumbar Vertebrae	0.04
Sternum	0.11
Ribs	0.07
Scapulae	0.17
Clavicles	0.24
Os coxae	0.11
Sacrum	0.13
Humeri, Proximal	0.15
Humeri, Upper Shaft	0.5
Humeri, Lower Shaft	0.45
Humeri, Distal	0.2
Radii, Proximal	0.2
Radii, Shaft	0.4
Radii, Distal	0.1
Ulnae, Proximal	0.15
Ulnae, Shaft	0.4
Ulnae, Distal	0.08
Wrists and Hands	0.15
Femora, Proximal	0.1
Femora, Upper Shaft	0.5
Femora, Lower Shaft	0.6
Femora, Distal	0.2
Patellae	0.13
Tibiae, Proximal	0.15
Tibiae, Shaft	0.5
Tibiae, Distal	0.1
Fibulae, Proximal	0.1
Fibulae, Shaft	0.3
Fibulae, Distal	0.1
Ankles and Feet	0.1

Table 4-25. *AM*, *TBV*, *TBS*, and *CBV* source f-values for the UF hybrid 15-year female skeleton.

	UF HYBRID 15Y FEMALE				
Skeletal Site	Cellularity	f_{TAM}	f_{TBV}	f_{TBS}	f_{CBV}
Cranium	55	0.108	0.193	0.121	0.149
Mandible	55	0.009	0.013	0.009	0.016
Cervical	75	0.035	0.019	0.024	0.014
Thoracic	75	0.124	0.051	0.071	0.028
Lumbar	75	0.152	0.051	0.078	0.014
Sternum	75	0.016	0.005	0.008	0.005
Ribs	75	0.114	0.044	0.053	0.062
Scapula	55	0.021	0.070	0.035	0.057
Clavicles	53	0.005	0.008	0.006	0.019
Os coxae	64	0.270	0.104	0.161	0.071
Sacrum	64	0.075	0.015	0.023	0.029
Humeri, Proximal	55	0.026	0.036	0.043	0.012
Humeri, Upper Shaft	35	0.003	0.000	0.000	0.030
Humeri, Lower Shaft	20	0.001	0.000	0.000	0.026
Humeri, Distal	0	0.000	0.021	0.022	0.018
Radii, Proximal	0	0.000	0.003	0.003	0.003
Radii, Shaft	0	0.000	0.000	0.000	0.022
Radii, Distal	0	0.000	0.007	0.007	0.003
Ulnae, Proximal	0	0.000	0.016	0.013	0.007
Ulnae, Shaft	0	0.000	0.000	0.000	0.026
Ulnae, Distal	0	0.000	0.002	0.002	0.001
Wrists and Hands	0	0.000	0.011	0.010	0.036
Femora, Proximal	55	0.033	0.065	0.069	0.022
Femora, Upper Shaft	35	0.006	0.000	0.000	0.056
Femora, Lower Shaft	20	0.004	0.000	0.000	0.064
Femora, Distal	0	0.000	0.127	0.100	0.021
Patellae	0	0.000	0.004	0.004	0.006
Tibiae, Proximal	0	0.000	0.030	0.044	0.030
Tibiae, Shaft	0	0.000	0.000	0.000	0.071
Tibiae, Distal	0	0.000	0.024	0.025	0.007
Fibulae, Proximal	0	0.000	0.003	0.004	0.003
Fibulae, Shaft	0	0.000	0.000	0.000	0.011
Fibulae, Distal	0	0.000	0.006	0.000	0.003
Ankles and Feet	0	0.000	0.072	0.064	0.059

Table 4-26. Skeletal-averaged absorbed fraction data for the UF hybrid 15-year female skeleton based on *PIRT* transport.

Energy (MeV)	ϕ (AM <– AM)	ϕ (AM <– TBS)	ϕ (AM <– TBV)	ϕ (AM <– CBV)	ϕ (TM_{50} <– TBS)	ϕ (TM_{50} <– TBV)	ϕ (TM_{50} <– AM)	ϕ (TM_{50} <– CBV)
0.001	1.00E+00	2.46E-01	7.47E-07	3.14E-08	2.16E-01	7.47E-07	1.37E-01	0.00E+00
0.003	9.99E-01	2.46E-01	8.27E-05	8.08E-06	2.33E-01	8.65E-05	1.37E-01	1.36E-06
0.005	9.97E-01	2.47E-01	3.06E-04	2.06E-05	2.34E-01	3.35E-04	1.37E-01	3.19E-06
0.010	9.89E-01	2.48E-01	1.59E-03	6.70E-05	2.34E-01	1.67E-03	1.36E-01	1.06E-05
0.015	9.77E-01	2.48E-01	3.72E-03	1.41E-04	2.33E-01	3.74E-03	1.35E-01	2.23E-05
0.020	9.62E-01	2.48E-01	6.29E-03	2.32E-04	2.31E-01	6.21E-03	1.33E-01	3.66E-05
0.030	9.24E-01	2.48E-01	1.27E-02	4.77E-04	2.26E-01	1.24E-02	1.29E-01	7.40E-05
0.040	8.80E-01	2.47E-01	2.05E-02	7.91E-04	2.19E-01	1.97E-02	1.24E-01	1.22E-04
0.050	8.33E-01	2.47E-01	2.94E-02	1.16E-03	2.12E-01	2.77E-02	1.19E-01	1.79E-04
0.060	7.86E-01	2.46E-01	3.90E-02	1.56E-03	2.03E-01	3.60E-02	1.13E-01	2.49E-04
0.080	7.10E-01	2.46E-01	5.93E-02	2.51E-03	1.74E-01	5.02E-02	1.04E-01	3.93E-04
0.10	6.68E-01	2.49E-01	8.02E-02	3.61E-03	1.44E-01	5.81E-02	9.81E-02	5.42E-04
0.15	6.14E-01	2.70E-01	1.33E-01	6.72E-03	1.02E-01	6.28E-02	9.40E-02	9.72E-04
0.20	5.80E-01	2.93E-01	1.78E-01	9.95E-03	8.23E-02	5.92E-02	9.55E-02	1.42E-03
0.30	5.41E-01	3.17E-01	2.26E-01	1.66E-02	6.48E-02	5.18E-02	9.80E-02	2.36E-03
0.40	5.21E-01	3.21E-01	2.41E-01	2.29E-02	5.82E-02	4.87E-02	9.75E-02	3.29E-03
0.50	5.06E-01	3.19E-01	2.45E-01	2.90E-02	5.47E-02	4.69E-02	9.62E-02	4.20E-03
0.60	4.93E-01	3.15E-01	2.45E-01	3.48E-02	5.22E-02	4.55E-02	9.46E-02	5.05E-03
0.80	4.69E-01	3.05E-01	2.40E-01	4.41E-02	4.84E-02	4.29E-02	9.11E-02	6.46E-03
1.0	4.47E-01	2.95E-01	2.32E-01	5.07E-02	4.54E-02	4.07E-02	8.74E-02	7.48E-03
1.5	3.99E-01	2.68E-01	2.12E-01	5.79E-02	3.98E-02	3.60E-02	7.87E-02	8.63E-03
2.0	3.59E-01	2.44E-01	1.93E-01	5.88E-02	3.55E-02	3.22E-02	7.13E-02	8.83E-03
3.0	2.98E-01	2.05E-01	1.61E-01	5.50E-02	2.91E-02	2.64E-02	5.93E-02	8.28E-03
4.0	2.53E-01	1.75E-01	1.37E-01	4.96E-02	2.46E-02	2.23E-02	5.05E-02	7.46E-03
5.0	2.18E-01	1.52E-01	1.19E-01	4.44E-02	2.12E-02	1.92E-02	4.37E-02	6.67E-03
6.0	1.91E-01	1.34E-01	1.05E-01	3.97E-02	1.86E-02	1.68E-02	3.84E-02	5.97E-03
8.0	1.52E-01	1.07E-01	8.33E-02	3.24E-02	1.48E-02	1.34E-02	3.06E-02	4.87E-03
10.0	1.26E-01	8.81E-02	6.87E-02	2.71E-02	1.22E-02	1.10E-02	2.52E-02	4.07E-03

Appendix C

A Skeletal Reference Dosimetry Model for the Adult Female

An Image-based Skeletal Tissue Model for the ICRP Reference Adult Female

Lindsay Sinclair[1], Deanna H. Pafundi[2], and Wesley E. Bolch[1]

[1]Department of Nuclear and Radiological Sciences, University of Florida
[2]Radiation Oncology Mayo Clinic, Rochester, MN

ABSTRACT

Modeling of the unique macro and microstructure of the skeleton has shown to be a challenging aspect of skeletal dosimetry. The skeleton is comprised of two main radiosensitive cell populations, hematopoietic stem cells and osteoprogenitor cells. Hematopoietic stem cells are found within the active marrow regions of spongiosa, while osteoprogenitor cells are found on the bone endosteum. Skeletal tissues include mineral bone (cortical or trabecular in structure), active and inactive marrow, cartilage, periosteum, and blood vessels. The skeletal model described in this study seeks to accurately represent the structure and composition of all skeletal tissues within an adult female phantom.

The skeletal tissue masses presented in this paper were derived from four data sets. The first are the polygon mesh and NURBS skeletal volumes of the UF hybrid adult female phantom. The UFHADF skeleton was modeled so that total skeletal masses for each bone site were matched with ICRP reference data. Initially, the skeleton was composed as a homogeneous mixture of all skeletal tissues, including cortical bone, trabecular bone, red and yellow marrow, miscellaneous skeletal tissues, and teeth.

The second source of data for this skeletal model includes ICRP70 (1995), ICRP89 (2002), and ICRU46 (1992). The skeletal tissue reference masses and densities were obtained from the ICRP reports. ICRU46 served as a reference for the density of soft tissue for an adult female and for the elemental composition of spongiosa.

The last two sources of data were based on image data sets from a 45 year-old female cadaver. All pertinent skeletal sites were excised and imaged by standard CT and microCT in order to get valuable information on skeletal macrostructure and microstructure.

The end result of this study was the creation of a heterogeneous skeletal tissue model for the adult female that closely matched the reference total skeletal tissue masses given by the ICRP. Active and inactive marrow masses were both within one percent of the ICRP reference values. The cortical bone mass differed by three percent, while the trabecular bone percent difference was 13. However, the CB/TB ratio from this model was 78/22, which closely matches the ICRP 80/20 ratio. In addition, the total skeletal mineral bone mass matched the ICRP reference value of 4000 g exactly.

INTRODUCTION

The composition of the skeleton is paramount in determining the effects of radiation exposure to the human body. The skeleton is comprised of two main radiosensitive cell populations, hematopoietic stem cells and osteoprogenitor cells. Hematopoietic stem cells are located in the active bone marrow, which can be found within trabecular spongiosa. Radiation exposures to these cells can be associated with leukemia risk. Osteoprogenitor cells are found on bone or endosteal surfaces. Stochastic effects such as bone cancer can be a result of radiation exposure to osteoprogenitor cells. When estimating the risk to radiosensitive regions of the skeleton, skeletal reference models are used to compute absorbed doses to these tissues. The skeletal tissue model presented here can be used to estimate radiation risk to a reference adult female.

Historically, the skeleton has been a challenging aspect to model in computational phantoms. This can be attributed to the highly variable and complex macrostructure and microstructure of the tissues which constitute the skeleton. Skeletal tissues include mineral bone, active and inactive marrow, cartilage, periosteum, and blood vessels. Mineral bone is an organic matrix composed mainly of the protein, collagen. This matrix is infused with inorganic material, calcium phosphate. (Triffitt 1980) The first step of bone formation is the creation of the organic matrix by osteoblasts, or bone-forming cells. The matrix is then mineralized, and then continually remodeled by osteoblasts and osteoclasts throughout life. (Frost 1980)

Mineral bone can generally be divided into either cortical or trabecular bone, based on structure. Cortical or compact bone forms the outer dense layer of osseous tissue throughout the skeleton. Cortical bone is found on the ends of bones surrounding trabecular bone and also

as a thicker shell on the shafts of the long bones. The trabecular or spongy bone is porous in structure and has a much lower bone volume fraction than compact bone. Bone marrow is found within the cavities of trabecular bone. (Frost 1963a)

As mentioned earlier, the two main radiosensitive cell types are osteoprogenitor cells and hematopoietic stem cells. Osteoprogenitor cells are found on the surfaces of bone and within the bone cavities. In modeling the skeletal system, the endosteum is used as a surrogate target tissue for osteoprogenitor cells. This study sets a layer within 50 microns of trabecular and cortical bone surfaces to represent the endosteum. (Bolch et al. 2007) Hematopoietic stem cells are found within the active marrow regions of trabecular spongiosa. Active marrow is used as a surrogate to model these cells. The skeletal model described in this study seeks to accurately represent the structure and composition of all skeletal tissues within an adult female phantom.

When evaluating risk to patients, for either short-term effects or secondary cancer induction from radiation, absorbed dose estimates to critical tissues are vital. In order to complete this task within the skeleton, skeletal tissue masses must be calculated and then applied to a computational phantom. While a third generation hybrid phantom is used in this study, the majority of computational phantoms can be divided into two earlier modeling techniques, stylized or mathematical and voxel or tomographic phantoms.

The earliest form of computational phantoms used for dose assessment for internal and external radiation exposures are stylized phantoms. Stylized phantoms consist of geometric surface equations to represent regions of human anatomy. The most widely used skeletal tissue models are based on Oak Ridge National Laboratory (ORNL) mathematical phantoms

developed in the late 1970s and early 1980s. The skeleton within these phantoms consists of a homogeneous mixture of cortical bone and spongiosa. (Snyder et al. 1974, Cristy 1980, 1981) The phantoms were developed to be used with the MIRD (Medical Internal Radiation Dose) schema to evaluate organ doses from internal radiation sources. (Cristy and Eckerman 1987, Han et al. 2006)

The second generation of computational phantoms are voxel or tomographic phantoms. They are based on medical images of patients who have undergone CT (computed tomography) or MR (magnetic resonance) imaging. Segmentation allows for delineation of internal anatomy. Voxel phantoms are much more anatomically realistic than stylized phantoms, since they based on real patient images. However, the shape and size of organs cannot be easily changed within tomographic phantoms; the phantoms are only uniformly scalable. Furthermore, the majority of these phantoms have a homogeneous skeletal composition, and various correction factors must be applied in order to get absorbed dose estimates to the red bone marrow and endosteum targets.

Several of the available voxel phantoms that have been published are based on incomplete image sets of human anatomy. (Gibbs et al. 1984, Williams et al. 1986, Veit et al. 1989, Zubal et al. 1994, Caon et al. 1999) More recent attempts to utilize a heterogeneous skeleton have been documented. Xu et al. (2000) developed a tomographic phantom from color photographic images from the Visible Human Project. The skeleton in VIP-man is divided into separately tagged voxels of mineral bone and red marrow. However, there is no delineation between cortical and trabecular bone, and no representation of yellow marrow. Another approach to differentiating skeletal tissues in voxel phantoms was to tag voxels within

the skeleton as cortical bone, spongiosa, and medullary marrow. (Zankl et al. 2007) Kramer et al. (2006a, 2006b) also utilized this approach in the MAX06 phantom. The distinction between cortical bone and spongiosa accounts for cortical bone shielding effects of marrow for transport involving low energy photons.

A third generation of computational phantoms called hybrid phantoms have been recently developed. Human anatomy within hybrid phantoms are made up of NURBS (Non-Uniform Rational B-Spline) and polygon mesh surfaces. They retain the anatomical realism of tomographic phantoms, and can also be easily modified to model different patient statures and weights. (Lee et al. 2007, Segars et al. 2008, Xu et al. 2007) A main contributor to the development of hybrid phantoms is the Bone Imaging & Dosimetry research group at the University of Florida. They have published hybrid phantoms representing the ICRP89 reference newborn, 1 year, 5 year, 10 year, 15 year and adult male and female. (Lee et al. 2007, 2008, 2009, Hurtado 2008) The UFHADF (UF hybrid adult female) phantom will be used in this study to create a heterogeneous skeletal model for the adult female.

Models of skeletal dosimetry currently used in a clinical setting, such as MIRDOSE and its successors (Stabin 1996, Eckerman and Stabin 2000, Stabin and Siegel 2003) are limited by several factors. These models assume an infinite cylinder of spongiosa, which can result in an overestimation of dose because there is no allowance for energy escape. Secondly, the current model does not allow for beta particle cross-fire from cortical bone to active marrow. Furthermore, the skeletal microstructure, including that of trabecular bone and marrow, are widely based on studies done at the University of Leeds in the 1960's and 1970's in which chord-length distributions were measured through trabecular bone and marrow cavities for 7

bone sites taken from a 44 year-old male. (Beddoe 1976) This data serves as a foundation for much of the skeletal attributes of ICRP reference man. (ICRP 1975)

The purpose of this study was to derive the masses of all the previously mentioned skeletal tissues in a bone site-specific manner, and then apply them to the UFHADF phantom. This allowed for significant improvements in the macro- and micro-architecture of the skeleton. For instance, spongiosa was modeled as a finite region within each bone site. Cross-fire effects were also taken into account from electron emissions in compact bone. The end result will be a heterogeneous skeleton from which a more accurate means of radiation transport can be implemented.

The skeletal tissue masses presented in this paper were derived from four data sets. The first are the polygon mesh and NURBS skeletal volumes of the UF hybrid adult female. The UFHADF skeleton was modeled so that total skeletal masses for each bone site were matched with ICRP reference data. Initially, the skeleton was composed as a homogeneous mixture of all skeletal tissues, including cortical bone, trabecular bone, red and yellow marrow, miscellaneous skeletal tissues, and teeth.

The second source of data for this skeletal model includes ICRP70 (1995), ICRP89 (2002), and ICRU46 (1992). The skeletal tissue reference masses and densities were obtained from the ICRP reports. ICRU46 served as a reference for the density of soft tissue for an adult female and for the elemental composition of spongiosa.

The last two sources of data were based on image data sets from a 45 year-old female cadaver. All pertinent skeletal sites were excised and imaged by standard CT and microCT in order to get valuable information on skeletal macrostructure and microstructure.

MATERIALS AND METHODS

The purpose of this study is to develop a comprehensive skeletal tissue model for the ICRP reference adult female. This model will be implemented into UFHADF, the UF hybrid adult female phantom and later, coupled to radiation transport codes to obtain absorbed dose estimates to the active bone marrow and endosteum. The development of a skeletal reference model is a two-part process: 1. skeletal tissue mass calculations and 2. skeletal dosimetry via radiation transport codes. This paper concentrates on the methodology behind calculating site-specific skeletal tissue masses.

The methodology presented here is based on mass derivations from Pafundi et. al (2009) for the ICRP reference newborn hybrid phantom. However, modifications were made to account for differences in skeletal structure between the newborn and adult model.

Image Acquisition and Analysis

The adult female skeletal model was initiated when a 45-year old female cadaver was made available to us through the State of Florida Anatomical Board. It was confirmed that skeleton of the female had no deterioration before the study was continued. The cadaver was first subjected to whole-body in-vivo CT imaging within the Department of Radiology at UF Shands hospital with a 64-slice Toshiba CT scanner. The in-vivo CT images were transferred to imaging workstations within ALRADS (Advanced Laboratory for Radiation Dosimetry Studies) at the UF Department of Nuclear and Radiological Engineering. This was done so that we would

have a complete data set of the subject available. The images were used when ex-vivo CT imaging of the skeletal site was not able to be performed (segmentation of the shafts of the long bones).

In order for ex-vivo CT imaging to take place a cadaver harvest was performed in which skeletal sites containing active marrow were excised. These bone sites included: the cranium, mandible, clavicles, scapulae, sternum, cervical, thoracic, and lumbar vertebrae, 2 upper, middle, and lower ribs, os coxae, sacrum, proximal and distal humeri, proximal and distal radii, proximal and distal ulnae, proximal and distal femorae, patellae, proximal and distal tibiae, and the proximal and distal fibulae. These major skeletal sites were harvested, cleaned, and then kept frozen for later use.

The next step performed was ex-vivo CT imaging of each skeletal site. These scans were completed at Shands at UF with the same CT scanner mentioned previously. Two scans for each bone were completed, one with a bone filter and one with a soft tissue filter in order to get optimal imaging of cortical bone and spongiosa boundaries, with 1 mm slices. Two vital parameters were extracted from these images, the co*rtical bone volume fraction* (CBVF) and the *spongiosa volume fraction* (SVF). These fractions sum to one, as they represent the total volume of homogeneous bone in a given skeletal site. Segmentation of cortical bone and spongiosa boundaries was completed, and volumes were calculated using 3D-Doctor™. These volume fractions will be later adjusted by an iterative process so that the total skeletal mineral bone mass matches the ICRP 89 (2002) value.

Following inspection of the ex-vivo scans, a region was selected within each bone to be imaged via microCT. The microCT imaging was completed by SCANCO (Scanco Medical AG,

Bruttisellen, Switzerland) at 30 micron resolution. The microCT imaging allowed for two parameters of skeletal microstructure to be obtained through image analysis software for almost all skeletal sites. These included the *marrow volume fraction* (MVF) and the *trabecular bone volume fraction* (TBVF). These volume fractions also sum to one, and represent the volume of spongiosa within each skeletal site. The image analysis software, *BIDUserInterface* (Rajon et al. 2006) converts the images into a binary format by selecting a threshold value through gradient inspection. Four main steps are taken to get the final binary image: (1) a region of interest (ROI) is extracted to ensure that no cortical bone remains in the image; (2) a median filter is applied to improve the signal-to-noise ratio (SNR); (3) a threshold value is determined; and (4) the ROI is segmented into either bone or marrow voxels based on the threshold value.

The final volume fraction to be determined for mass calculations is the shallow marrow volume fraction (SMVF). This is the volume of spongiosa occupied by marrow within 50 microns of bone surfaces. As mentioned earlier, this parameter will be used to determine the surrogate target tissue for osteoprogenitor cells. The SMVF is calculated by importing the microCT images for each skeletal site into the PIRTSMVF code. (Shah et al. 2005)

Mass Calculations

Miscellaneous Skeletal Tissues

After obtaining all of the relevant volume fractions from the macro and microstructure, the next step is to distribute the miscellaneous skeletal tissue mass. Miscellaneous skeletal tissues (MST) include blood vessels and periosteum. (ICRP 2002) Since these tissues cannot be

identified in CT data sets, they are just included in the homogeneous skeletal volumes of the adult female phantom. When comparing total skeletal tissue masses to that of ICRP 89, the MST must be taken out. Miscellaneous skeletal tissues are first distributed by volume to all skeletal sites, where X represents one skeletal site. (Equation 1)

$$V_{MST}^{X} = V_{MST} * (\frac{V_{HB*}^{X}}{V_{HB*}^{Total}}), \quad (1)$$

The volumes marked with an asterisk represent those including MST. V_{HB*} refers to the volume of homogeneous bone already defined within the phantom. V_{MST} was calculated by multiplying the mass of 160 g, as given by ICRP89 as the total amount of MST within the skeleton, by the density of soft tissue for an adult female, 1.03. (ICRU46 1992)

Next they are further partitioned into skeletal tissues including active marrow (AM*), inactive marrow (IM*), and mineral bone(MB*) including cortical (CB*) and trabecular bone (TB*) volumes. (Equation 2)

$$V_{MST-AM}^{X} = V_{MST}^{X} * (\frac{V_{AM*}^{X}}{V_{HB*}^{X}}), \quad (2)$$

$$V_{MST-IM}^{X} = V_{MST}^{X} * (\frac{V_{IM*}^{X}}{V_{HB*}^{X}})$$

$$V_{MST-MB}^{X} = V_{MST}^{X} * (\frac{V_{MB*}^{X}}{V_{HB*}^{X}})$$

$$V_{MST-CB}^{X} = V_{MST-MB}^{X} * \left(\frac{V_{CB*}^{X}}{V_{MB*}^{X}}\right)$$

$$V_{MST-TB}^{X} = V_{MST-MB}^{X} * \left(\frac{V_{TB*}^{X}}{V_{MB*}^{X}}\right)$$

Marrow Volumes and Masses

In the adult, marrow can be found within spongiosa cavities or in the medullary cavities of the shafts of the long bones. In the medullary cavities of the long bones the marrow is

assumed to be 100 percent inactive marrow, while active marrow remains in the proximal and distal ends of the bones. (ICRP 2002) The active and inactive marrow volumes are calculated from the NURBS homogeneous bone volumes, the spongiosa volume fraction (SVF), marrow volume fraction(MVF), and the cellularity factor, CF (fraction of marrow that is hematopoetically active). (ICRP 1995) (Equation 3)

$$V_{TAM*}^{X} = V_{HB*}^{X} * SVF^{X} * MVF^{X} * CF^{X} \quad (3)$$

$$V_{TIM*}^{X} = V_{HB*}^{X} * SVF^{X} * MVF^{X} * (1 - CF^{X})$$

$$V_{TAM}^{X} = V_{TAM*}^{X} - V_{MST-AM}^{X}$$

$$V_{TIM}^{X} = V_{TIM*}^{X} - V_{MST-IM}^{X}$$

The subscripts TAM (trabecular active marrow) and TIM (trabecular inactive marrow) are adopted to distinguish between the inactive marrow located within trabecular cavities and the medullary marrow located within the shafts of the long bones. The medullary marrow volume is calculated in the same way as the trabecular inactive marrow volume, except the MVF is equal to 1, since there is no trabeculation within the shafts. Since there was no microCT imaging completed for the hands and feet, and Whitwell (1973) conducted a study which showed comparable microstructure among the ribs and these bone regions, the MVF for the ribs was assigned to the wrists and hands and ankles and feet. The cellularity factors were obtained from Table 41 in ICRP70. For the inactive marrow, the volume is multiplied by (1-CF) instead of just CF, in order to obtain the fraction of marrow that hematopoietically inactive. The MST is then subtracted from the marrow volumes and multiplied by the correct ICRP density (1.03 for active marrow, 0.98 for inactive marrow) in order to compare to the active and inactive marrow masses from ICRP 89.

Mineral Bone Masses and Volumes

Total mineral bone within the adult female skeleton is composed of trabecular and cortical bone. The equations used to calculate the mineral bone volumes including miscellaneous skeletal tissues are shown below. (Equation 4)

$$V_{MB*}^{X} = V_{TB*}^{X} + V_{CB*}^{X} \quad (4)$$

$$V_{TB*}^{X} = V_{HB*}^{X} * SVF^{X} * TBVF^{X}$$

$$V_{CB*}^{X} = V_{HB*}^{X} * CBVF^{X}$$

These volumes are based on the adult female phantom homogeneous bone volumes, as well as the macro and microstructure parameters determined from previous image processing techniques. The initial SVF and CBVF were obtained from manual image segmentation, and were adjusted through an iterative process until the total mineral bone mass matched the ICRP 89 (2002) value of 4000 g. The equations for mineral bone volumes excluding MST are shown in Equation 5.

$$V_{MB}^{X} = V_{MB*}^{X} - V_{MST-MB}^{X} \quad (5)$$

$$V_{TB}^{X} = V_{TB*}^{X} - V_{MST-TB}^{X}$$

$$V_{CB}^{X} = V_{CB*}^{X} - V_{MST-CB}^{X}$$

The masses of mineral bone, trabecular bone, and cortical bone are calculated from multiplying the equations above by the ICRP 89 (2002) density for mineral bone, 1.9 g/cm^3.

Shallow Marrow Masses and Volumes

As previously discussed, the shallow marrow volume or endosteum is used as a surrogate target tissue for osteoprogenitor cells. It encompasses a layer of cells 50 microns

within trabecular bone surfaces or the cortical bone/medullary cavity interface in the shafts of the long bones. The target layer along trabecular bone surfaces is defined as TAM_{50}, and the layer along the shafts on the long bones, CIM_{50}. The equations for these volumes are shown below. (Equation 6 and 7)

$$V^X_{TAM50*} = V^X_{Spongiosa} * SMVF^X * CF^X \quad (6)$$

$$V^X_{CIM50*} = V^X_{Medullary\ marrow*} * SMVF^X_{Shaft} * (1 - CF)^X \quad (7)$$

In equation 6, the $V^X_{Spongiosa}$ refers to the volume of spongiosa for skeletal site, X. It is the product of the phantom homogeneous bone volume and the spongiosa volume fraction. The $SMVF^X$ is calculated from the PIRTSMVF code by importing the microCT image into the code. In equation 7, since microCT images were not obtained for the shafts of the long bones, this volume must be calculated in a different manner. The shafts of the long bones were modeled as concentric cylinders, with an effective radius, $r_{medullary\ marrow}$. (Equation 8) From the effective radius the shallow marrow volume fraction for the shafts was calculated. (Equation 9)

$$r_{medullary\ marrow} = \sqrt{\frac{\frac{V^X_{medullary\ marrow*}}{2}}{\pi * h}} \quad (8)$$

$$SMVF^X_{Shaft} = 1 - \left(\frac{r^X_{medullary\ marrow*} - 0.005}{r^X_{medullary\ marrow*}}\right)^2 \quad (9)$$

In equations 7 and 8, $V^X_{Medullary\ marrow*}$ refers to the total volume of medullary marrow within the shafts. It is the product of the skeletal site volume from the female phantom and the medullary marrow volume fraction from segmentation in 3D-Doctor™. The h in equation 8 is the height of the shaft region, measured in *Rhinoceros™*.

RESULTS AND DISCUSSION

The volumes and masses of all skeletal tissues including active and inactive marrow, cortical and trabecular bone, and miscellaneous skeletal tissues were calculated based on 1) ICRP Reference skeletal tissue masses from ICRP70 and ICRP89, 2) the skeletal volumes from the ICRP-based UF hybrid adult female phantom, 3) in-vivo and ex-vivo CT images of all marrow-containing skeletal sites, and 4) microCT images of all active marrow-containing sites. This study targeted total skeletal tissue masses provided in ICRP 89 (2002), but distributed them among all marrow-containing skeletal sites based on volume ratios and imaging data.

Volume fractions for Spongiosa, Marrow, Cortical and Trabecular Bone

Table 1 shows the SVF (spongiosa volume fraction), CBVF (cortical bone volume fraction), TBVF (trabecular bone volume fraction) and MVF (marrow volume fraction) used to calculate all skeletal tissue masses. The SVF and CBVF were initially determined through manual image segmentation in 3D-Doctor™, and later adjusted through an iterative process to match ICRP reference masses. The values shown are the final volume fractions used in the mass calculations. The volume fractions for the cranium, all vertebral sites, and the proximal femur are averages of multiple samples obtained for that given bone site. The MVF and TBVF were determined by gradient inspection using BIDUserInterface. (Rajon et al. 2006) All of the MVFs for the shafts of the long bones are valued at 1.0, as there is no trabeculation, and all of the marrow in the medullary cavity is assumed to be inactive marrow.

Miscellaneous Skeletal Tissue Distribution

Table 2 shows how the ICRP value of 160 g of miscellaneous skeletal tissue was partitioned. First, it was distributed to skeletal sites based on volume ratios of the homogeneous bones within the UFHADF phantom. Then, the volumes were further divided among all skeletal tissues: active and inactive marrow, and cortical and trabecular bone.

Marrow Volumes and Masses

Table 3 shows the trabecular active and inactive marrow volumes and masses for the adult female skeleton. These values do not include miscellaneous skeletal tissues. The entire skeleton was calculated to have an active marrow volume of 874.26 cm^3 assuming the ICRP density of 1.03 g/cm^3 for active marrow. The total skeletal mass of active marrow came out to be 900.49 g, almost equal to the ICRP reference mass of 900 g. The ICRP reference mass for trabecular inactive marrow was 1800 g. The final value for this skeletal tissue model was 1777.3, slightly over a 1 percent difference. The total volume was 1813.6 cm^3, assuming the ICRP reference density of 0.98 g/cm^3 for inactive marrow. The largest mass of active marrow for a given bone site was found to be in the os coxae, which shows good agreement from the active marrow percent distribution table in ICRP 89.

Mineral Bone Volumes and Masses

Table 4 lists the masses for mineral bone and its constituents, trabecular and cortical bone. The values listed exclude the masses of miscellaneous skeletal tissues. These masses were calculated based on their respective volumes and the density of mineral bone, 0.98, found

in ICRP89. The mineral bone mass for the entire skeleton matched exactly with the ICRP reference mass of 4000g. The cortical and trabecular bone masses differed slightly from reference values, with the trabecular bone mass equaling 900.5 g, and cortical bone mass being 3107.1 g. These values exhibit a 13 and 3 percent difference from ICRP. However, ICRP 89 clearly states that 80 % of total mineral bone mass is cortical, and 20 % is trabecular. The masses from this study indicate a very similar 78/22 percent distribution.

Shallow Marrow Volumes and Masses

The shallow marrow distribution by skeletal site is reported in Table 5. The first column is the amount of spongiosa for a given bone site that was computed as shallow marrow. These values came directly from the PIRTSMVF code with the exception of all the shafts of the long bones. Table 6 lists the average lengths of the shafts of the long bones. The longest shaft was found to be the femur at 28.7 cm, and the shortest was the ulna, 17.4 cm. Ten measurements were taken for each long bone shaft. The calculated medullary marrow radius was used to calculate the shallow marrow volume fraction for the shafts of the long bone listed in column 2 of table 5. Column 3 is the percent of total marrow calculated as shallow marrow. Volumes and masses of shallow active and inactive marrow are listed in the last four columns. The total amount of shallow active marrow was around 147g.

CONCLUSION

The end result of this study was the creation of a heterogeneous skeletal tissue model for the adult female that closely matched the reference total skeletal tissue masses given by the ICRP. Active and inactive marrow masses were both within one percent of the ICRP reference values. The cortical bone mass differed by three percent, while the trabecular bone percent difference was 13. However, the CB/TB ratio from this model was 78/22, which closely matches the ICRP 80/20 ratio. In addition, the total skeletal mineral bone mass matched the ICRP reference value of 4000 g exactly. Shallow marrow volumes and masses were also calculated so that they can serve as a surrogate target region for osteoprogenitor cells.

In order to complete the skeletal dosimetry model for the adult female, the volumes from this study will be realized within the UFHADF. This subsegmentation of the skeleton is completed using the software, *Rhinoceros™* (McNeel North America, Seattle, WA). Utilizing *Rhinoceros™*, cortical bone, spongiosa, and medullary marrow volumes will be targeted, completing the heterogeneous skeletal tissue model. The next step is to voxelize the phantom using an in-house *MATLAB™* (The Mathworks, Inc., Natick, MA) code, *Voxelizer* (Lee et al. 2007), so that radiation transport can be executed. An in-house IDL (ITT Visualization Solutions, Boulder, CO) code *Voxel_Counter* will be used to verify that the voxel volumes are within one percent of the original volumes. Next, the voxelized version of UFHADF will be visually inspected using the program, *ImageJ* (National Institutes of Health Public Domain, Bethesda, MD). Radiation transport will be accomplished using PIRT (Paired Image Radiation Transport) (Shah et al. 2005). PIRT tracks the energy deposition of particles through the macrostructure and microstructure simultaneously. Finally, the skeletal tissue masses from this project will be

used to obtain specific absorbed fraction data from the PIRT runs. When all of these steps are accomplished, the skeletal reference model for the ICRP adult female will be complete.

REFERENCES

Beddoe AH, Darley PJ, and Spiers FW 1976 Measurements of trabecular bone structure in man. Phys.Med. Biol. **21**(4) 589-607

Caon M, Bibbo G, and Pattison J 1999 An EGS4-ready tomographic computational model of a 14-year-old female torso for calculating organ doses from CT examinations. Physics in Medicine and Biology **44**(9) 2213-2225

Cristy, M. 1980. *Mathematical phantoms representing children of various ages for use in estimates of internal dose.* U.S. Nuclear Regulatory Commission Rep. NUREG/CR-1159 (also Oak Ridge National Laboratory Rep. ORNL/NUREG/TM-367).

Cristy, M. 1981. Active bone marrow distribution as a function of age in humans. *Phys. Med. Biol*.26: 389–400.

Cristy M and Eckerman K F 1987 *Specific Absorbed Fractions of Energy at Various Ages from Internal Photon Sources* vols 1–7 ORNL/TM-8381 (Oak Ridge, TN: Oak Ridge National Laboratory)

Eckerman K F and Stabin M G 2000 Electron absorbed fractions and dose conversion factors for marrow and bone by skeletal regions *Health Phys.* **78** 199-214

Frost, H.M. (1980). Skeletal physiology and bone remodeling. In: Fundamental and clinical bone physiology, ed. By M.R. Urist. Philadelphia: J. B. Lippincott Co., 208-241

Frost, H.M. (1963a) Bone remodeling dynamics. Springfield, Illinois: Charles C. Thomas.

Gibbs SJ, Pujol A, Chen TS, Malcolm AW, and James AE 1984 Patient Risk from Interproximal Radiography. Oral Surgery Oral Medicine Oral Pathology Oral Radiology and Endodontics **58**(3) 347-354

Han E, BolchWand Eckerman K 2006 Revisions to the ORNL series of adult and pediatric computational phantoms for use with the MIRD schema *Health Phys.* **90** 337–56

Hurtado J L, Lee C, Lodwick D, Geode T, Williams J L and Bolch W E in press Hybrid computational phantoms representing the reference adult male and adult female: Construction and applications to retrospective dosimetry *Health Phys*

International Commission on Radiological Protection (ICRP) (1975) Publication 23, Report of the task group on reference man. Oxford: Pergamon Press.

ICRP (1995). Basic anatomical and physiological data for use in radiological protection: the skeleton. ICRP Publication 70, Ann. ICRP 25 (2).

ICRP 2002 ICRP Publication 89: basic anatomical and physiological data for use in radiological protection—reference values *Ann. ICRP* **32** 1–277

ICRU 1992 Photon, electron, proton and neutron interaction data for body tissues *ICRU Report* No 46 (Bethesda,MD: International Commission on Radiation Units and Measurements)

Kramer R, Khoury H J, Vieira J W and Kawrakow I 2006a Skeletal dosimetry in the MAX06 and the FAX06 phantoms for external exposure to photons based on vertebral 3D-microCT images *Phys. Med. Biol.* **51** 6265–89

Kramer R, Khoury H J, Vieira J W and Lima V J 2006b MAX06 and FAX06: update of two adult human phantoms for radiation protection dosimetry *Phys. Med. Biol.* **51** 3331–46

Lee C, Lodwick D, Hasenauer D, Williams J L, Lee C and Bolch W E 2007 Hybrid computational phantoms of the male and female newborn patient: NURBS-based whole-body models *Phys. Med. Biol.* **52** 3309–33

Lee C, Lodwick D, Williams J L and Bolch W E 2008 Hybrid computational phantoms of the 15-year male and female adolescent: applications to CT organ dosimetry for patients of variable morphometry *Med Phys* **35** 2366-2382

Lee C, Lodwick D, Hurtado J, Pafundi D, Williams J, Bolch W 2009 The UF Family of Reference Hybrid Phantoms for Computational Radiation Dosimetry *Phys Med Biol* **?**

Pafundi D, Lee C, Watchman C, Bourke V, Aris J, Shagina N, Harrison J, Fell T, Bolch W. 2009. An Image-based Skeletal Tissue Model for the ICRP Reference Newborn. Phys med Biol. 54: 4497-4531

Rajon D, Pichardo J, Brindle J, Kielar K, Jokisch D, Patton P and Bolch W 2006 Image segmentation of trabecular spongiosa by visual inspection of the gradient magnitude *Phys. Med. Biol.* **51** 4447–67

Segars W P, Mahesh M, Beck T J, Frey E C and Tsui B M 2008 Realistic CT simulation using the 4D XCAT phantom *Med Phys* **35** 3800-3808

Shah AP, Rajon D, Patton P, Jokisch D, and Bolch W 2005c Accounting for beta-particle energy loss to cortical bone via Paired-Image Radiation Transport (*PIRT*). Med Phys **32**(5) 1354-1366

Segars W P, Mahesh M, Beck T J, Frey E C and Tsui B M 2008 Realistic CT simulation using the 4D XCAT phantom *Med Phys* **35** 3800-3808

Shah AP, Rajon D, Patton P, Jokisch D, and Bolch W 2005c Accounting for beta-particle energy loss to cortical bone via Paired-Image Radiation Transport (*PIRT*). Med Phys **32**(5) 1354-1366

Snyder, W.S., Ford, M.R., Warner, G.G., and Watson, S.B. 1974. *A tabulation of dose equivalent per microcurie-day for source and target organs of an adult for various radionuclides: Part 1.* Oak Ridge National Laboratory Rep. ORNL-5000.

Stabin M G and Siegel J A 2003 Physical models and dose factors for use in internal dose assessment *Health Phys* **85** 294-310

Stabin MG. MIRDOSE: personal computer software for internal dose assessment in nuclear medicine. *J Nucl Med.* 1996;37:538 –546.

Triffitt, J.T. (1980) The organic matrix of bone tissue. In: Fundamental and clinical bone physiology, ed. By M.R. Urist. Philadelphia: J.B. Lippincott Co., 45-82.

Veit R, Zankl M, Petoussi N, Mannweiler E, Williams G, and Drexler G 1989 Tomographic anthropomorphic models, Part I: Construction technique and description of models of an 8-week-old baby and a 7-year-old child. Neuherberg, Germany: GSF-National Research Center for Environment and Health.

Williams G, Zankl M, Abmayr W, Veit R, and Drexler G 1986 The calculation of dose from external photon exposures using reference and realistic human phantoms and Monte-Carlo methods. Physics in Medicine and Biology **31**(4) 449-452

Xu X G, Taranenko V, Zhang J and Shi C 2007 A boundary-representation method for designing whole-body radiation dosimetry models: pregnant females at the ends of three gestational periods--RPI-P3, -P6 and -P9 *Phys Med Biol* **52** 7023-7044

Xu XG, Chao TC, and Bozkurt A 2000 VIP-man: An image-based whole-body adult male model constructed from color photographs of the visible human project for multiparticle Monte Carlo calculations. Health Physics **78**(5) 476-486

Zankl M, Eckerman K F and Bolch W E 2007 Adult male and female voxel-based models representing the ICRP
reference adult—the skeleton *Radiat. Prot. Dosim.* **127** 174–86

Zubal IG, Harrell CR, Smith EO, Rattner Z, Gindi G, and Hoffer PB 1994 Computerized 3-Dimensional Segmented Human Anatomy. Medical Physics **21**(2) 299-302

Table 1. Skeletal Site-Specific Volume Fractions

Skeletal Site	MVF	TBVF	SVF	CBVF
Cranium	0.3160	0.6840	0.4125	0.58749
Mandible	0.8502	0.1498	0.4965	0.50345
Cervical	0.8205	0.1795	0.6415	0.35853
Thoracic	0.8856	0.1144	0.7890	0.21102
Lumbar	0.8728	0.1272	0.8488	0.15119
Sternum	0.9173	0.0827	0.7385	0.26153
Ribs	0.9096	0.0904	0.5706	0.42943
Scapulae	0.9461	0.0539	0.6082	0.39179
Clavicles	0.9211	0.0789	0.5638	0.43617
Os coxae	0.9529	0.0471	0.7698	0.23017
Sacrum	0.8476	0.1524	0.7423	0.25772
Humeri, Proximal	0.9071	0.0929	0.8811	0.11886
Humeri, Upper Shaft	1.0000	0.0000	0.3468	0.65322
Humeri, Lower Shaft	1.0000	0.0000	0.3468	0.65322
Humeri, Distal	0.8291	0.1709	0.7644	0.23555
Radii, Proximal	0.8805	0.1195	0.7448	0.25519
Radii, Shaft	1.0000	0.0000	0.3353	0.66472
Radii, Distal	0.8671	0.1329	0.8253	0.17471
Ulnae, Proximal	0.7312	0.2688	0.8120	0.18795
Ulnae, Shaft	1.0000	0.0000	0.3338	0.66623
Ulnae, Distal	0.9620	0.0380	0.8184	0.18158
Wrists and Hands	0.9096	0.0904	0.3482	0.65181
Femora, Proximal	0.77275	0.2273	0.9008	0.09917
Femora, Upper Shaft	1.0000	0.0000	0.5230	0.47701
Femora, Lower Shaft	1.0000	0.0000	0.5230	0.47701
Femora, Distal	0.7966	0.2034	0.8558	0.14419
Patellae	0.8135	0.1865	0.8588	0.14116
Tibiae, Proximal	0.8417	0.1583	0.8830	0.11698
Tibiae, Shaft	1.0000	0.0000	0.4708	0.52919
Tibiae, Distal	0.8284	0.1716	0.8509	0.14909
Fibulae, Proximal	0.8780	0.1220	0.8344	0.16564
Fibulae, Shaft	1.0000	0.0000	0.3058	0.69422
Fibulae, Distal	0.8185	0.1815	0.7428	0.25724
Ankles and Feet	0.9096	0.0904	0.6812	0.31877

Table 2. Miscellaneous Skeletal Tissue Volume and Mass Distribution

Skeletal Site	MST - Total Vol	MST - Total Mass	MST - Mineral Bone Vol	MST - Mineral Bone Mass	MST - TAM Vol	MST - TAM Mass	MST - TIM Vol	MST - TIM Mass	MST - CBV Vol	MST - CBV Mass	MST - TBV Vol	MST - TBV Mass
Cranium	18.35	18.71	15.96	16.28	0.91	0.93	1.48	1.51	10.78	10.99	4.31	4.40
Mandible	1.53	1.56	0.89	0.90	0.25	0.25	0.40	0.41	0.77	0.79	0.09	0.09
Cervical	2.54	2.59	1.20	1.23	0.94	0.95	0.40	0.41	0.91	0.93	0.21	0.22
Thoracic	7.28	7.43	2.19	2.24	3.56	3.63	1.53	1.56	1.54	1.57	0.42	0.43
Lumbar	8.60	8.78	2.23	2.27	4.46	4.55	1.91	1.95	1.30	1.33	0.56	0.57
Sternum	1.23	1.26	0.40	0.41	0.58	0.60	0.25	0.26	0.32	0.33	0.06	0.06
Ribs	9.80	10.00	4.71	4.81	3.56	3.63	1.53	1.56	4.21	4.29	0.33	0.34
Scapulae	9.70	9.90	4.12	4.20	2.12	2.16	3.46	3.53	3.80	3.88	0.23	0.24
Clavicles	1.62	1.65	0.78	0.80	0.28	0.28	0.56	0.58	0.71	0.72	0.05	0.05
Os coxae	20.27	20.68	5.40	5.51	7.14	7.28	7.73	7.89	4.67	4.76	0.50	0.51
Sacrum	6.16	6.29	2.29	2.33	1.86	1.90	2.02	2.06	1.59	1.62	0.50	0.51
Humeri, Proximal	4.03	4.11	0.81	0.82	1.13	1.15	2.09	2.13	0.48	0.49	0.25	0.25
Humeri, Upper Shaft	2.14	2.18	1.39	1.42	0.11	0.11	0.63	0.64	1.39	1.42	0.00	0.00
Humeri, Lower Shaft	1.88	1.92	1.23	1.25	0.00	0.00	0.65	0.67	1.23	1.25	0.00	0.00
Humeri, Distal	2.56	2.62	0.94	0.96	0.00	0.00	1.63	1.66	0.60	0.62	0.23	0.23
Radii, Proximal	0.40	0.41	0.14	0.14	0.00	0.00	0.26	0.27	0.10	0.10	0.02	0.02
Radii, Shaft	1.49	1.51	0.99	1.01	0.00	0.00	0.50	0.51	0.99	1.01	0.00	0.00
Radii, Distal	0.72	0.74	0.21	0.21	0.00	0.00	0.52	0.53	0.13	0.13	0.06	0.06
Ulnae, Proximal	1.36	1.38	0.55	0.56	0.00	0.00	0.81	0.82	0.25	0.26	0.21	0.21
Ulnae, Shaft	1.76	1.80	1.17	1.20	0.00	0.00	0.59	0.60	1.17	1.20	0.00	0.00
Ulnae, Distal	0.25	0.26	0.05	0.05	0.00	0.00	0.20	0.20	0.05	0.05	0.00	0.00
Wrists and Hands	3.65	3.73	2.50	2.55	0.00	0.00	1.16	1.18	2.38	2.43	0.09	0.09
Femora, Proximal	5.76	5.88	1.75	1.79	1.40	1.43	2.61	2.66	0.57	0.58	0.75	0.77
Femora, Upper Shaft	3.97	4.05	1.89	1.93	0.31	0.32	1.76	1.80	1.89	1.93	0.00	0.00
Femora, Lower Shaft	4.53	4.62	2.16	2.20	0.00	0.00	2.37	2.42	2.16	2.20	0.00	0.00
Femora, Distal	7.52	7.67	2.39	2.44	0.00	0.00	5.12	5.23	1.08	1.11	1.06	1.08
Patellae	0.81	0.82	0.24	0.25	0.00	0.00	0.56	0.58	0.11	0.12	0.10	0.10
Tibiae, Proximal	5.96	6.08	1.53	1.56	0.00	0.00	4.43	4.52	0.70	0.71	0.65	0.66
Tibiae, Shaft	5.31	5.41	2.81	2.86	0.00	0.00	2.50	2.55	2.81	2.86	0.00	0.00
Tibiae, Distal	2.19	2.23	0.65	0.66	0.00	0.00	1.54	1.58	0.33	0.33	0.26	0.26
Fibulae, Proximal	0.50	0.51	0.13	0.14	0.00	0.00	0.37	0.37	0.08	0.08	0.03	0.03
Fibulae, Shaft	0.81	0.82	0.56	0.57	0.00	0.00	0.25	0.25	0.56	0.57	0.00	0.00
Fibulae, Distal	0.49	0.50	0.19	0.20	0.00	0.00	0.30	0.30	0.13	0.13	0.05	0.05
Ankles and Feet	11.68	11.92	4.44	4.53	0.00	0.00	7.24	7.39	3.72	3.80	0.36	0.37
Total Skeleton	156.86	160.00	68.90	70.28	28.61	29.18	59.35	60.54	53.52	54.59	11.38	11.61
ICRP 89 Reference	156.86	160.00										

Table 3. Trabecular Active and Inactive Marrow Volumes and Masses

Skeletal Site	TAM Volume (cm3)	TAM Mass (g)	TIM Volume (cm3)	TIM Mass (g)
Cranium	27.77	28.60	45.31	44.40
Mandible	7.52	7.74	12.27	12.02
Cervical	28.61	29.47	12.26	12.02
Thoracic	108.85	112.12	46.65	45.72
Lumbar	136.33	140.42	58.43	57.26
Sternum	17.85	18.39	7.65	7.50
Ribs	108.78	112.04	46.62	45.69
Scapulae	64.84	66.78	105.79	103.67
Clavicles	8.50	8.75	17.25	16.91
Os coxae	218.10	224.64	236.27	231.55
Sacrum	56.89	58.59	61.63	60.40
Humeri, Proximal	34.42	35.45	63.92	62.64
Humeri, Upper Shaft	3.39	3.50	19.23	18.85
Humeri, Lower Shaft	0.00	0.00	19.94	19.54
Humeri, Distal	0.00	0.00	49.67	48.67
Radii, Proximal	0.00	0.00	7.99	7.83
Radii, Shaft	0.00	0.00	15.22	14.91
Radii, Distal	0.00	0.00	15.77	15.46
Ulnae, Proximal	0.00	0.00	24.61	24.12
Ulnae, Shaft	0.00	0.00	17.96	17.60
Ulnae, Distal	0.00	0.00	6.07	5.95
Wrists and Hands	0.00	0.00	35.34	34.64
Femora, Proximal	42.91	44.20	79.70	78.10
Femora, Upper Shaft	9.51	9.79	53.89	52.81
Femora, Lower Shaft	0.00	0.00	72.36	70.91
Femora, Distal	0.00	0.00	156.57	153.44
Patellae	0.00	0.00	17.26	16.91
Tibiae, Proximal	0.00	0.00	135.34	132.63
Tibiae, Shaft	0.00	0.00	76.36	74.83
Tibiae, Distal	0.00	0.00	47.19	46.25
Fibulae, Proximal	0.00	0.00	11.20	10.98
Fibulae, Shaft	0.00	0.00	7.53	7.38
Fibulae, Distal	0.00	0.00	9.11	8.92
Ankles and Feet	0.00	0.00	221.24	216.82
Total Skeleton	874.26	900.49	1813.58	1777.31
ICRP 89 Reference		900.00		1800.00
Ratio		1.00		0.99

Table 4. Cortical, Trabecular, and Mineral Bone Masses

Skeletal Site	Excluding MST		
	Trabecular Bone Mass (g)	Cortical Bone Mass (g)	Total Mineral Bone Mass
Cranium	302.22	625.80	926.38
Mandible	6.67	44.83	51.45
Cervical	17.14	52.89	69.88
Thoracic	38.63	89.23	127.40
Lumbar	54.65	75.52	129.46
Sternum	4.40	18.71	23.08
Ribs	29.68	244.30	273.65
Scapulae	18.63	220.73	239.20
Clavicles	4.23	41.09	45.28
Os coxae	43.11	270.87	313.54
Sacrum	40.86	92.24	132.73
Humeri, Proximal	19.29	27.79	46.92
Humeri, Upper Shaft	0.00	80.98	80.98
Humeri, Lower Shaft	0.00	71.35	71.35
Humeri, Distal	19.66	35.07	54.52
Radii, Proximal	2.08	5.91	7.97
Radii, Shaft	0.00	57.32	57.32
Radii, Distal	4.64	7.32	11.91
Ulnae, Proximal	17.36	14.80	32.00
Ulnae, Shaft	0.00	68.13	68.13
Ulnae, Distal	0.46	2.66	3.11
Wrists and Hands	6.72	138.21	144.88
Femora, Proximal	69.33	33.19	101.70
Femora, Upper Shaft	0.00	109.87	109.87
Femora, Lower Shaft	0.00	125.40	125.40
Femora, Distal	76.43	62.92	138.88
Patellae	7.58	6.63	14.14
Tibiae, Proximal	48.72	40.47	88.83
Tibiae, Shaft	0.00	163.07	163.07
Tibiae, Distal	18.70	18.96	37.54
Fibulae, Proximal	3.00	4.81	7.77
Fibulae, Shaft	0.00	32.49	32.49
Fibulae, Distal	3.87	7.32	11.16
Ankles and Feet	42.46	216.25	258.03
Total Skeleton	900.48	3107.12	4000.00
ICRP 89 Reference	800.00	3200.00	4000.00
Ratio	1.13	0.97	1.00

Table 5. Distribution of Shallow Marrow by Skeletal Site

Skeletal Site	SMVF (% of SV)	SMVF (% of Marrow)	Shallow Inactive Marrow Volume	Shallow Inactive Marrow Mass	Shallow Active Marrow Volume	Shallow Active Marrow Mass	Shallow Marrow (% of Total)
Cranium	16.92	53.55	25.06	24.56	15.36	15.82	10.78
Mandible	23.54	27.69	3.51	3.44	2.15	2.21	1.51
Cervical	13.38	16.31	2.06	2.02	4.82	4.96	1.87
Thoracic	13.84	15.63	7.53	7.38	17.57	18.10	6.80
Lumbar	8.46	9.69	5.85	5.73	13.65	14.06	5.29
Sternum	16.12	17.57	1.39	1.36	3.24	3.34	1.25
Ribs	17.46	19.20	9.24	9.06	21.57	22.22	8.35
Scapulae	14.78	15.62	17.06	16.72	10.46	10.77	7.34
Clavicles	11.67	12.66	2.26	2.21	1.11	1.14	0.90
Os coxae	15.03	15.77	38.48	37.71	35.52	36.59	19.84
Sacrum	10.76	12.70	8.08	7.92	7.46	7.68	4.17
Humeri, Proximal	10.81	11.91	7.86	7.71	4.23	4.36	3.22
Humeri, Upper Shaft	0.02	0.02	0.00	0.00	0.00	0.00	0.00
Humeri, Lower Shaft	0.02	0.02	0.00	0.00	0.00	0.00	0.00
Humeri, Distal	11.36	13.70	7.03	6.89	0.00	0.00	1.84
Radii, Proximal	10.72	12.18	1.00	0.98	0.00	0.00	0.26
Radii, Shaft	0.03	0.03	0.00	0.00	0.00	0.00	0.00
Radii, Distal	11.02	12.70	2.07	2.03	0.00	0.00	0.54
Ulnae, Proximal	11.24	15.38	3.91	3.83	0.00	0.00	1.02
Ulnae, Shaft	0.02	0.02	0.00	0.00	0.00	0.00	0.00
Ulnae, Distal	7.01	7.29	0.46	0.45	0.00	0.00	0.12
Wrists and Hands	9.59	10.55	3.85	3.77	0.00	0.00	1.01
Femora, Proximal	9.70	12.55	10.33	10.13	5.56	5.73	4.23
Femora, Upper Shaft	0.01	0.01	0.01	0.01	0.00	0.00	0.00
Femora, Lower Shaft	0.01	0.01	0.01	0.01	0.00	0.00	0.00
Femora, Distal	7.16	8.98	14.52	14.23	0.00	0.00	3.80
Patellae	6.12	7.52	1.34	1.31	0.00	0.00	0.35
Tibiae, Proximal	13.11	15.57	21.77	21.33	0.00	0.00	5.70
Tibiae, Shaft	0.01	0.01	0.01	0.01	0.00	0.00	0.00
Tibiae, Distal	13.80	16.66	8.12	7.96	0.00	0.00	2.13
Fibulae, Proximal	11.42	13.01	1.50	1.47	0.00	0.00	0.39
Fibulae, Shaft	0.04	0.04	0.00	0.00	0.00	0.00	0.00
Fibulae, Distal	18.89	23.07	2.17	2.13	0.00	0.00	0.57
Ankles and Feet	10.20	11.21	25.62	25.11	0.00	0.00	6.71
Total Skeleton			232.13	227.49	142.70	146.99	100.00

Table 6. Height and Radii of the Medullary Cavities within the long bone of UFHADF

Skeletal Site	Measured Height (cm) Medullary Marrow	Measured Height Std. Dev. (cm)	Calculated Radius (cm) Medullary Marrow
Humerii, Upper Shaft	9.755	0.095	0.617
Humerii, Lower Shaft	9.995	0.117	0.573
Radii, Shaft	17.532	0.159	0.378
Ulna, Shaft	17.443	0.032	0.411
Femora, Upper Shaft	14.642	0.065	0.844
Femora, Lower Shaft	14.108	0.048	0.918
Tibia, Shaft	23.744	0.050	0.727
Fibula, Shaft	23.761	0.054	0.228